SYNTHESIS AND CHARACTERIZATION OF IRON OXYCHLORIDE INTERCALATED BY ORGANOSULFUR ELECTRON DONORS

By

Susan Mary Kauzlarich

A DISSERTATION

Submitted to

Michigan State University

in partial fulfillment of the requirements

for the degree of

DOCTOR OF PHILOSOPHY

Department of Chemistry

1985

ABSTRACT

SYNTHESIS AND CHARACTERIZATION OF
IRON OXYCHLORIDE INTERCALATED BY ORGANOSULFUR
ELECTRON DONORS

By

Susan Mary Kauzlarich

In an effort to develop a new type of low-dimensional conductor, the intercalation chemistry of FeOCl with tetrathiolene molecules was explored. New intercalation compounds of the organic electron donors, TTF (tetrathiafulvalene), TMTTF (tetramethyl-TTF), TTN (tetrathianaphthalene), and TTT (tetrathiatetracene) with the inorganic host FeOCl were prepared by direct reaction of solutions of the organosulfur compound with solid FeOCl. The new phases obtained were $FeOCl(TTF)_{1/8.5}$, $FeOCl(TMTTF)_{1/13}$, $FeOCl(TTN)_{1/9}(toluene)_{1/21}$ and $FeOCl(TTT)_{1/9}(toluene)_{1/23}$.

The pressed powder electrical conductivity of FeOCl intercalated with these tetrathiolenes is about 10^3-10^4 times that of the pristine material ($\sigma_{RT}(FeOCl) \sim 10^{-6} (\Omega\text{-cm})^{-1}$). The temperature dependence of the conductivity is consistent with FeOCl and its intercalates being semiconductors with apparent bandgaps of 0.6 eV and ca. 0.3-0.4 eV, respectively. The highest conductivity ($\sigma_{RT} \sim 10^{-2}$ $(\Omega\text{-cm})^{-1}$) is observed for $FeOCl(TMTTF)_{1/13}$. Infrared spectroscopy indicates that the tetrathiolene molecule exists as a radical cation within the layers. Variable temperature magnetic susceptibility data for FeOCl indicates that there is strong short range magnetic ordering between

90 and 300 K. Comparison of the susceptibility data for the intercalates with that of FeOCl suggests that short range magnetic interactions are also important for the intercalates.

The combination of X-ray powder diffraction and EXAFS spectroscopy shows that these intercalates are, in general, well-ordered, crystalline solids. Upon intercalation the b axis (the interlayer distance) expands and doubles. In addition, alternate layers move one-half unit cell along the ac plane, giving rise to extinctions in the X-ray powder diffraction data consistent with a body-centered unit cell. The X-ray powder diffraction data are consistent with the tetrathiolene molecule being oriented perpendicular to the layers, with the exception of $FeOCl(TMTTF)_{1/13}$ in which the TMTTF molecule is oriented parallel to the layers.

Detailed neutron powder diffraction and wideline ^1H and ^2H NMR studies were carried out on $FeOCl(TTF)_{1/8.5}$, the best characterized and the most crystalline intercalate. The neutron powder diffraction data are consistent with a space group of Immm or I222 for the intercalate. A "soft" sphere model was proposed to account for the data; it assumes that sulfur atoms of the TTF molecule have a nonspherical electronic distribution that can be described by a pseudo-sp^3 hybridization. The neutron data provide evidence for long range ordering of the TTF molecule within FeOCl. ^1H and ^2H wideline NMR studies indicate that there is more than one type of ordering of the TTF molecules in $FeOCl(TTF)_{1/8.5}$, characterized by different average TTF environments and/or dynamics.

To my family and Larry

ACKNOWLEDGEMENTS

I would like to thank Professor Bruce A. Averill for his support and encouragement throughout the course of this work. I am also indebted to Dr. Boon K. Teo and Dr. John Faber for their helpful and generous collaboration. I would like to thank Dr. Jeff Ellena for his work on the NMR studies and for many helpful discussions.

I am grateful to Professor James L. Dye for serving as my advisor at Michigan State University and to his group, O. Fussa, M. Tinkham, M. Faber, S. Dawes and R. Huang, for many enlightening discussions and for their friendship.

In addition, I would like to thank Dr. M. R. Antonio, Dr. W. E. Cleland and M. Rogers for their advice and help during the course of this work. I thank C. Hulse and E. Ponzetto for being great company and S. Hefler for sharing a lab with me.

I would like to express my sincere thanks to my family and Larry who have provided me with considerable support and continuous encouragement throughout this work.

TABLE OF CONTENTS

	Page
LIST OF TABLES	vi
LIST OF FIGURES	viii
SUMMARY OF ABBREVIATIONS	xiv
INTRODUCTION	1
EXPERIMENTAL	12
Materials and Methods	12
Preparation of FeOCl	18
General Preparation of Intercalates	21
$FeOCl(TTF)_x(toluene)_y$	21
$FeOCl(TTF \text{ or } d_4\text{-}TTF)_x$	23
$FeOCl(TMTTF)_x$	23
$FeOCl(TTN \text{ or } TTT)_x(toluene)_y$	23
$FeOCl(Pyridine)_x$	24
SYNTHESIS OF FeOCl AND ITS TETRATHIOLENE INTERCALATES	25
MOX	26
Intercalation	29
Solvent effects	30
Effects of FeOCl decomposition and $FeCl_3$ upon intercalation	33
Preliminary results using other guests	36
Preliminary results using hosts other than FeOCl	37
STRUCTURAL STUDIES OF THE INTERCALATES	38
X-Ray Diffraction Results	38
Extended X-Ray Absorption Fine Structure	49

Page

Hard Sphere Model 67

Neutron Difraction Results 74

Soft Sphere Model 90

SOLID STATE NMR STUDIES 97

^{1}H NMR 98

^{13}C NMR 116

^{2}H NMR 124

ELECTRONIC PROPERTIES OF THE INTERCALATES 132

Infrared Spectroscopy 132

Optical Spectra 144

Conductivity 148

X-Ray Absorption Near Edge Structure 149

Magnetic Studies of FeOCl and the Intercalates 153

Variable temperatuare magnetic susceptibility 153
Neutron diffraction 157

SUMMARY 162

LIST OF REFERENCES 169

LIST OF TABLES

Table		Page
1	Chemical analysis for FeOCl and the $FeOCl(O)_x(S)_y$ compounds where O = organosulfur and S = solvent	20
2	Chemical analysis for two samples of FeOCl whose variable temperature magnetic susceptibility is shown in Figure 7	27
3	Kinetic data for FeOCl + TTF(0.24 M in dimethoxyethane)	32
4	Chemical analysis for $FeOCl(TMTTF)_x$ prepared under different reaction conditions	34
5	Calculated and observed X-ray powder diffraction data for FeOCl (Cu $K\alpha_1$ = 1.54056 A using silicon as an internal standard)	40
6	X-ray powder diffraction data for $FeOCl(TTF)_{1/9}(tol)_{1/21}$, Co $K\alpha$ = 1.7902 A	41
7	X-ray powder diffraction data for the intercalates showing the calculated and observed d-spacings for the cell parameters given	43
8	The distances and coordination numbers obtained from the EXAFS analysis for FeOCl and the intercalates	65
9	Debye-Waller factors (A^2) obtained from the best fit to the experimental data using theoretical functions	66
10	Cell parameters, final positional, and thermal parameters for FeOCl at 300 and 10 K	77
11	Cell constants and figures of merit obtained for twenty reflections from neutron powder diffraction data for $FeOCl(TTF)_{1/8.5}$	82
12	Observed and calculated d-spacings (A) of the neutron powder diffraction spectra for $FeOCl(TTF)_{1/8.5}$ with the proposed indexing scheme: a = 3.7836(4) Å, b = 25.9629(3) A and c = 3.3410(4) A	83

Table		Page
13	Atomic positions refined for $FeOCl(TTF)_{1/8.5}$ including carbons, space group = Immm (data set length 3.80 - 1.0 Å, R = 7.2%)	89
14	Definitions of the abbreviations used in the parameter listing for the NMR spectra	100
15	Linewidths and relative areas of the single pulse ^1H spectrum of TTF	103
16	Linewidths and relative areas of the Θ_0-τ-Θ_{90} ^1H spectrum of TTF	105
17	Linewidths and relative area of echo ^1H spectra for $FeOCl(TTF)_{1/8.5}$	111
18	Position of the $a_g\nu_3$ band observed in the Raman data with the values for the charge transfer	135
19	Infrared spectral features of $FeOCl(TTF)_{1/8.5}$ and the TTF infrared absorptions of TTF(CA), (ss)	137
20	Infrared spectral features of $FeOCl(d_4\text{-TTF})_{1/9}$ and the d_4-TTF infrared absorptions of d_4-TTF(CA), (ss)	138
21	Infrared spectral features for $FeOCl(TMTTF)_{1/13}$ and the TMTTF infrared absorptions of $(TMTTF)_2X^1$ (X^1 = BF_4^-, ClO_4^-, and PF_6^-)	140
22	Infrared spectral features for $FeOCl(TTT)_{1/9}(tol)_{1/23}$ and the infrared absorptions of TTT(X), X = Cl^-, Br^-, and SCN^- and $TTT^\bullet$	142
23	Infrared spectral features for $FeOCl(TTN)_{1/9}(tol)_{1/21}$ and the infrared absorptions of $TTN^\bullet$	143
24	Two-probe pressed powder conductivity measurements for FeOCl and the intercalates	151
25	Effective moments calculated for high spin Fe^{+3}, FeOCl, and the intercalates 300 K using spin-only formula	156

LIST OF FIGURES

Figure		Page
1	The structure of TTF-TCNQ showing the segregated stacking of the TTF (donor) and TCNQ (acceptor) molecules	3
2	A representation of the structure of $(TMTSF)_2X$ showing the electronic density of the anion ($X = PF_6^-$)	4
3	A view of two layers of the FeOCl structure	7
4	An illustration of the expansion of the TaS_2 layers upon intercalation of octadecylamine	8
5	Schematic drawings of the organosulfur molecules intercalated into FeOCl	11
6	An illustration of the reaction flask used for intercalation	22
7	Molar susceptibility vs temperature (K) for two preparations of FeOCl (see Table 2)	28
8	A schematic of FeOCl showing four unit cells	39
9	X-ray powder diffraction data plotted as intensity vs 2θ for (a) FeOCl, (b) $FeOCl(TTF)_{1/9}(tol)_{1/21}$, (c) $FeOCl(TTN)_{1/9}(tol)_{1/23}$ and (d) $FeOCl(TTT)_{1/7}$	47
10	(a) Fe K-edge transmission X-ray absorption spectrum and (b) the background subtracted Fe EXAFS data of FeOCl	50
11	(a) Fe K-edge transmission X-ray absorption spectrum and (b) the background subtracted Fe EXAFS data of $FeOCl(TTF)_{1/8.5}$	51
12	(a) Fe K-edge transmission X-ray absorption spectrum and (b) the background subtracted Fe EXAFS data of $FeOCl(TMTTF)_{1/13}$	52
13	(a) Fe K-edge transmission X-ray absorption spectrum and (b) the background subtracted Fe EXAFS data of $FeOCl(TTN)_{1/9}(tol)_{1/23}$	53

Figure		Page
14	(a) Fe K-edge transmission X-ray absorption spectrum and (b) the background subtracted Fe EXAFS data of $FeOCl(TTT)_{1/7}$	54
15	Fourier transforms of the Fe K-edge transmission EXAFS $k^3\chi(k)$ vs r for (a) FeOCl, (b) $FeOCl(TTF)_{1/8.5}$ and (c) $FeOCl(TMTTF)_{1/13}$	57
16	Fourier transforms of the Fe K-edge transmission EXAFS $k^3\chi(k)$ vs r for (a) $FeOCl(TTT)_{1/7}$ and (b) $FeOCl(py)_{1/3.6}$	58
17	Comparison of the Fourier transforms of the Fe K-edge transmission EXAFS $k^3\chi(k)$ vs r for FeOCl (solid curve) and $FeOCl(TTN)_{1/9}(tol)_{1/22}$ (dotted curve) with peak assignments	59
18	(a) ΔE vs Δr for Fe--Fe nonbonded near neighbors and (b) B vs σ for FeOCl, $FeOCl(TTF)_{1/9}(tol)_{1/21}$, $FeOCl(TTN)_{1/9}(tol)_{1/22}$ and for $FeOCl(TTT)_{1/7}$	62
19	(a) ΔE vs Δr for Fe--Fe (c-axis) and (b) B vs σ for FeOCl, $FeOCl(TTF)_{1/9}(tol)_{1/21}$, $FeOCl(TTN)_{1/9}(tol)_{1/22}$ and $FeOCl(TTT)_{1/7}$	63
20	(a) ΔE vs Δr for Fe--Fe (a-axis) and (b) B vs σ for FeOCl, $FeOCl(TTF)_{1/9}(tol)_{1/21}$, $FeOCl(TTN)_{1/9}(tol)_{1/22}$ and $FeOCl(TTT)_{1/7}$	64
21	Schematic representation of the orientation of the (top) TTF (bottom) TTT, TTN molecules predicted by the hard sphere model	70
22	Geometrical basis for equations 6-12 for TTF orientation based on the hard sphere model	71
23	Geometrical basis for equations 13-15 for the TTN and TTT orientation based on the hard sphere model	73
24	Nuclear scattering (barns) vs atomic weight	75

Figure Page

25 Profile refinement of the 150° TOF detector bank data for FeOCl at 300 K showing the low d region. The observed data are indicated by points and the calculated results by a solid line. Marks directly beneath the pattern indicate the positions of reflections. A difference curve appears at the bottom 78

26 Profile refinement of the 150° TOF detector bank data for FeOCl at 10 K showing the low d region. The observed data are indicated by points and the calculated results by a solid line. Marks directly beneath the pattern indicate the positions of reflections. A difference curve appears at the bottom 79

27 Graph of sigma vs d including error bars obtained from the fit of $FeOCl(TTF)_{1/8.5}$ and Si at 300 K 81

28 Profile refinement of the 90° bank for $FeOCl(TTF)_{1/8.5}$ using only Fe, O, Cl in the refinement (low d region). The observed data are indicated by points, and the calculated results by a solid line. Marks directly beneath the pattern indicate the positions of reflections. A difference curve appears at the bottom 85

29 Profile refinement of the 90° bank for $FeOCl(TTF)_{1/8.5}$ including carbons (low d region). The observed data are indicated by points, and the calculated results by a solid line. Marks directly beneath the pattern indicate the positions of reflections. A difference curve appears at the bottom 86

30 Profile refinement of 90° bank for $FeOCl(TTF)_{1/8.5}$ including data to 1.0 Å. The observed data are indicated by points, and the calculated results by a solid line. Marks directly beneath the pattern indicate the positions of reflections. A difference curve appears at the bottom 88

31 Illustration of the lateral shift of the chloride ion layers of FeOCl upon intercalation 91

Figure		Page
32	Schematic representation of the possible orientation of TTF taking into account the lateral shift of the layers for both a (a) soft and (b) hard sphere model	92
33	Schematic representation of the orientation of TTN and TTT taking into account the lateral shift of the FeOCl layers	94
34	Illustration of the TTF molecule on the bc plane showing the number of cells the molecule spans	95
35	(a) FT ^1H NMR of TTF obtained from a single pulse radio frequency, (b) Expanded scale (Table 14 defines the abbreviations used in the parameter listing)	99
36	The ^1H FT NMR spectrum obtained for TTF (a) after removing the first 100 μs of the FID, (b) by subtraction of (a) from the full FT NMR spectrum of TTF	102
37	^1H FT NMR spectrum for TTF obtained by employing a Θ_0-τ-Θ_{90} pulse sequence	104
38	^1H FT NMR spectrum obtained for TTF by a Θ_0-τ-Θ_0 pulse	106
39	^1H FT NMR spectrum obtained for $FeOCl(TTF)_{1/8.5}$ obtained by a single radio frequency pulse	107
40	^1H FT NMR spectrum for $FeOCl(TIF)_{1/8.5}$ obtained by a Θ_0-τ-Θ_{90} pulse sequence	108
41	^1H FT NMR spectrum for $FeOCl(TTF)_{1/8.5}$ obtained Θ_0-τ-Θ_0 pulse sequence	109
42	^1H FT NMR using the same parameters as those shown in Figure 37, drawn to the same scale as Figures 43 and 44	113
43	(a and b) ^1H FT NMR for $FeOCl(TTF)_{1/8.5}$ hole burning experiments using a field strength of 145 Hz. Arrows indicate location of preirradiation	114

Figure		Page
44	(a and b) ^{1}H FT NMR for $FeOCl(TTF)_{1/8.5}$ hole burning experiments using a field strength of 43 Hz. Arrows indicate location of preirradiation	115
45	(a) ^{1}H-coupled-^{13}C FT NMR spectrum of TTF in $CDCl_3$, (b) The expanded scale showing the peaks corresponding to TTF	117
46	^{13}C CPMAS spectrum for TTF	118
47	^{13}C CPMAS spectrum for $TTF_3Br_2 \cdot H_2O$	120
48	^{13}C CPMAS spectrum for TTF(CA) (ss)	121
49	^{13}C CPMAS spectrum for TTF(CA) (ms)	122
50	A schematic representation of a quadrupolar powder pattern resulting from a sterically rigid C-D bond	125
51	^{2}H FT NMR of d_4-TTF obtained from a single 90° pulse	126
52	The ^{2}H quadrupole echo spectrum for $FeOCl(d_4\text{-TTF})_{1/9}$	128
53	The ^{2}H quadrupolar-dipolar echo spectrum for $FeOCl(d_4\text{-TTF})_{1/9}$	129
54	Infrared spectra of FeOCl and $FeOCl(TTF)_{1/8.5}$ with assignments. Values for TTF(CA) are in parenthesis	133
55	The infrared spectrum for $FeOCl(d_4\text{-TTF})$ with assignments. Values for d_4-TTF(CA) are in parenthesis	139
56	Optical spectra of (flurolube mulls between NaCl plates) for FeOCl(---), $FeOCl(TTF)_{1/8.5}$ (——), and TTF(CA)(ss)(•••••). The baseline is indicated also (--•••--). Absorption is an arbitrary scale	145
57	Optical spectra (flurolube mulls between NaCl plates) for FeOCl(-•••••-), $FeOCl(TMTTF)_{1/13}$(——), $FeOCl(TTN)_{1/9}(tol)_{1/21}$(•••••) and $FeOCl(TTT)_{1/9}(tol)_{1/23}$ (---). Absorption is an arbitrary scale	146

Figure		Page
58	$\ell n\rho$ vs 1/T for two probe pressed powder conductivity measurements	150
59	The Fe K-edge X-ray absorption edge spectrum for (a) FeOCl and various materials (b) and FeOCl and $FeOCl(TTF)_{1/8.5}$	152
60	χ molar vs T for FeOCl, $FeOCl(TMTTF)_{1/13}$ and $FeOCl(TTF)_{1/8.5}$ with lines drawn through the points	154
61	χ molar vs T for FeOCl, $FeOCl(TTN)_{1/9}(tol)_{1/21}$ and $FeOCl(TTT)_{1/9}(tol)_{1/23}$ with lines drawn through the points	155
62	Neutron powder diffraction for FeOCl 300 K (top) and 10 K (bottom) data	158
63	Magnetic lattice for FeOCl (8 unit cells) showing the direction of spins proposed by Adam and Buisson	159
64	Neutron powder diffraction for $FeOCl(TTF)_{1/8.5}$, 300 K (top) and 10 K (bottom) data	161

SUMMARY OF ABBREVIATIONS

4-AP:	4-aminopyridine
BFBT:	Best Fit Based on Theory
CA:	chloranil
CHESS:	Cornell High Energy Synchrotron Source
Cl_4TTN:	tetrachloroTTN
DBTTF:	dibenzoTTF
DME:	dimethoxyethane
DMTSF/DETSF:	dimethyl/diethyltetraselenofulvalene
DTT:	dithiotetracene
MeCN:	acetonitrile
EXAFS:	Extended X-ray Absorption Fine Structure
FABM:	Fine Adjustment Based on Models
GPPD:	General Purpose Powder Diffractometer
ILL:	Institute Laue Langevin
IPNS:	Intense Pulsed Neutron Source
py:	pyridine
TMTSF:	tetramethyltetraselenofulvalene
TOF:	Time of flight
TTF:	tetrathiafulvalene
TMTTF:	tetramethylTTF
TTN:	tetrathianaphthalene
TTT:	tetrathiatetracene
TCNQ:	tetracyano-p-quinodimethane
tol:	toluene
XANES	X-ray Absorption Near Edge Structure

INTRODUCTION

The traditional view that solid-state systems are an area of interest primarily to physicists has changed rapidly within the past twenty years. Chemists are actively investigating the synthesis and properties of solid-state low-dimensional conductive materials.[1-5] The activity in this field was initially stimulated by the hypothesis that a one-dimensional organic compound could be designed that would exhibit room temperature superconductivity.[6,7] Further stimulus was provided by the discovery of systems with high electrical conductivity (comparable to that of conductors such as copper) along one or more axes. These compounds have potential uses as antistatic coatings, as electronic and optical devices, as lightweight batteries, and as superconductors.

There are basically three categories of well-studied low-dimensional conducting materials: (1) those containing linear polymers; (2) those containing linear chains of transition metals; and (3) those containing stacks of donor and acceptor molecules. Compounds such as $K_2[Pt(CN)_4]0.3Br \cdot 3H_2O$ (Krogmann's salt) fall into the first category; in these materials, it is the overlap of the transition metal d-orbitals that provides a pathway for electrical conduction.[8] In the case of linear polymers such as $(SN)_x$ and $(CH)_xX_y$ (doped polyacetylene), electrons can travel both along and between the chains

of atoms.[9,10] Doping of the polymeric metal phthalocyanines $(MPcX)_n$ (where M = Al, Ga, Cr, Si, Ge, Sn and Co, Pc = phthalocyanine, and X = F, O, S and CN)[11-13] by iodine causes these materials to become highly conducting; the conductivity is attributed to the stacking arrangement of the phthalocyanine ligand as well as to partial charge transfer from the iodine to the macrocycle.[14] TTF-TCNQ (tetrathiafulvalene-tetracyanoquinodimethane) is the prototypical member of the last category. The high conductivity of this compound is due to the presence of segregated stacks of donor (TTF) and acceptor (TCNQ) molecules (Figure 1) and to the occurrence of partial charge transfer between the two.[15] Compounds of this general type that crystallize as mixed stacks are usually insulators.[16] Although a great deal of interest in organic metals has stemmed from their technological potential, their use in industry has been limited due to the fragility of the crystals as well as to the difficulties in synthesis.

Synthetic strategies under investigation in other laboratories include the use of selenium and tellurium analogues of organic donors, more complex π systems, a variety of inorganic anions, and electrochemical synthesis. All of these strategies have had some success. The use of the selenium analog of the organic electron donor molecule, TMTTF (tetramethyl-TTF), provided the first organic superconductor at ambient pressure, $(TMTSF)_2ClO_4$ (TMTSF=tetramethyltetraselenofulvalene, see Figure 2).[17] The critical temperature for this compound is 1.3 K.[18] When the anion is replaced by other anions $(TMTSF)_2X$ ($X = PF_6^-$, AsF_6^-, SbF_6^-, BF_4^- and NO_3^-), the material undergoes a superconducting

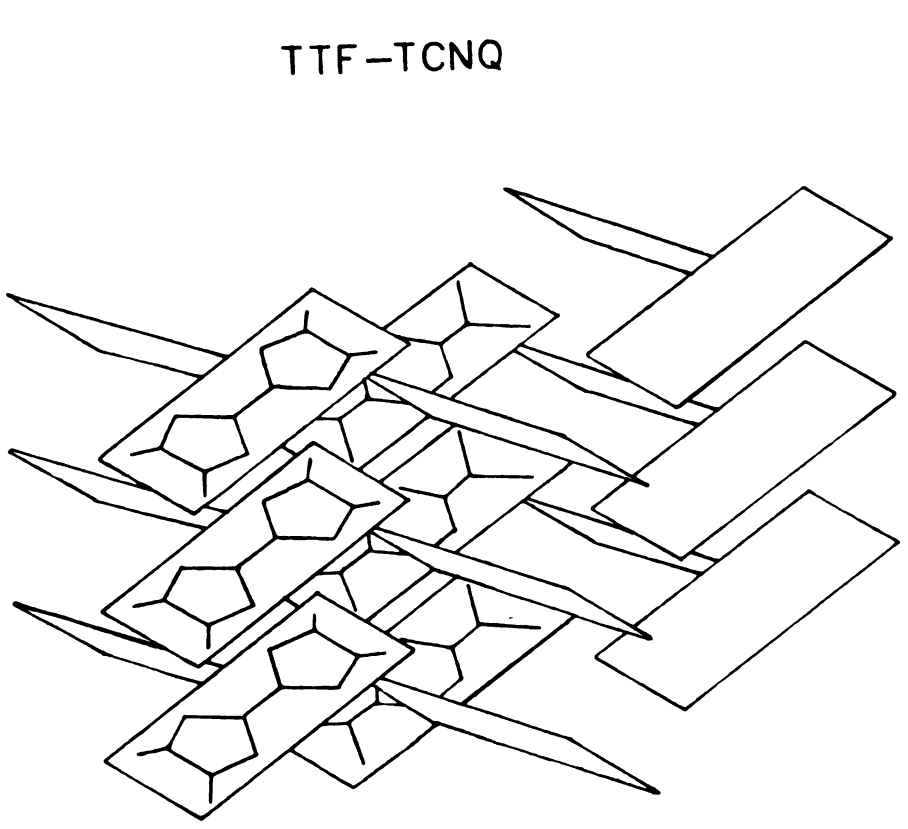

Figure 1. The structure of TTF-TCNQ showing the segregated stacking of the TTF (donor) and TCNQ (acceptor) molecules

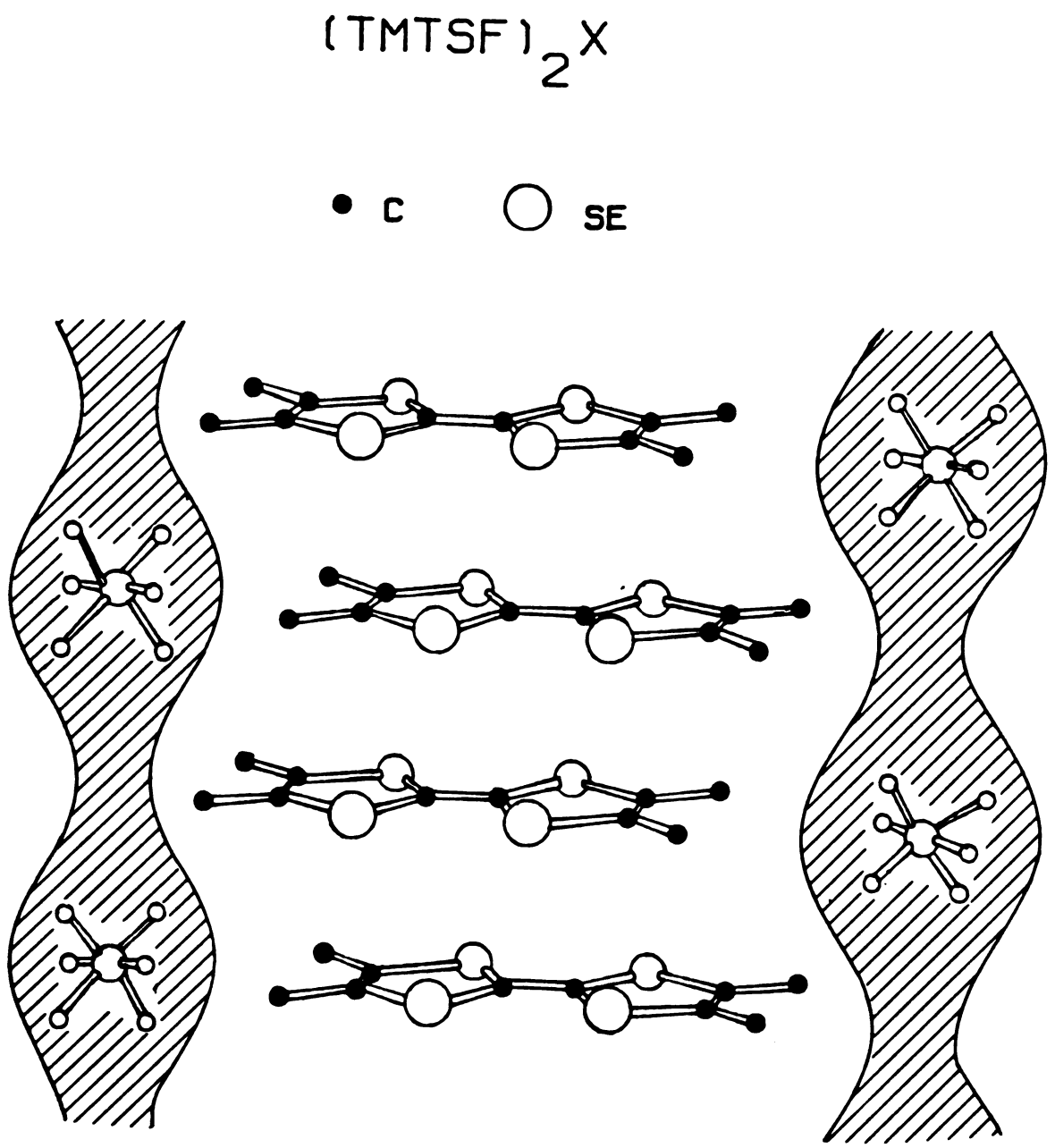

Figure 2. A representation of the structure of $(TMTSF)_2X$ showing the electronic density of the anion ($X = PF_6^-$)

transition only under high pressures.[19] The most recent addition to the class of organic superconductors is a triiodide salt of bis(ethylenedithiolo)tetrathiafulvalene (BEDT-TTF, referred to as "ET"), which is superconducting at 1.5 K at ambient pressure.[20] The selenium-selenium or sulfur-sulfur interactions between the stacks of either the TMTSF or ET charge transfer salt are important in determining whether the material will conduct and undergo a superconducting transition. The ET charge transfer compounds lack the columnar stacking that is the most prominent feature in $(TMTSF)_2X$ and other organic metals.[20] It appears to form a two-dimensional network in which the interstack S-S contact distances are less than the sum of the van der Waals radii (3.6 A). Thus, the primary S-S interactions are between the loosely connected zig-zag stacks, not within a stack as in the case for $(TMTSF)_2X$.[20] In order to maximize the S-S, or for TMTSF, the Se-Se overlap and thus superconductivity, fine tuning the structure of these compounds by varying the anions of these structural types is currently being pursued by a number of groups.[20-22]

In addition to the structural constraints outlined above, a further criterion is that the electron donor (or acceptor) molecules achieve a nonintegral oxidation state in the material.[2,4,23,24] This is essential to provide a partially filled valence band and low energy for charge transport through the material.[4,16,23-26] The combination of these two requirements, overlapping S-S or Se-Se interactions and partial charge transfer, significantly restricts the number of highly conductive materials. Although the $(ET)I_3$ compound is superconducting, the reaction procedure results in more than one phase, of which only one is superconducting.[20]

A desire to enforce the formation of segregated stacks of cations led to the consideration of intercalation chemistry as a general route to new low-dimensional materials. Intercalation, in its simplest conception, can be viewed as the insertion of a species into a layered matrix by expanding one axis and preserving the identity of both the guest and host species.[27] A variety of transition metal compounds are known to exhibit a lamellar structure in which layers containing metal atoms lie between parallel layers of chalcogen or halogen atoms.[28-31] Examples are the Group IVB, VB and VIB transition metal dichalcogenides (e.g., TaS_2, ZrS_2, $NbSe_2$, MoS_2), the transition metal oxyhalides (e.g., FeOCl, VOCl), and the transition metal phosphorus trisulfides (e.g., $MnPS_3$, $FePS_3$); the structure of FeOCl is shown in Figure 3. In all cases the layers are held together by weak van der Waals interactions, which accounts for the fact that small molecules can be easily intercalated (or inserted) into these solids.[27,29-32] The expansion of the layers of TaS_2 by 51 Å upon intercalation of octadecylamine is shown in Figure 4. This is rather an extreme example, but it illustrates the fact that preferred orientation of a guest molecule within the host layers can be achieved while preserving the identity of both.[33]

One of the important questions in intercalation chemistry is the orientation of the intercalant with respect to the host layers. Although in most cases direct structural evidence is lacking, for NbS_2[34] and TaS_2[35] intercalated by deuteropyridine, neutron diffraction studies have shown that the pyridine is oriented perpendicular to the layers, with the lone pair electrons on the nitrogen atom directed

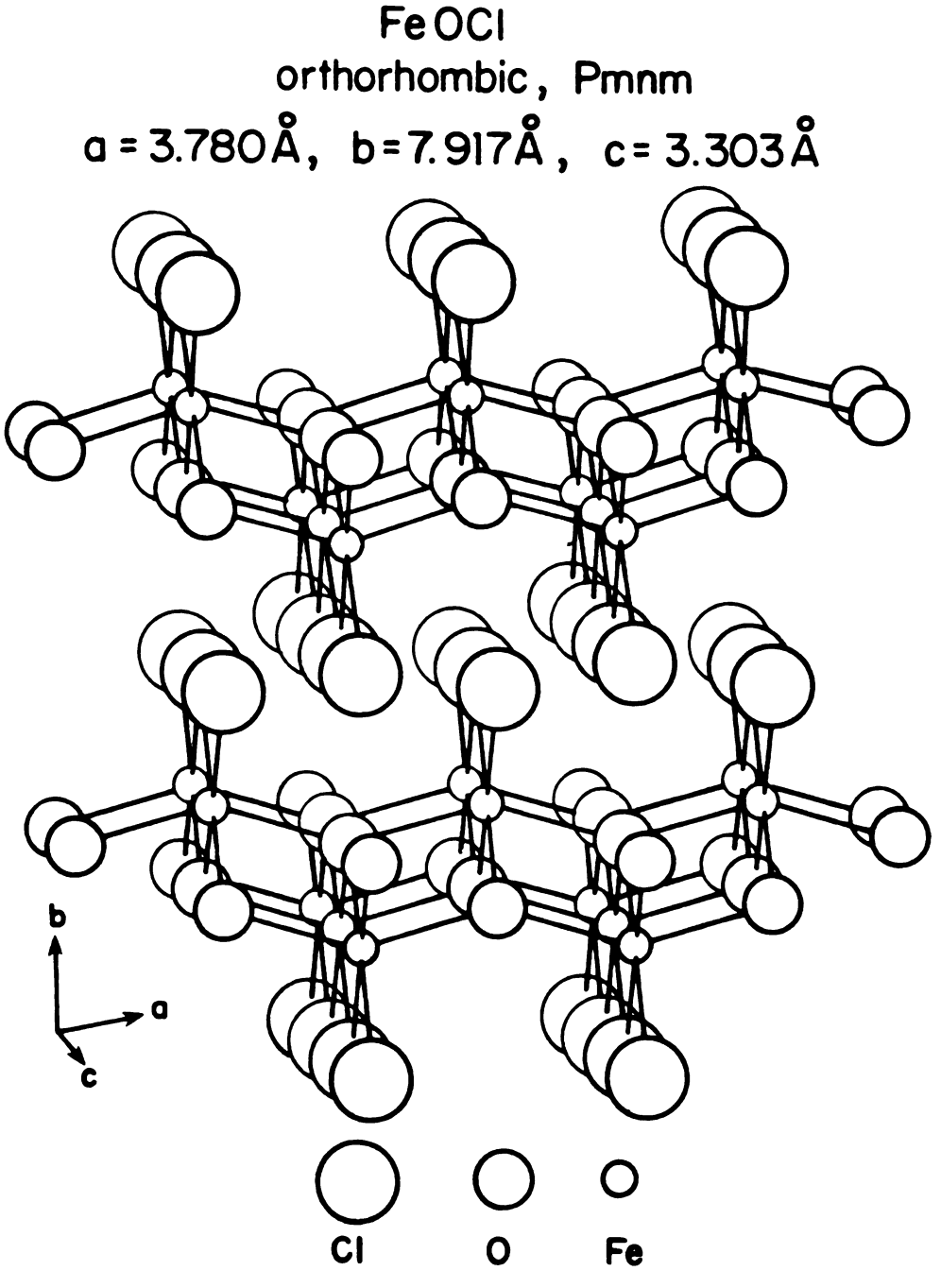

Figure 3. A view of two layers of the FeOCl structure

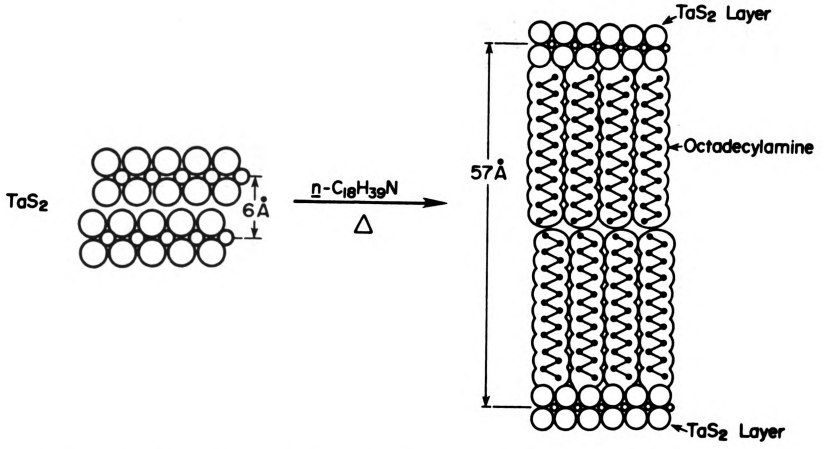

Figure 4. An illustration of the expansion of the TaS_2 layers upon intercalation of octadecylamine

parallel to the layers. A similar orientation has been proposed for pyridine intercalated into FeOCl.[36] Studies on the cobaltocene intercalant of both TaS_2,[37,38] and FeOCl[39] are consistent with an orientation similar to that of pyridine; the molecule appears to be oriented with the C_5 axis parallel to the layers.

Replacing the anions in $(TMTSF)_2X$ (Figure 2) with a layered material such as FeOCl provides visual evidence that a synthetic route to low-dimensional conductors might be successful. The use of a layered material can enforce the stacking of organic electron donors that have the potential to stack similarly to the pyridine or cobaltocene molecules. Since intercalation compounds generally adopt stoichiometries approximating close packing of the intercalant molecules, the resulting orbital overlap should allow facile charge transfer between adjacent molecules. Partial charge transfer from the guest to the host layers should result in a highly conducting material. Although the band structure for the metal oxyhalides has not been determined, a chemical analogy can be proposed. Thus, FeOCl, in which the Fe^{+3} is relatively easy to reduce, is expected to be most susceptible to intercalation by electron donors (such as TTF). Metal oxyhalides such as VOCl and TiOCl, in which the metal is relatively easy to oxidize, may be most easily intercalated by oxidants (such as TCNQ). A wide variety of polar organic compounds[40] as well as organometallic species[30,41-43] are known to intercalate into FeOCl, resulting in a significant expansion of the interlayer distance and increased conductivity (10^3-10^4) over that of FeOCl ($\sigma_{RT} = 10^{-7}$ $(ohms\text{-}cm)^{-1}$).

As discussed herein, the intercalation chemistry of FeOCl has been expanded to include TTF and the other tetrathiolene molecules shown in Figure 5. The following new phases have been obtained: $FeOCl(TTF)_{1/8.5}$, $FeOCl(TMTTF)_{1/13}$, $FeOCl(TTN)_{1/9}(tol)_{1/22}$, (TTN = tetrathianaphthalene), and $FeOCl(TTT)_{1/9}(tol)_{1/23}$, (TTT = tetrathiatetracene). A number of physical techniques were used to obtain information on the properties of these materials. The techniques included X-ray powder diffraction, EXAFS (Extended X-ray Absorption Fine Structure) spectroscopy, infrared and optical spectroscopy, variable temperature magnetic susceptibility and conductivity studies on all the intercalates. In addition, detailed neutron powder diffraction and wideline ^1H and ^2H NMR studies were performed on the $FeOCl(TTF)_{1/8.5}$ and $FeOCl(d_4\text{-}TTF)_{1/9}$ compounds, which could be easily synthesized in large amounts and appeared to be highly crystalline. EXAFS and X-ray powder diffraction provide information on the short and long range order, respectively, of the host. Neutron powder diffraction and NMR provide information on the static and dynamic ordering, respectively, of the guest species. Electronic information was obtained by infrared and optical spectroscopy as well as from conductivity measurements. The magnetic studies help to ascertain the changes in the host lattice that occur upon intercalation. All these techniques, taken together, have led to a better understanding of this system and has provided some insight on the details of the reactions and the resulting properties of the intercalates. The synthesis and characterization of these new materials will be discussed and evaluated as a route towards low dimensional conductors.

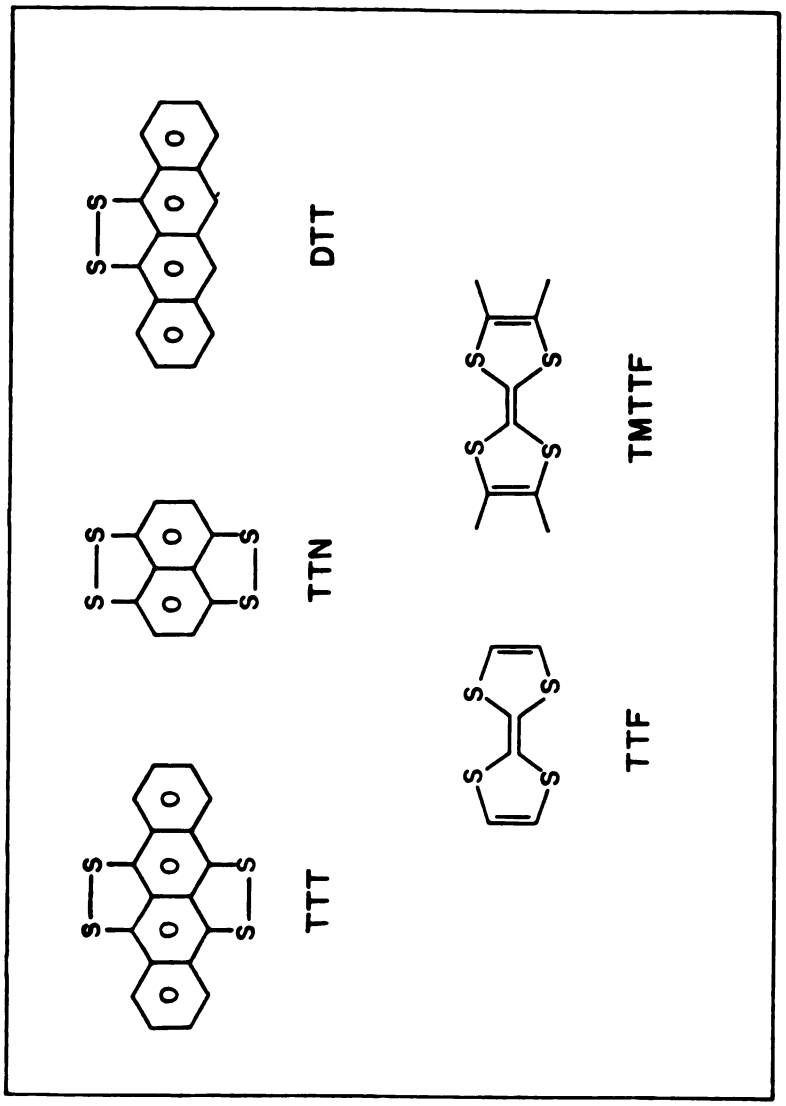

Figure 5. Schematic drawings of the organosulfur molecules intercalated into FeOCl

EXPERIMENTAL

Materials and Methods

Preparation of all intercalates was performed under an inert atmosphere of argon dried by passage through supported phosphorus pentoxide (Aquasorb). Solutions and solvents were degassed prior to use by repeated evacuation and flushing with dry argon. All other solvents were distilled once from appropriate drying agents, except acetone which was reagent or spectroscopic grade (Scientific Products).

TTF, obtained from Parish or Aldrich Chemical Co., was recrystallized once from cyclohexane/hexanes.[44] High purity TTF and TMTSF, obtained from Strem Chemical Co., were handled exclusively under inert atmosphere. TMTTF,[45] BDTTF,[46,47] TTF(CA),[48] VOCl,[49,50] and $TTF_3Br_2H_2O$[51] were prepared by published procedures. d_4-TTF was prepared by a literature method[52] substituting d_1-EtOH for d_1-MeOH. TTT, prepared by a published procedure,[53,54] was purified by Soxhlet extraction[55] and subsequently by ten to fifteen sublimations at 210°C at 10^{-2} torr. DTT was obtained as a blue side product in the sublimation.[54] High purity 2H-TaS_2 was a gift from F. J. DiSalvo of Bell Laboratories, Murray Hill, New Jersey. TTN and Cl_4TTN were gifts from B. K. Teo of Bell Laboratories, Murray Hill, New Jersey. Cl_4TTN was used without further purification, whereas TTN was purified by Soxhlet

extraction with benzene and recrystallized by addition of MeCN to the saturated benzene solution.[56] CA was purchased from Eastman (practical grade) and recrystallized once from toluene. 3-Bromo-2-butanone, stabilized with MgO, was purchased from Alfa Chemical Co. and distilled prior to use in the preparation of TMTTF. Peracetic acid (35%), P_4S_{10}(Gold Label), decalin, and perchloric acid (69-72%) were purchased from Aldrich Chemical Co., KSCOEt[57] was prepared by a published procedure and these materials used in the preparation of TMTTF. All other reagents used in the preparation of published compounds were common reagent grade and used without further purification. The identity of the prepared tetrathiolenes was verified by melting point, infrared spectroscopy and elemental analysis.

Solution electronic spectra were recorded on a Cary 219 spectrophotometer. Solid state spectra of Fluorolube mulls between NaCl or quartz plates were recorded on a Cary 17DI spectrophotometer at the University of Virginia. Infrared spectra were obtained on a Perkin-Elmer Model 1430 grating spectrophotometer at the University of Virginia, using KBr pellets (Harshaw Chemical Co., Solon, Ohio; stabilized infrared quality).

Proton, deuterium and carbon-13 NMR spectra of TTF, d_4-TTF, $FeOCl(TTF)_{1/8.5}$, and $FeOCl(d_4\text{-}TTF)_{1/9}$ were recorded by J. Ellena on a Nicolet NT-360 spectrometer at the University of Virginia. Digitization rates of up to 2 MHz were achieved with a Nicolet 2090 digital oscilloscope. All spectra were obtained at 20 ± 2°C, chemical shifts are reported relative to TMS ($(CH_3)_4Si$). Proton spectra (361 MHz) were recorded with a standard Nicolet transmitter and probe. The

NT-360 was equipped with a Henry Radio Tempo 2006 amplifier and home-build probe for deuterium operation at 55.4 MHz. The 90° pulse width was 5 microseconds. Solution carbon-13 spectra were recorded at 90.8 MHz. Proton-carbon-13 cross polarization and magic angle spinning were used to obtain carbon-13 spectra of solids at 37.7 MHz on a Nicolet NT-150 at the Colorado State University Regional NMR Center by J. Frye. In all experiments the delay time between data acquisition and the following pulse was adjusted so that an increase in delay time had no effect on the spectral lineshapes. Standard cyclops[58,59] phase cycling and data routing for echo experiments was the same as that described by Bloom et al.[60] and Griffin.[61] During echo experiments data acquisition was begun before the top of the echo and points collected prior to the echo peak were removed before Fourier transformation. The only spectra phase correction necessary for echo spectra was that required to correct for misalignment of the transmitter and receiver phases (no first order phase correction was used). Flipback pulses[62] were used to accelerate data acquisition in CPMAS experiments.

Temperature dependent magnetic susceptibilities were measured from 5-300 K on all samples at Michigan State University on a SHE Corp. SQUID susceptometer. The samples were run in a Delrin bucket able to hold approximately 50 mg of material. The empty bucket was run separately before each sample and the data were fit using KINFIT4, a nonlinear least-squares fitting program available at Michigan State. Selected samples were run and analyzed at the University of Virginia on a similar instrument by D. Holtman.

Temperature dependent two-probe powder conductivity measurements were taken with an apparatus (described elsewhere[63]) at Michigan State University in Professor J. L. Dye's laboratory. Constant voltage was supplied by a Heathkit Regulated Low Voltage Power Supply and the current measured by a 610 BR Keithley electrometer. All samples measured obeyed Ohm's law. Typical data acquisition of points from 25 to -60°C, cycled once, took twelve to sixteen hours. The current was measured every two degrees, and the temperature was measured by a thermocouple situated inside the cryostat cavity. Additional four- and two-probe single crystal conductivity measurements were obtained with the help of John Papioannou, a research associate in Professor Dye's laboratory. A two-probe conductivity cell, modeled on the same design as that used in Professor Dye's laboratory, was constructed at the University of Virginia. All measurements were conducted at room temperature. The samples were 3-4 mm long and were held in a 2 mm diameter precision bore Pyrex cell. The sample could be pressed to a maximum pressure of ca. 800 Pa. The constant voltage source was a home-made D.C. power source capable of supplying 1.3 to 24 volts. The current was measured by a Keithley Model 600 electrometer or a Model 177 microvolt digital multimeter.

X-ray diffraction data were recorded on a General Electric powder diffractometer with either Cu or Co Kα radiation using Pt powder (Aldrich 99.999% pure) as an internal standard. High precision data were obtained on a Huber Model 621 powder camera by asymmetric transmission and back-reflection using Cu Kα_1 radiation and silicon (Hipure, Spex Industries, Metuchen, New Jersey) as a standard at the

University of Virginia Materials Science Department X-Ray Laboratory. At Michigan State University, X-ray powder diffraction data were obtained on a small radius Guinier powder camera in Professor H. Eick's laboratory or on a Siemens powder diffractometer in Professor T. Pinnavia's laboratory using Cu Kα radiation. Film from the Huber powder camera was measured on a Huber Model 622 film reader capable of ±0.01 degrees accuracy. Lattice parameters were verified by using an X-ray program based on the relationship of spacing to reciprocal cell edges,[64] written by D. Holtman for a HP-87 minicomputer (Department of Chemistry, University of Virginia). Single crystal diffraction photographs were obtained at the University of Virginia on a precession camera.

EXAFS (Extended X-Ray Absorption Fine Structure) and XANES (X-Ray Absorption Near Edge Structure) spectra were obtained at CHESS (Cornell High Energy Synchrotron Source) using experimental stations C-1 and C-2. Spectra were obtained on four different occasions on the same and different sample preparations to ensure reproducibility. The samples were diluted with boron nitride in a glove bag under nitrogen atmosphere, pressed into homogeneous pellets in aluminum cells (3x19 mm), and sealed with 1-mil Kapton tape. The sample concentration was adjusted to obtain a value of $\mu\chi = 1$ in order to minimize thickness effects. All the data were taken in the parasitic mode with the electron storage ring operating at an average current of 10 mA and at energies of 4.7 or 5.0 GeV. All spectra were taken with a beam width of 15 mm and resolution of 1-2 eV. The monochromator was detuned by 50% to avoid contributions from higher harmonics. Typical spectra

of the Fe K-edge took 15-20 minutes and were taken in four regions during the energy scan in order to obtain constant k steps ($Å^{-1}$). The spectra of the compounds were taken by transmission where the incident and transmitted beam intensities were measured by ionization chambers at 8 and 30 cm in length, respectively, and filled with nitrogen (flow type). The spectra were analyzed at Bell Laboratories, Murray Hill, New Jersey in collaboration with B. K. Teo, using programs described elsewhere,[65] which were adapted to run on a DEC PDP Model 11/45 minicomputer.

Neutron powder diffraction data were collected and analyzed at Argonne National Laboratory at the Intense Pulsed Neutron Source (IPNS) in collaboration with J. Faber, Jr. The samples (FeOCl, $FeOCl(TTF)_{1/8.5}$, and $FeOCl(d_4\text{-}TTF)_{1/9}$), were run at room temperature and 10 K in a vanadium cell placed in a displex unit on the General Purpose Powder Diffractometer (GPPD). The structure was refined using Rietveld profile analysis program.[66] Initial values of the unit cell parameters for the intercalates were determined from X-ray powder diffraction data. For FeOCl, initial atomic positions were taken from single crystal X-ray work.[67] The FeOCl structure was refined satisfactorily using 21 parameters in the final refinement (2θ zero, background, half width parameter, lattice parameters, an asymmetry parameter, a scale factor, and an anisotropic parameter). The structures of $FeOCl(TTF)_{1/8.5}$ and $FeOCl(d_4\text{-}TTF)_{1/9}$ were refined using only Fe, O and Cl atoms over a limited data range (1.359 - 3.797 Å). Initial atomic positions were calculated from an idealized model[39] using Immm or I222 as a space group. It was found that I222 with 2

Fe, 2 O and 2 Cl atoms gave the best weighted profile R: R = 8.773% ($R_{expected}$ = 1.997%). A Fourier difference map showed significant density between the layers; it was necessary to include a representation of the intercalated TTF molecule. Upon inclusion of the carbon atoms of TTF a much larger data range could be fit (occupational parameters of the carbons were allowed to vary).

Mass spectra were obtained as a service at either Michigan State University by E. Oliver or at the University of Virginia by E. K. Johnson on a Finnegan MAT, Model 4600 GC/MS. Elemental analyses were performed by Galbraith Laboratories, Inc., Knoxville, Tennessee.

Preparation of FeOCl

The overall reaction scheme is shown below. The two methods used

$$\alpha\text{-}Fe_2O_3 + 4/3\ FeCl_3 \longrightarrow 3\ FeOCl$$

are as follows.

Method A. α-Fe_2O_3 (Baker Chemicals) was dried overnight under vacuum over $CaSO_4$ at 120°C. The Pyrex reaction tube (ℓ = 14.5 cm, id = 1.5 cm and V = 25.62 cc) was cleaned with ethanolic KOH overnight, rinsed with 6N HCl, then 95% EtOH, and dried in an oven at 110°C overnight. In a drybox, the reaction tube was charged with 4.22 gm of α-Fe_2O_3 and 5.18 gm anhydrous $FeCl_3$ (Aldrich). The tube was sealed under dynamic vacuum (10^{-2} torr) and the contents mixed well by a vortex stirrer. The tube was placed in a Lindberg one-zone furnace at 350°C with the empty end of the tube outside the heating coils in order to produce a temperature gradient. After one week, the reaction tube was allowed to cool to room temperature inside the furnace. Large red-violet crystals were deposited at the cool end and

microcrystalline powder was deposited about half way down the tube. In addition, green $FeCl_3$ crystals were formed at the cool end in some preparations. The reaction tube was opened in air, the crystals separated and washed on a coarse glass frit with reagent grade acetone to remove $FeCl_3$. In addition, the frit allowed any unreacted α-Fe_2O_3 to be removed by acting as a sieve. The solid typically was washed with approximately 1-2 liters of acetone and dried over $CaSO_4$ under vacuum overnight. The yield was typically 95-100%.

Method B. α-Fe_2O_3 (52.70 gm) was dried overnight at 110°C and added to anhydrous $FeCl_3$ (71.38 gm). The reactants were transferred into a quartz tube (ℓ = 60 cm, id = 5 cm, V = 1.178×10^{-3} cc, cleaned in the same manner as Method A) in an argon atmosphere glove bag. The tube was evacuated for two hours and sealed under dynamic vacuum (10^{-2} torr). The tube was placed in a Lindberg three zone furnace and the temperature was raised to 370°C at the reactant end and 350°C at the other over a period of an hour. After one week the temperature was raised to 390°C at the reactant end and reduced to 310°C at the other. After another week, the tube was allowed to cool to room temperature inside the furnace. The yield was 99-100%. From the cool end, large crystals were obtained, and from the hot end, microcrystalline powder. The powder was washed on a medium glass frit with about 5 liters of reagent grade acetone, then with absolute EtOH (1 liter). The solid was placed in a vacuum oven at 110°C overnight, and subsequently in Schlenk tubes under argon. The elemental analysis is listed in Table 1.

Table 1. Chemical analysis for FeOCl and the $FeOCl(O)_x(S)_y$ compounds where O = organosulfur and S = solvent

	O	x	S	y	(calc) (obs) %C	%H	%Cl	%Fe	%S
FeOCl							33.04	52.05	
							32.47	52.33	
FeOCl	TTF	1/8.5		-	6.45	0.36	26.99	42.13	11.49
					6.53	0.70	26.07	42.13	11.42
FeOCl	TTF	1/11	tol	1/21	8.10	0.58	27.20	42.84	8.95
					7.47	0.91	27.10	42.46	8.12
FeOCl	TMTTF	1/13	-	-	7.26	0.73	27.85	43.87	7.75
					7.32	0.79	27.44	44.13	7.89
FeOCl	TTN	1/9.22	tol	1/22	12.15	0.58	25.53	40.22	10.02
					12.56	0.74	24.83	40.56	10.10
FeOCl	TTT	1/9.5	tol	1/23	17.78	0.87	23.88	37.61	9.09
					14.59	0.81	23.09	37.64	8.74
FeOCl	py	1/3.6	-	-	12.91	1.16	27.43	43.20	3.01[a]
					13.59	1.20	26.52	43.55	3.05

[a]Percent nitrogen.

General Preparation of Intercalates

FeOCl (100 mg) and the intercalant (100 mg) were weighed and transferred in a dry box to a Teflon stoppered reaction flask (Figure 6), which contained a teflon coated stir bar (10 x 4 mm). Approximately 15-25 ml of an appropriate solvent was added via cannula or anaerobic syringe to the reaction flask. The reaction mixture was degassed; the flask was evacuated and sealed via the Teflon stopcock. The flask was wrapped with aluminum foil to ensure uniform heating as well as protection from light (TTF is photosensitive). It was placed in an oil bath whose temperature was controlled by a variable resistor and had typical fluctuations of ±5°C. After a period of one to six weeks, the reaction flask was removed and the mixture transferred to an anaerobic glass frit under argon. The black microcrystalline solid was washed with freshly distilled solvent and subsequently with degassed reagent grade acetone. The solid was dried at room temperature for twelve hours under vacuum. Intercalation was verified by weight gain, X-ray powder diffraction, mass spectrometry, and elemental analysis.

Elemental analyses for the intercalates obtained are listed in Table 1.

$FeOCl(TTF)_x(toluene)_y$

25-30 ml of toluene was added to the FeOCl and TTF solids (mole ratio (2:1)) to produce a bright yellow solution. This reaction takes a minimum of one week at 70°C. The absorption peaks in the optical spectra of the acetone eluant could be assigned to TTF^+.[68] In

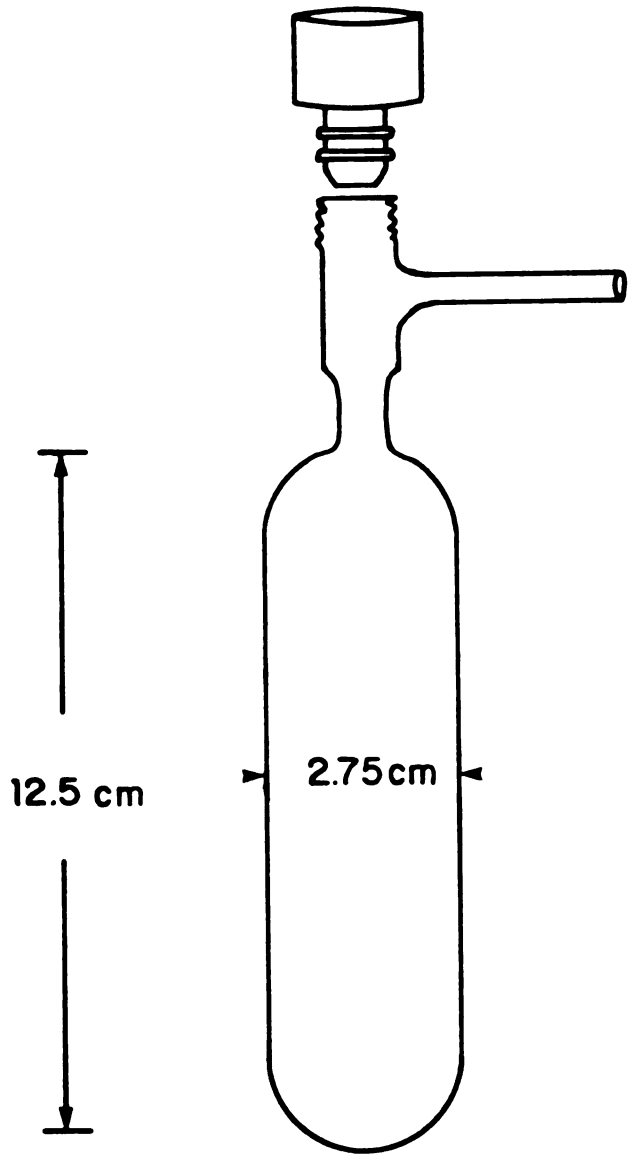

Figure 6. An illustration of the reaction flask used for intercalation

addition, there was a strong peak at 360 nm which was assigned to $FeCl_3$. $1/9 < x < 1/12$, $1/18 < y < 1/25$.

FeOCl(TTF or d_4-TTF)$_x$

5-7 mM concentrations of intercalant in DME solution were used in these reactions. The mole ratio of FeOCl to intercalant was 2:1. The reaction took 10 days at 50°C. The optical spectra of the acetone eluant consisted of absorption peaks due to TTF^+ and a very small amount of $FeCl_3$. No solvent molecule was detectable by mass spectrometry. $1/8 < x < 1/9$.

FeOCl(TMTTF)$_x$

TMTTF is only slightly soluble in MeCN. Therefore, a saturated solution was prepared by dissolving TMTTF in a minimum amount of warm MeCN. This solution was transferred via cannula to the reaction flask. The mole ratio of FeOCl to TMTTF was 2:1. Once in contact with solid FeOCl, the solution gradually turned from yellow-orange to yellow-green color. The reaction took a minimum of 13 days at 55°C. Optical spectra of the MeCN eluant indicated the presence of $TMTTF^+$.[52] $1/13 < x < 1/14$.

FeOCl(TTN or TTT)$_x$(toluene)$_y$

Mole ratios were 6:1 and 3:1 for TTN and TTT intercalants, respectively. These compounds are sparingly soluble in only a few solvents such as DMF, hot toluene and methylene chloride. There was always undissolved intercalant in the reaction mixture, which was heated at 70°C. The TTN and TTT reactions took 28 and 45 days,

respectively. Both reaction mixtures were washed thoroughly (Soxhlet extraction with methylene chloride for 3 days or 8 to 10 hours of continuous washing with toluene). As with the other acetone eluants, the optical spectra could be assigned to the radical cation.[69] $1/7 < x < 1/9$, $1/19 < y < 1/26$.

FeOCl(Pyridine)$_x$

The preparation of FeOCl(py)$_x$ where $x = 1/3$ or $1/4$ is a published procedure.[70] It was found that the pyridine solution turned yellow over a period of time; this depended on the FeOCl preparations. Even FeOCl samples of very high purity (measured by low temperature variable susceptibility) turned the pyridine solution yellow after one week at 70°C. The optical spectra could be assigned to $FeCl_3$. $x = 1/3.4$.

SYNTHESIS OF FeOCL AND ITS TETRATHIOLENE INTERCALATES

Absolute criteria regarding an acceptable purity for "single phase" products are not possible, since results depend greatly on the particular compound and the physical methods used to characterize them. For example, the Debye-Scherrer method for powder patterns may give inadequate resolution[71] and can easily miss up to 10% of a second phase. Unfortunately, a significant number of articles explain at length the physical properties of certain materials, but provide little or no information regarding the preparation or the phase purity of the material studied. There are many articles on intercalation compounds of FeOCl, in which the elemental analysis show serious discrepancies between the calculated and observed percentages. In addition, often little or no X-ray powder diffraction data are available.

This chapter discusses some of the problems encountered in the synthesis of the tetrathiolene intercalation compounds of FeOCl. These observations do not constitute a rigorous study but are derived from the results of many different preparations with varied time, solvent, temperature, etc. of the reactions.

MOX

There are three procedures outlined in the literature for the preparation of FeOCl: (1) the reaction of Fe_2O_3 with HCl,[72] (2) the reaction of $FeCl_3$ with water or water-saturated oxygen[73,74] and (3) the reaction of α-Fe_2O_3 with $FeCl_3$. The last reaction has been reported with various preparation temperatures and ratios of reactants and reaction times.[67,75,76] It has been called a vapor transport reaction,[76] but there is little evidence for this type of mechanism. In the absence of water, the product does not deposit at the cooler end of the reaction tube. Absence of any volatile FeO_xCl_y products in addition to FeOCl indicates that this is not a vapor transport reaction. In this work, careful drying of the α-Fe_2O_3 has been found to be important in order to obtain high purity FeOCl. Although a temperature gradient was generally used in the reaction, it was found that the microcrystalline product formed at the hot end of the reaction tube unless water was present. Very large FeOCl crystals (2 x 0.5 cm) deposited at the cool end in some preparations along with the excess $FeCl_3$ that was used in the reaction when small amounts of water were present.

FeOCl is water sensitive; the extent of its hydrolysis has been studied by monitoring the Cl-Fe ratio as a function of time and water pressure.[72] It was found that in a dry atmosphere FeOCl seems to be indefinitely stable, but it decomposes completely in 3 days in 100% humidity. The decomposition product is not detectable by X-ray powder diffraction; it has been suggested to be γ-FeOOH (lepidocrite),[77] which has a similar structure. A small amount of impurity could

easily go unnoticed in FeOCl. In solid state reactions such as that of Fe_2O_3 and $FeCl_3$ it is sometimes difficult to ensure a product free from impurities. Small amounts of impurities in FeOCl can have a significant effect on rates of intercalation reactions and the physical properties of the intercalate. The elemental analysis for two distinct samples of FeOCl prepared by the same method is listed in Table 2. These apparently identical preparations (by powder X-ray diffraction) of FeOCl also show quite different variable temperature magnetic susceptibility curves (Figure 7). Low temperature magnetic susceptibility is sensitive to small amounts of impurities, and thus is a good technique for ascertaining the purity of FeOCl.[41]

Table 2. Chemical analysis for two samples of FeOCl whose variable temperature magnetic susceptibility is shown in Figure 7

		Fe%	Cl%
	calculated	52.05	33.04
FeOCl[a]	observed	52.33	32.47
FeOCl[b]	observed	49.19	29.18

[a]Represented in Figure 7 by Δ.
[b]Represented in Figure 7 by O.

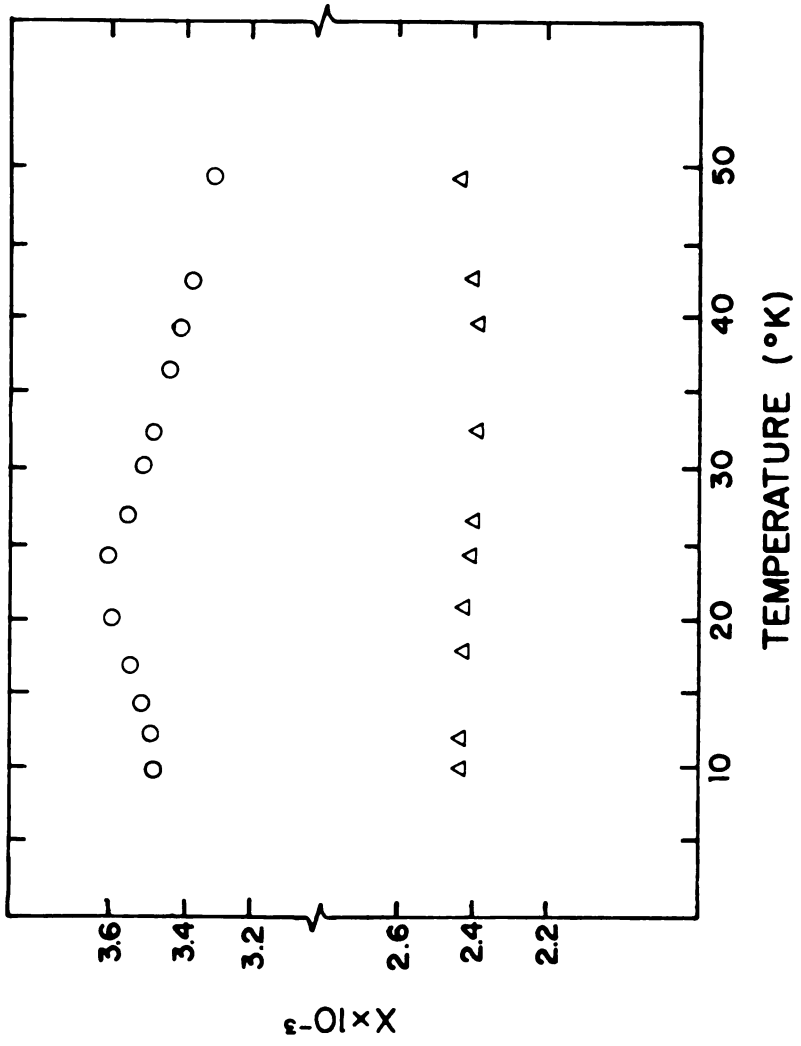

Figure 7. Molar susceptibility vs temperature (K) for two preparations of FeOCl (see Table 2)

Apparently FeOBr does not exist.[28,78] Attempts using α-Fe_2O_3 with anhydrous $FeBr_3$[79] or with $FeBr_3$ and As_2O_3[80] in a sealed tube at reaction temperatures of 500 and 400°C, respectively, proved unsuccessful. This is due to the decomposition of $FeBr_3$ at elevated temperatures. $FeOCl(4\text{-AP})_{1/4}$ (4-AP = 4-aminopyridine) has been reported to undergo deintercalation ahd chloride-methoxide exchange using MeOH.[81] FeOCl is reported to be indefinitely stable to MeOH at 80°C,[82] but when $FeOCl(4\text{-AP})_{1/4}$ is soaked in MeOH at 80°C it forms $FeOOCH_3$, which has the FeOCl type structure with the chlorides replaced by methoxides. It was suggested that the expansion of the interlayer distance on intercalation of FeOCl makes it easy for methoxide to replace the chlorides.[82] The 4-aminopyridine intercalate is the only one reported to undergo this type of reaction with FeOCl, although there is recent evidence that MeOH cointercalates as well when used as a solvent.[36] FeOCl also undergoes exchange with NH_3 to form $FeONH_2$, but little work has been done with this compound.[83] This type of approach, deintercalation and exchange, may be more promising for the synthesis of FeOBr.

Intercalation

Intercalation reactions may be represented chemically by the addition reaction $L + xG \longrightarrow LG_x$. L represents the contents of one unit cell of the layered material and x represents the number of guest species (usually a fraction) associated with that unit cell. In general, for intercalation reactions, the number of guest molecules in a unit cell is expressed as 1/x where x is an integer. This convention will be followed throughout the text except when clear identification

of particular preparations of an intercalate phase is necessary in order to aid in the discussion of the synthesis.

Solvent effects

Solvent effects in the case of the intercalation of FeOCl have been noted.[84,85] Investigation of the intercalation of Lewis bases indicates that the rate of intercalation depends upon the acid strength of the solvent used.[85] In the case of metallocenes, solvent and steric effects are more important than differences in ionization potentials of the guest species.[84] It was found that materials which did not intercalate with toluene as the solvent were easily intercalated with DME as the solvent. It was suggested that DME facilitates electron transfer from the guest to the host by stabilization of the radical cation. DME cointercalates with some of the metallocenes, but there is no evidence (MS or IR) that it cointercalates with TTF.

All intercalation reactions of tetrathiolenes and related compounds were run with various solvents such as toluene, MeCN and DME. Intercalation with TTF using toluene was first performed in our laboratory.[86] Since then, various synthetic procedures have been examined using DME and MeCN as solvents, as well as no solvent. The intercalation reactions of TTN and TTT required longer reaction times (22-45 days) at higher temperature (65-70°C) than the other tetrathiolenes. This is due to their extremely low solubility in most solvents.

Solvents clearly play a role in the intercalation process: total intercalation of TTF is achieved in 10 days at 55°C using DME as a solvent whereas only 40% intercalation is observed using MeCN under

the same conditions.[87] Even without solvent TTF will intercalate slowly: about 20% intercalation was observed by reacting TTF and FeOCl in a sealed tube at 135°C for a 24 hour period. A study of the kinetics of the FeOCl-TTF intercalation reaction suggests that impurities in the guest species aid in the rate of reaction (Table 3). The TTF used in this study was either a high purity Strem (99.9%) or Aldrich (97% pure) product. The final intercalation products were identical by X-ray powder diffraction and variable temperature magnetic susceptibility. Further studies are necessary with FeOCl of known particle size in order to obtain a quantitative measure of the effect of impurities on the rate of intercalation.

TMTTF is soluble in toluene, methylene chloride and hot MeCN. Due to the initial success of toluene as a solvent for TTF, it was used as a solvent for the intercalation reaction of FeOCl with TMTTF. Repeated attempts at a reaction temperature of 85°C always produced a two phase system in addition to 40-80% unreacted FeOCl. The use of lower temperatures produced similar results, but required longer reaction times. The powder X-ray diffraction showed two low angle peaks, corresponding to d = 13.59 and 11.94 A, in addition to that of the FeOCl (010) reflection, suggestive of the presence of two b axis parameters for the intercalated phase. The observed d spacings are consistent with the TMTTF in two orientations: one lying perpendicular and the other parallel to the FeOCl layers. The same phenomenon occurs with FeOCl(p-phenylenediamine)$_{1/9}$.[85] Its b axis parameters are 13.61 and 11.42 A, consistent with the orientation of the plane of the phenyl ring perpendicular and parallel to the host layers. In the

Table 3. Kinetic data for FeOCl + TTF (0.24 M in dimethoxyethane)

time (days)	h k ℓ	99.9% TTF (%)[a]	97% TTF (%)[a]
3	0 2 0[b]	78	60
	0 1 0[c]	100	100
6	0 2 0[b]	100	100
	0 1 0[c]	33	6
10	0 2 0[b]	100	100
	0 1 0[c]	4	-
14	0 2 0[b]	100	100
	0 1 0[c]	2	1
18	0 2 0[b]	100	100
	0 1 0[c]	-	-

[a]Percentages were calculated from the measured intensity of the 0 2 0 reflection of the intercalate and the 0 1 0 reflection of FeOCl and reported as I/I (strongest peak).

[b]The 0 2 0 reflection for the intercalate.

[c]The 0 1 0 reflection for FeOCl.

case of p-phenylenediamine no evidence for unintercalated FeOCl was observed. Further efforts with MeCN provided a one phase system for $FeOCl(TMTTF)_{1/x}$, in which the plane of the TMTTF molecule is parallel to the layers.

Stabilization of the radical cation by DME has been cited as the reason for facile intercalation of metallocenes into FeOCl.[84] For TTF, DME appears to induce a faster rate of intercalation than toluene or MeCN. TMTTF is insoluble in DME. The fact that only MeCN results in complete intercalation of TMTTF into FeOCl suggests a similar explanation to that proposed for the solvent effects for the TTF and the metallocene reactions. MeCN, a more polar solvent than toluene, may stabilize the radical cation of TMTTF. Although this stabilization of the cation may in general be important for intercalation, the use of iodine to generate the radical cation of TTF in situ had no effect on the rate of intercalation, which was monitored by X-ray powder diffraction.

Effects of FeOCl decomposition and $FeCl_3$ upon intercalation

Elemental analysis of several TMTTF intercalation reactions has afforded some insight on the effects of FeOCl decomposition upon intercalation. Table 4 shows the chemical analysis for the products of the reactions discussed below.

FeOCl was made in large quantity and several reactions were prepared with TMTTF in MeCN. One of the reactions showed immediate decomposition upon addition of the hot TMTTF MeCN solution. The decomposition could be observed by the change in color of a small amount of FeOCl from purple to orange-red. The chemical analysis of

Table 4. Chemical analysis for $FeOCl(TMTTF)_x$ prepared under different reaction conditions

Conditions	x	(calc) (obs)	C	H	S	Fe	Cl (%)
21 days	0.068		6.52	0.66	6.98	44.59	28.33
T = 65°C			6.61	0.59	6.74	44.83	28.58
55 days	0.077		7.24	0.73	7.73	43.87	27.85
T = 65°C			7.32	0.79	7.89	44.13	27.44
21 days	0.074		7.01	0.71	7.50	44.05	28.03
decomposed FeOCl			6.69	0.56	7.82	42.61	28.04
T = 65°C							
23 days	0.083		7.76	0.78	8.28	43.29	27.48
$T \geq 70°C$			8.66	0.98	7.93	43.80	24.04

the resulting intercalate is significantly low in iron content compared to the calculated value. The stoichiometry (ignoring this discrepancy) is $FeOCl(TMTTF)_{0.074}$. This is a slightly higher amount of TMTTF than that in a sample which showed no visible signs of FeOCl decomposition ($FeOCl(TMTTF)_{0.068}$). When reactions proceeded at temperatures greater than 70°C, decomposition occurred and the resulting chloride analysis was low. The decomposition of FeOCl in intercalation reactions has been noted with the intercalation reactions involving metallocenes at temperatures greater than 80°C.[42] If

the discrepancy between the calculated and observed percentage of chloride is disregarded, the stoichiometry obtained is $FeOCl(TMTTF)_{0.083}$. These differences are greater than can be accounted for by errors in the analysis (see Table 4). It appears as if the decomposition of the host increases the rate of reaction. This effect has been noted for the MS_2 intercalates, where excess sulfur in the solution (obtained from small amounts of decomposition of the host) increases the rate of reaction.[88] Subtle changes in the stoichiometry are also observed (based on analytical data) using longer reaction times. A reaction time of 55 days increased the TMTTF content in FeOCl from 0.068 to 0.077 per FeOCl. This constitutes about a 1% increase in the intercalant analysis which is significant. The changes which involve only the TMTTF content in FeOCl appear to have little effect on the resulting physical properties.

The reaction of FeOCl with pyridine at 70°C for 7 days forms the compound $FeOCl(Py)_{1/3}$.[89] Analytical and mass spectrometry studies indicated the formation of bipyridine and chloropyridine.[32] It was suggested that redox mechanism similar to that proposed for $TaS_2(py)_{1/2}$ might be valid for the $FeOCl(py)_{1/3}$ reaction.[90] It has also been suggested that small amounts of water (<100 ppm) aid the intercalation reaction by forming pyH^+.[32,91] In the preparation of $FeOCl(py)_{1/x}$ a slightly different phase was obtained than that reported in the literature. The pyridine used in this reaction was reagent grade, dried 24 hours over activated 4 A molecular sieves, in contrast to the published procedure in which the pyridine was distilled from sodium hydroxide. The stoichiometry obtained from this

preparation was $FeOCl(py)_{1/3.4}$. The infrared spectrum obtained for the $FeOCl(py)_{1/3.4}$ sample is identical to that reported for $FeOCl(py)_{1/3}$[92] in which peaks corresponding to bipyridine were identified.[36] It was noted in different preparations that sometimes the reaction mixture turned yellow immediately, indicative of the presence of $FeCl_3$ as an impurity in FeOCl. Even with very pure FeOCl samples (as determined from low temperature magnetic susceptibility), it was noted that the pyridine solution turned faintly yellow by the end of 7 days at 70°C. Although this discoloration has not been reported, at least one other scientist working in this area has made the same observation.[93] The optical spectra corresponded to that of $FeCl_3 \cdot 6H_2O$. The presence of small amounts of $FeCl_3$ may be important to this intercalation reaction.

Preliminary results using other guests

DTT could be successfully intercalated into FeOCl using DME as a solvent, but the few Bragg peaks obtained in the X-ray powder diffraction pattern were very broad, and no further work was done with this compound. DBTTF appears to intercalate into FeOCl very slowly (50% after 6 months at 65°C) using toluene as a solvent. Cl_4TTN, TMTSF and DM/DETSF in toluene at 70°C or in methylene chloride at 30°C have not been intercalated to date. These three intercalants are fairly insoluble in most solvents and further studies are necessary in order to ascertain whether intercalation of these materials is possible.

Preliminary results using hosts other than FeOCl

Alternative hosts whose intercalation chemistry was investigated were VOCl and 2H-TaS_2. Although TaS_2 is easily intercalated by pyridine,[94] intercalation with TTF, TMTTF, DBTTF, and TMTSF was unsuccessful with tolune as a solvent at 100°C for 9 days. Attempts with TaS_2 and TTF under more strenuous reaction conditions (sealed tube at 180°C, 24 hours) were also unsuccessful; the X-ray diffraction pattern was that of pristine TaS_2. The intercalation of VOCl with TTF or CA (chloranil) in toluene at 70°C, and in acetone, methylene chloride or MeCN at 28°C for two weeks was unsuccessful. The failure of these reactions may be attributed to the low temperature used; 28°C was initially used both because of the low boiling point of methylene chloride and to minimize decomposition of the intercalant. Attempts to intercalate pyridine into VOCl were also unsuccessful despite published procedures.[95,96] The literature preparation uses a reaction temperature of 80°C whereas only 70°C was used to attempt the synthesis. Temperature and/or impurities can have significant effects upon intercalation, as has been shown in the proceeding paragraphs for FeOCl. A study of these effects upon the intercalation of VOCl is in progress in this laboratory and will provide complementary data to this work on FeOCl.

STRUCTURAL STUDIES OF THE INTERCALATES

X-Ray Diffraction Results

The FeOCl structure consists of stacked neutral layers formed from distorted cis-$(FeCl_2O_4)^{7-}$ octahedra, which share half their edges to produce a central sheet of $(FeO)_n^+$ with Cl^- layers outermost on either side of the sheet.[67] The iron atoms share a single oxygen atom along the a axis, and both a chloride and an oxygen atom along the c axis (Figures 3 and 8). FeOCl crystallizes in an orthorhombic space group, Pmnm, with a = 3.780 A, b = 7.917 A, and c = 3.303 A. These cell dimensions agree very well with the Bragg reflections observed in the X-ray powder diffraction (Table 5).

X-ray powder diffraction data of $FeOCl(TTF)_{1/9}(tol)_{1/21}$ could be simulated by a monoclinic cell with the c axis corresponding to the interlayer distance.[97] Although the positions of the calculated reflections were in close agreement to those of the observed reflections (Table 6), extinctions in the experimental data could not be rationalized. A model originally proposed for $FeOCl(metallocene)_{1/x}$[39] was considered for $FeOCl(tetrathiolene)_{1/x}$. In this model, the b axis expands and doubles upon intercalation, producing symmetric vacancies for the guest molecules. Alternate layers move one-half unit cell along the ac plane, giving rise to extinctions consistent with a body centered unit cell of symmetry Immm or I222. The X-ray

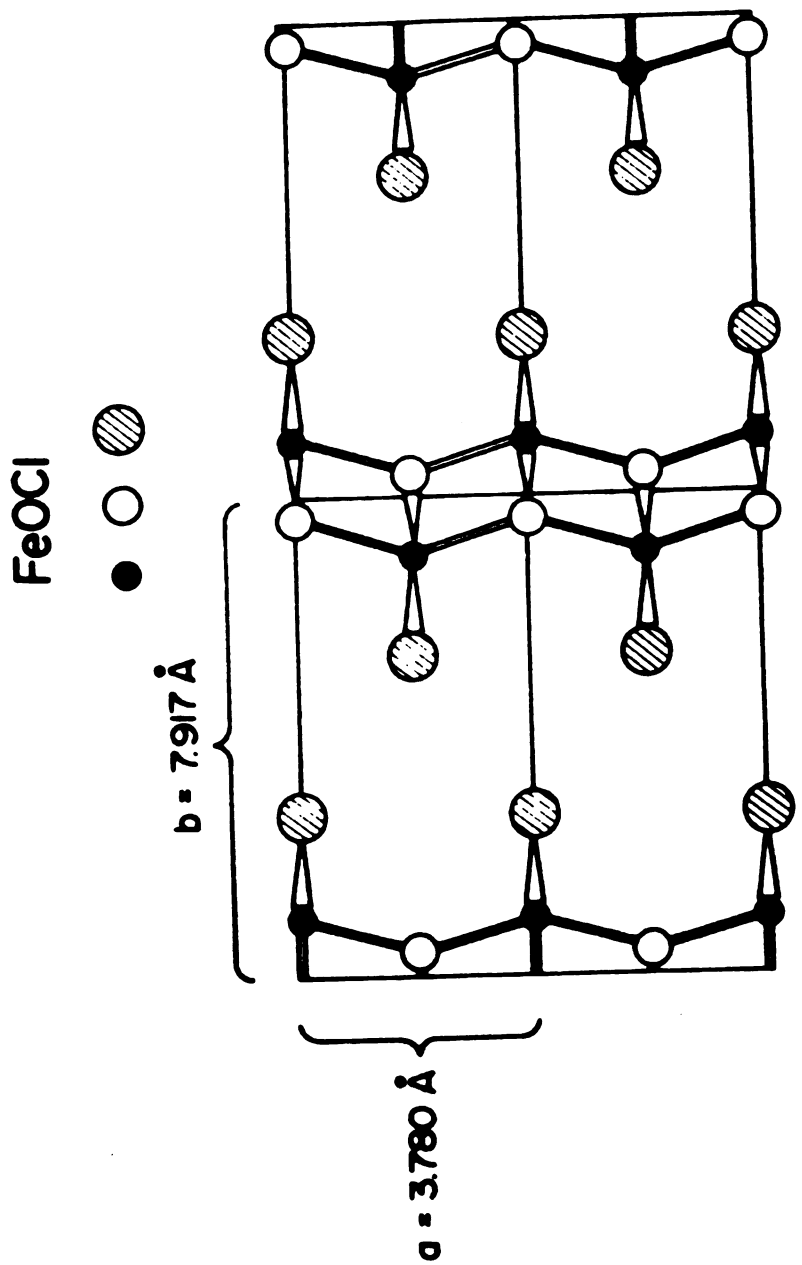

Figure 8. A schematic of FeOCl showing four unit cells

Table 5. Calculated and observed X-ray powder diffraction data for FeOCl (Cu $K\alpha_1$ = 1.54056 A using silicon as an internal standard)

I^a	d^b_{obs}	h k ℓ	d^b_{calc}
s	7.9158	0 1 0	7.9170
s	3.4093	1 1 0	3.4111
m	2.5364	0 1 2	2.5361
m	2.3735	1 1 1	2.3729
m	2.1787	1 3 0	2.1638
w	1.9785	0 4 0	1.9792
m	1.8895	2 0 0	1.8900
w	1.8350	2 0 1	1.8383
w	1.8082	1 1 3	1.8100
w	1.6503	0 0 2	1.6515
m	1.6167	0 1 2	1.6167
vw	1.5482	1 4 1	1.5487
m	1.5132	2 2 1	1.5155
mw	1.4855	1 1 2	1.4865
w	1.3916	2 3 1	1.3932
m	1.2420	2 0 2	1.2436
vvw	1.0602	0 2 3	1.0607

$\underline{a}$ = 3.780 A, $\underline{b}$ = 7.917 A, $\underline{c}$ = 3.303 A

[a]Relative intensities.

[b]d-spacings in A.

Table 6. X-ray powder diffraction data for $FeOCl(TTF)_{1/9}(tol)_{1/21}$, Co Kα = 1.7902 A

I^a	d^b_{obs}	h k ℓ	d^b_{calc}
100	13.08	0 0 1	13.205
20	6.60	0 0 2	6.602
10	3.475	2 0 0	3.480
1	3.079	$\bar{4}$ 0 5	3.075
1	2.742	$\bar{2}$ 1 5	2.739
1	2.636	0 0 5	2.641
6	2.493	$\bar{4}$ 0 3	2.491
1	1.338	0 1 4	2.337
1	1.880	0 0 7	1.886
1	1.811	0 1 6	1.833
1	1.644	0 0 8	1.651
2	1.505	2 2 0	1.450

$\underline{a}$ = 3.84 x 2 A, $\underline{b}$ = 3.31 A, $\underline{c}$ = 14.43 A, β = 115°

[a]Relative intensities.

[b]d-spacings in A.

powder diffraction data and lattice cell parameters for the $FeOCl(tetrathiolene)_{1/x}$ compounds are given in Table 7. In all cases, the data are consistent with the model proposed by Halbert[39] described above. Early in this work, extinctions were not considered; it was thought that intercalation would decrease the number of observable X-ray peaks due to disorder of the lattice structure.[36] The decrease in the number of Bragg peaks of the intercalate compared to FeOCl can be attributed to the space group; body-centering increases the number of extinctions by including the requirement of $2n = h+k+\ell$. X-ray powder diffraction peaks for the intercalates are slightly broader than those for pristine FeOCl. TTT is the largest of the organosulfur molecules, and the TTT intercalate has the broadest X-ray peaks (Figure 9). $FeOCl(TTT)_{1/9}(tol)_{1/21}$ may contain unintercalated FeOCl: the broad peak observed in the X-ray powder diffraction at about 8 A is always present. The peak at 8 A can be attributed to either the (0 1 0) reflection of FeOCl ($\underline{b}$ = 7.917 A) or to the (0 4 0) reflection of the intercalate ($\underline{b}$ = 30.89 A). Very few reflections are observed for this compound and only the $\underline{b}$ axis could be obtained from the X-ray powder diffraction data. $FeOCl(TMTTF)_{1/13}$ shows the smallest expansion along the $\underline{b}$ axis; presumably the intercalant is oriented parallel to the layers. For some samples, containing a higher content of TMTTF, the X-ray powder diffraction data showed additional diffraction peaks to those reported in Table 7, which could not adequately be accounted for. A model was proposed[97] which was based on the sulfur atoms of the intercalant and the chlorine atoms of FeOCl interacting as hard spheres of fixed van der Waals radii.

Table 7. X-ray powder diffraction data for the intercalates showing the calculated and observed d-spacings for the cell parameters given

I^a	d^b_{obs}	h k ℓ	d^b_{calc}
	$FeOCl(TTF)_{1/9}(tol)_{1/21}$		
s	13.1694	0 2 0	13.078
s	6.5378	0 4 0	6.5390
s	3.4776	1 3 0	3.4773
w	3.0770	1 5 0	3.0702
m	2.7664	0 5 1	2.8077
vw	2.5021	1 0 1	2.5011
m	2.4838	0 $\bar{7}$ 1	2.4850
w	2.4549	1 2 1	2.4566
m	2.3365	1 4 1	2.3361
m	1.8960	2 0 0	1.8960
w	1.8757	2 2 0	1.8764
mw	1.8077	1 10 1	1.8077
w	1.6638	0 0 2	1.6638
vw	1.6511	0 2 2	1.6505
vw	1.5085	2 7 1	1.5074
vw	1.2507	3 3 0	1.2509

$\underline{a}$ = 3.792 A, $\underline{b}$ = 26.1560 A, $\underline{c}$ = 3.3276 A

Table 7 (cont'd)

I^a	d^b_{obs} $FeOCl(TTF)_{1/8.5}$	h k ℓ	d^b_{calc}
s	13.099	0 2 0	13.009
m	6.511	0 4 0	6.505
s	3.474	1 3 0	3.471
m	3.065	1 5 0	3.062
m	2.8212	0 5 1	2.8116
s	2.4842	0 7 1	2.4849
w	2.4604	1 $\dot{2}$ 1	2.4603
m	2.3419	1 4 1	2.3381
w	2.1880	0 9 1	2.1862
m	1.8937	2 0 0	1.8937
mv	1.8748	2 2 0	1.8740
mw	1.8048	1 10 1	1.8048
mw	1.6706	0 0 2	1.6706
w	1.6568	0 2 2	1.6570
vw	1.5699	2 5 1	1.5705
m	1.5056	1 3 2	1.5053

$\underline{a}$ = 3.7874 Å, $\underline{b}$ = 26.0193 Å, $\underline{c}$ = 3.3412 Å

Table 7 (cont'd)

I^a	d^b_{obs}	h k ℓ	d^b_{calc}
	$FeOCl(TMTTF)_{1/13}$		
s	11.588	0 2 0	11.672
m	5.834	0 4 0	5.836
m	3.394	1 3 0	3.4034
s	2.7082	0 5 1	2.7043
m	2.3586	0 7 1	2.3519
vvw	2.0457	0 9 1	2.0434
m	1.8923	2 0 0	1.8923
mw	1.8679	2 2 0	1.8679
m	1.6587	0 0 2	1.6587
w	1.6421	0 2 2	1.6422
w	1.5514	2 5 1	1.5504
vw	1.5288	1 12 1	1.5341
mw	1.5082	1 3 2	1.4910
vw	1.4758	2 7 1	1.4742
vw	1.4711	2 10 0	1.4698
mw	1.2478	3 3 0	1.2453
mw	1.2406	2 2 2	1.2403

$\underline{a}$ = 3.7846 Å, $\underline{b}$ = 23.3444 Å, $\underline{c}$ = 3.3174 Å

Table 7 (cont'd)

I^a	d^b_{obs} $FeOCl(TTN)_{1/9}(tol)_{1/22}$	h k ℓ	d^b_{calc}
s	15.479	0 2 0	15.443
m	7.7014	0 4 0	7.722
m	3.5559	1 3 0	3.5583
w	3.2338	1 5 0	3.2317
w	2.9300	0 5 1	2.9332
w	2.6595	0 7 1	2.6595
w	2.3903	0 9 1	2.3909
w	2.2501	1 6 1	2.2513
w	2.1449	0 11 1	2.1474
m	1.8958	2 0 0	1.8960
m	1.8858	2 2 0	1.8819
m	1.8085	1 12 1	1.7945
m	1.5019	1 3 2	1.5091
mw	1.4841	2 9 1	1.4856

$\underline{a}$ = 3.7920 A, $\underline{b}$ = 30.8860 A, $\underline{c}$ = 3.3329 A

[a]Relative intensities.

[b]d-spacings in A.

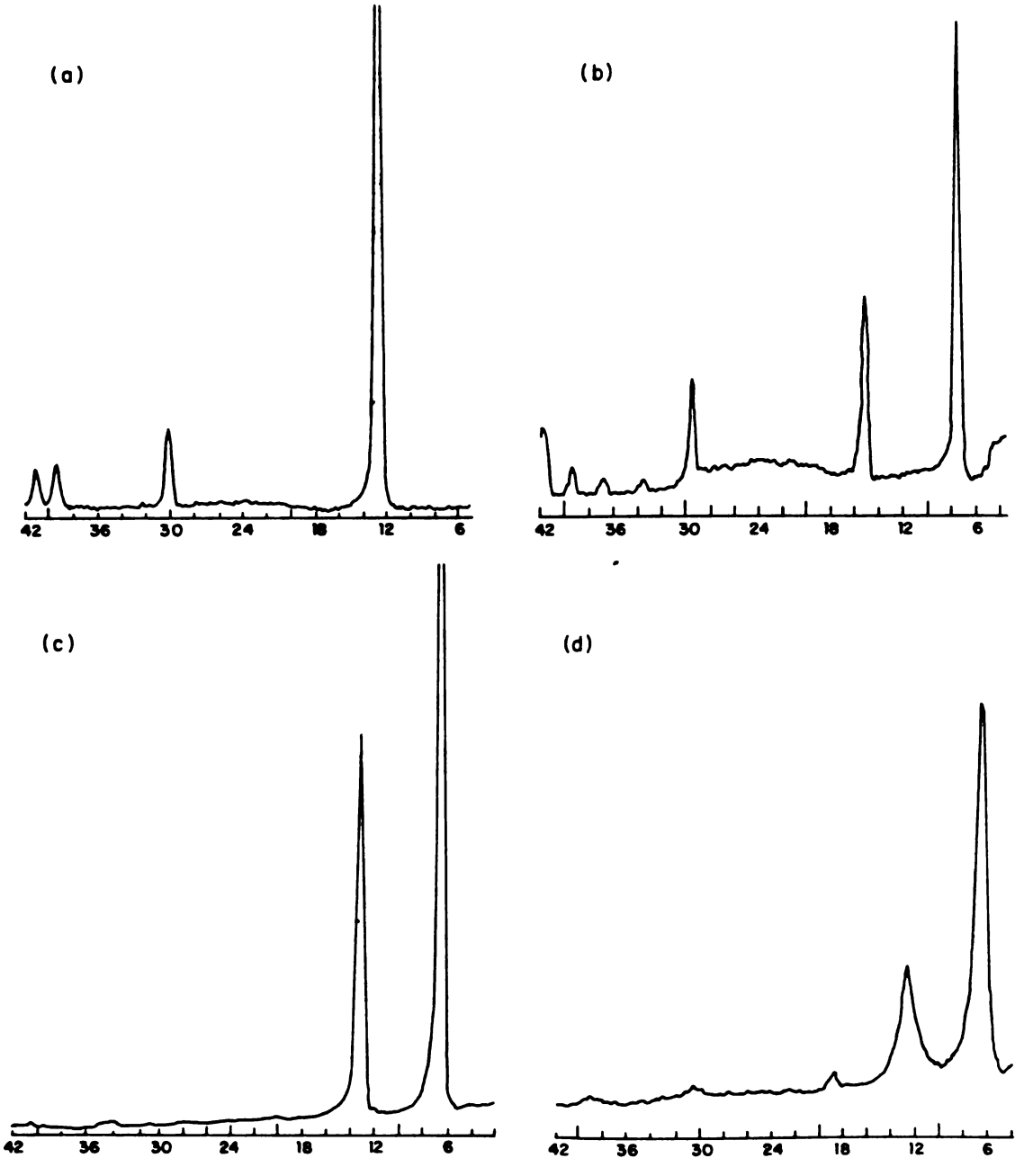

Figure 9. X-ray powder diffraction data plotted as intensity vs 2θ for (a) FeOCl, (b) $FeOCl(TTF)_{1/9}(tol)_{1/21}$, (c) $FeOCl(TTN)_{1/9}(tol)_{1/23}$ and (d) $FeOCl(TTT)_{1/7}$

Reevaluation of the X-ray and neutron powder diffraction data has led to another model in which the sulfur and the chloride atoms can be closer together than the sum of their van der Waals radii, due to a nonspherical electron distribution around the sulfur atom of TTF. This is referred to as the soft sphere model for lack of a better descriptive title. In this model, the FeOCl layers are "locked" into place by the TTF molecule. This type of locking also occurs with metallocenes intercalated into TaS_2.[98] Both models will be described in detail later in this chapter.

Single crystal studies on $FeOCl(TTF)_{1/x}$ have been carried out. A longer reaction time (4-5 months) is required for the intercalation of FeOCl crystals than for powder. Microscopic examination showed that the surface of many of the $FeOCl(TTF)_{1/x}$ crystals was puckered, and usually the "crystals" were aggregates, consisting of several sheets stacked one upon the other.

In general, the smaller crystals appeared to give better X-ray diffraction patterns. "Single crystals" of three different reactions were mounted and precession photographs obtained. One preparation was vacuum dried, and the other two were dried by passing dry argon over the crystals. All the photographs for the larger crystals showed broad streaks or spots that were not well defined. The smaller crystals provided better diffraction, but the photographs were interpreted as resulting from a twinned or otherwise imperfect crystal.

Intercalation structures have been determined by calculated electron density maps based on X-ray powder diffraction data,[99,100] EXAFS,[101-104] neutron powder diffraction,[34,35] and more recently by

solid state NMR.[37,105,106] The latter two techniques were applied to the FeOCl-TTF system, the best characterized and most crystalline of the FeOCl-tetrathiolene intercalates. Further structural information on all the intercalates was obtained by EXAFS spectroscopy.

Extended X-Ray Absorption Fine Structure Results

In recent years, there have been several excellent theoretical derivations and reviews of EXAFS (Extended X-Ray Absorption Fine Structure), and the reader is referred to these works for a formal discussion of EXAFS theory and its application.[107-111] The following section will discuss experimental results that were analyzed by accepted procedures described in greater detail elsewhere.[65,112-115] Theoretical background for EXAFS will only be included where necessary to aid the reader in understanding the results described herein.

The Fe K-edge transmission X-ray absorption spectra of FeOCl and the intercalates are shown in Figures 10-14(a). The absorption spectrum exhibits modulations of the transmitted X-ray intensity above the absorption edge: these modulations are referred to as Extended X-ray Absorption Fine Structure (EXAFS). The spectrum is typically plotted as the $\ell n(I_0/I)$ vs E, where I = intensity and E = energy in units of eV. If the absorbing atom is near other atoms, the final state wavefunction of the photoelectron may be modified by scattering due to neighboring atom(s). This results in an interference effect in the final state of the photoelectron and modifies the absorption cross section.

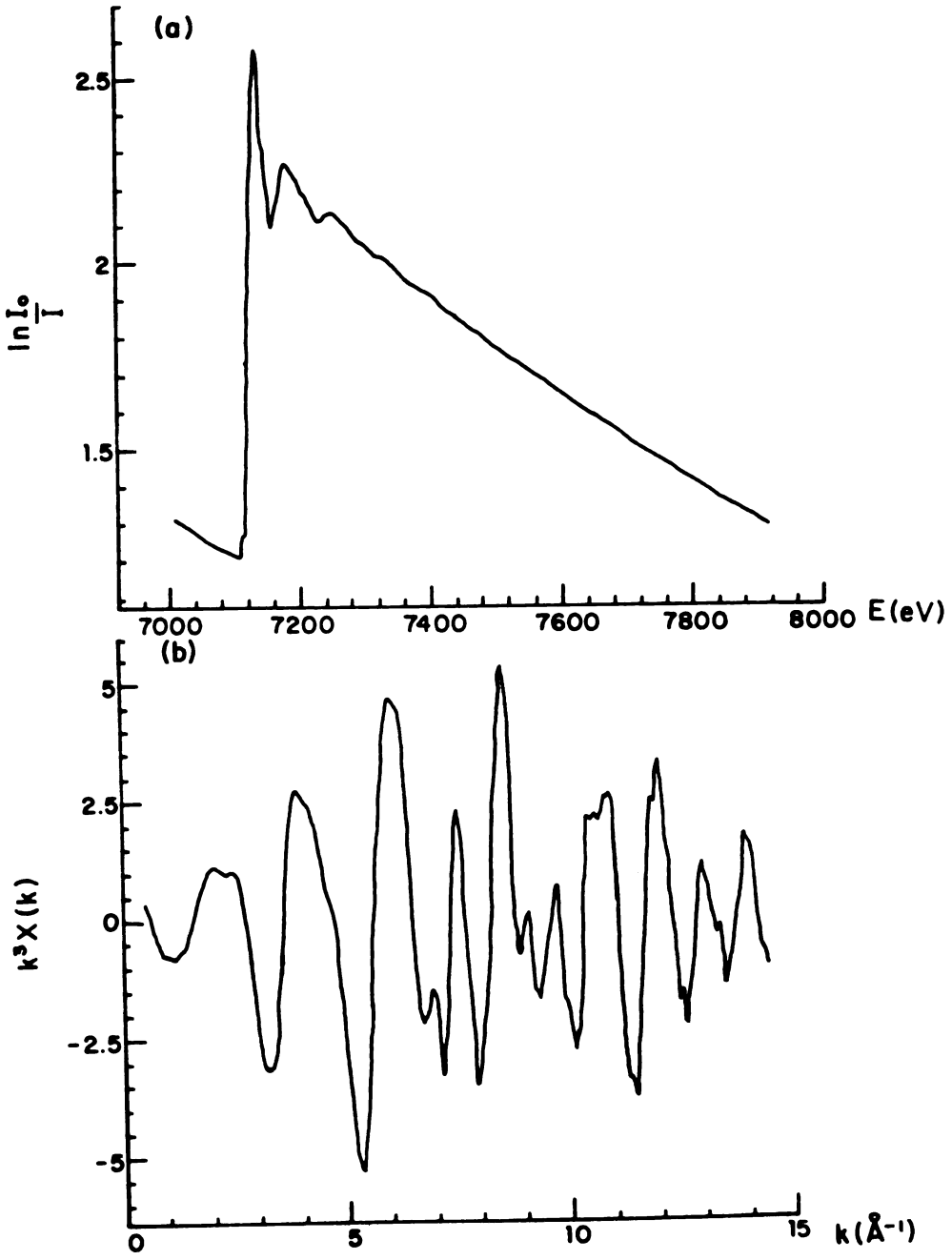

Figure 10. (a) Fe K-edge transmission X-ray absorption spectrum and (b) the background subtracted Fe EXAFS data of FeOCl

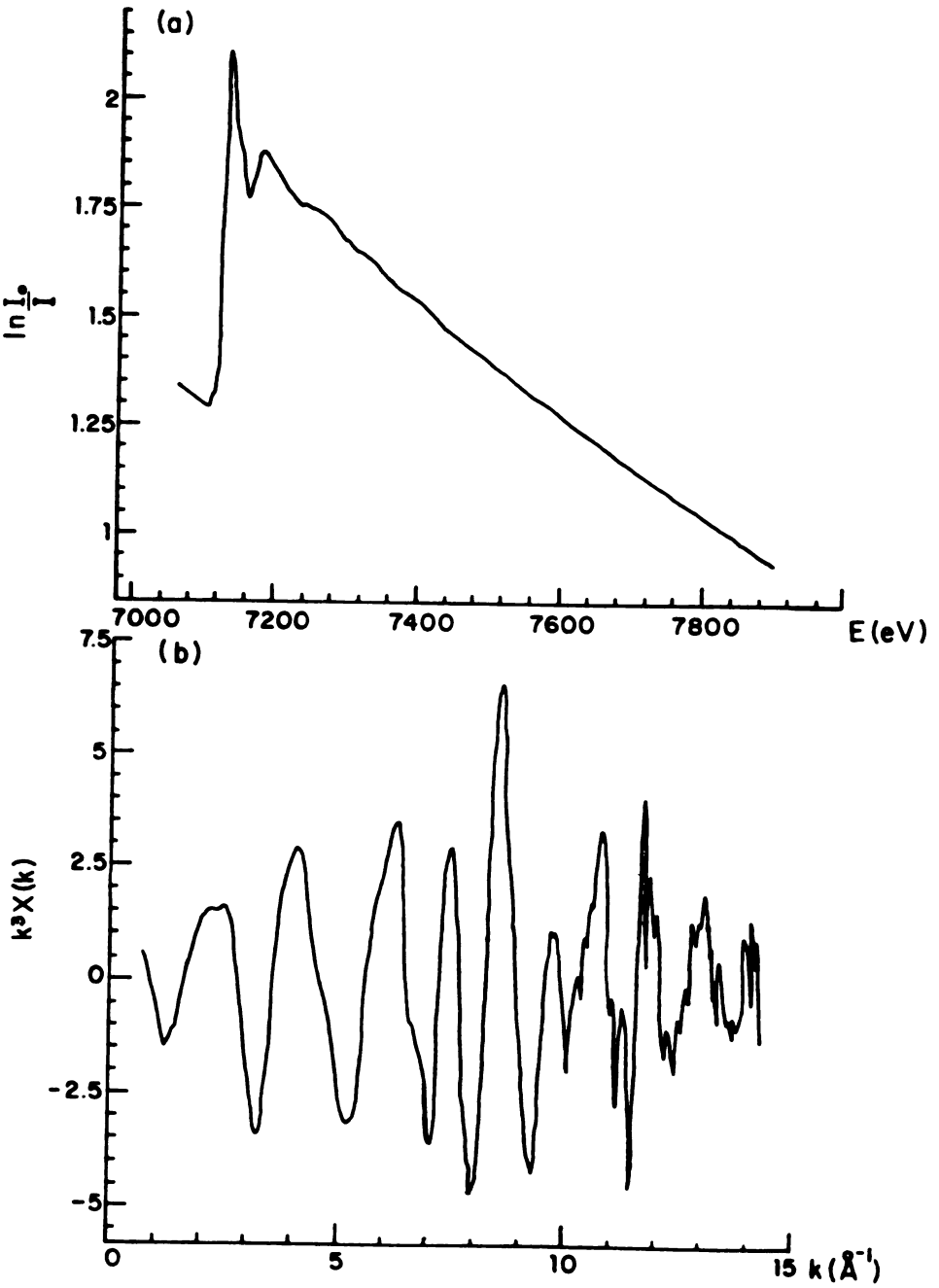

Figure 11. (a) Fe K-edge transmission X-ray absorption spectrum and (b) the background subtracted Fe EXAFS data of $FeOCl(TTF)_{1/8.5}$

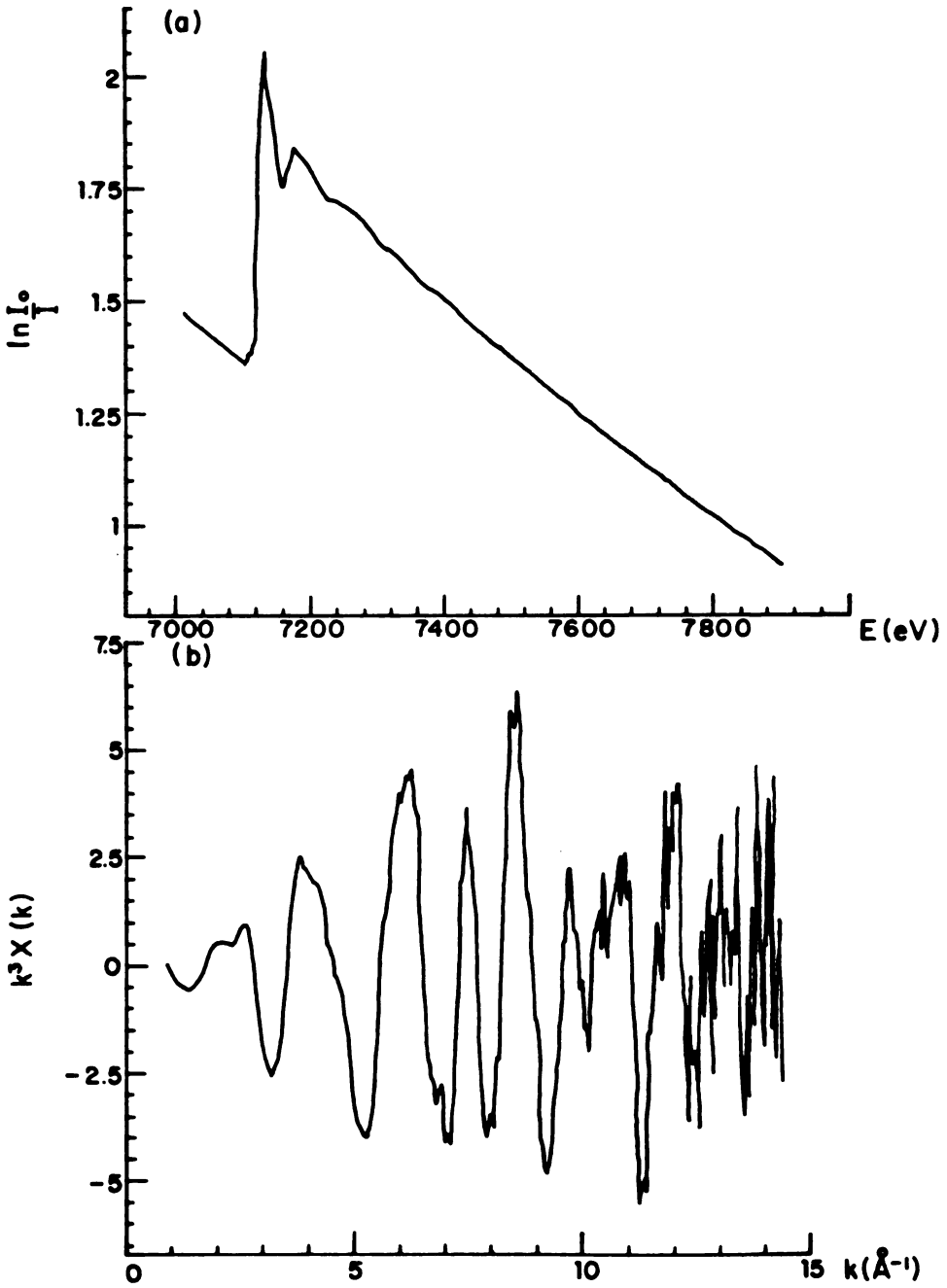

Figure 12. (a) Fe K-edge transmission X-ray absorption spectrum and (b) the background subtracted Fe EXAFS data of $FeOCl(TMTTF)_{1/13}$

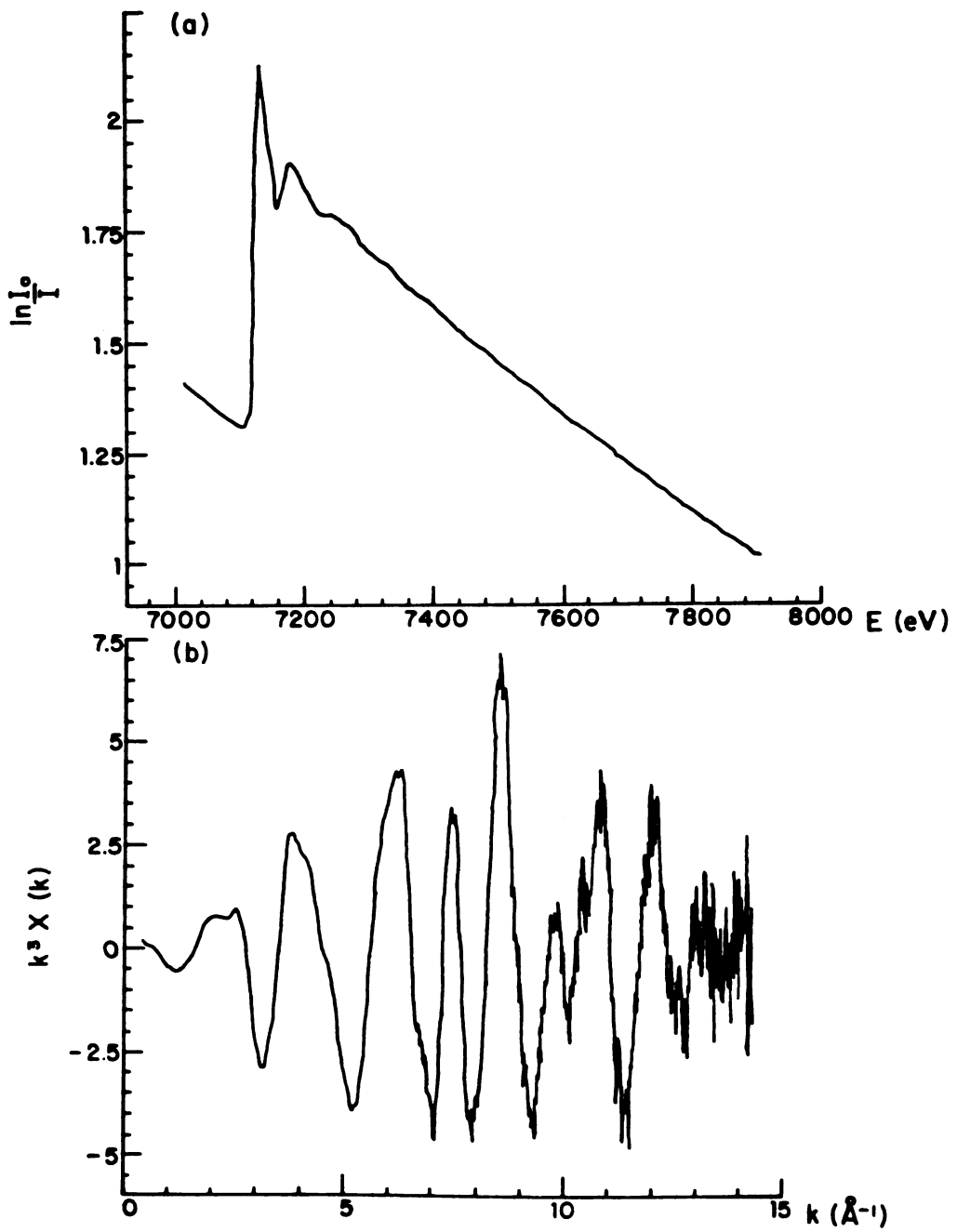

Figure 13. (a) Fe K-edge transmission X-ray absorption spectrum and (b) the background subtracted Fe EXAFS data of $FeOCl(TTN)_{1/9}(tol)_{1/23}$

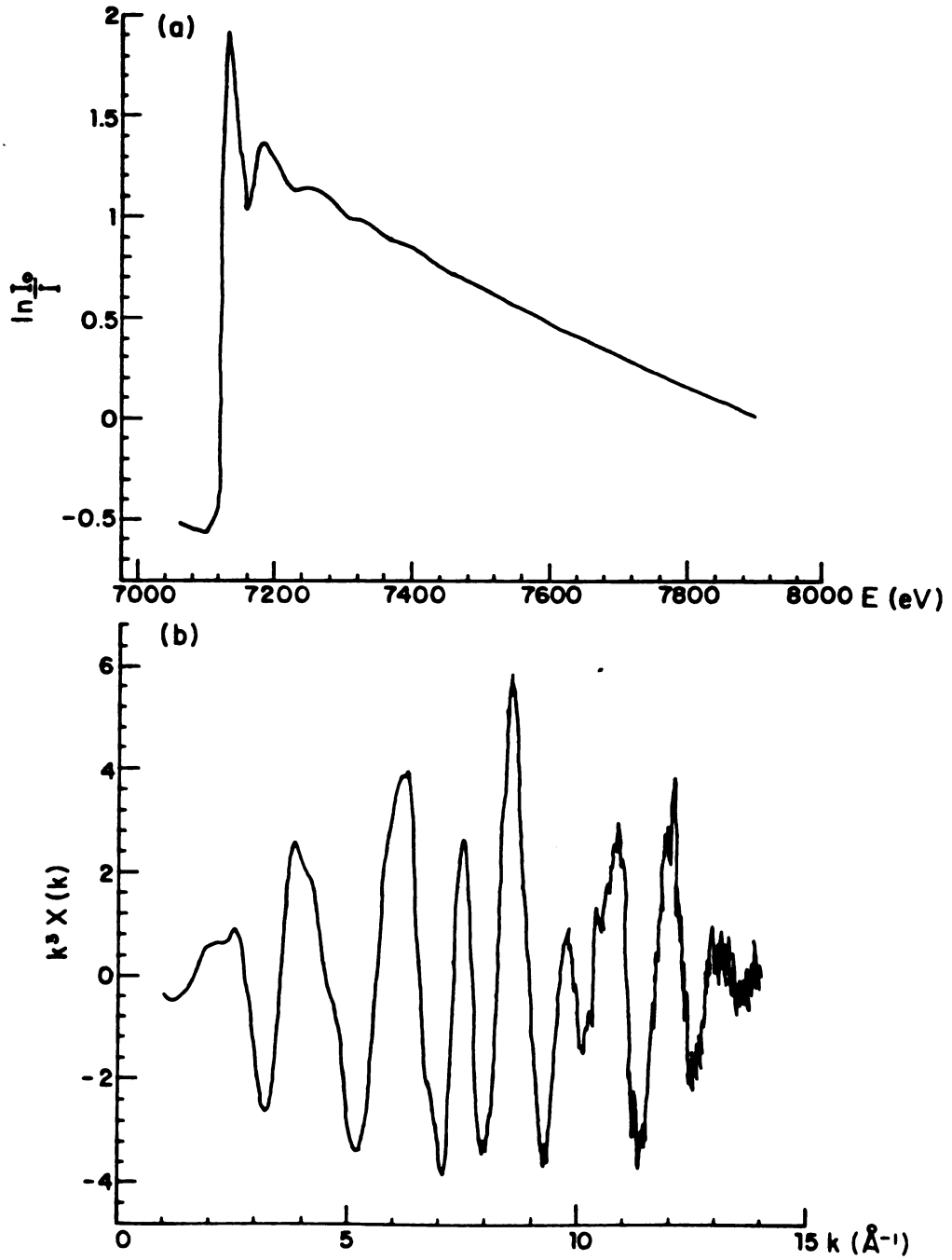

Figure 14. (a) Fe K-edge transmission X-ray absorption spectrum and (b) the background subtracted Fe EXAFS data of $FeOCl(TTT)_{1/7}$

The background absorption for all compounds was removed in k-space using a cubic spline function of four sections, $\Delta k = 3.48\ A^{-1}$ (equation 1).

$$k(A^{-1}) = \sqrt{(2m/h^2)(E-E_0^{exp})} \qquad (1)$$

The normalized oscillatory part of the absorption coefficient in the form $k^3\chi(k)$ vs k, was obtained by dividing by the edge jump $\Delta\mu_0$, and by correcting for the fall-off of $\mu(k)$ with Victoreen's true absorption coefficient equation.[116,117] The edge jump, used to normalize the data, was taken as the step in the absorption cross section across the K absorption edge. The edge jump was measured as the difference between the EXAFS and pre-near-edge region absorption. For all these spectra, the edge position energy, E_0, was determined as the photon energy at half-height of the absorption edge jump plus 13 eV (7124 eV). This provided a Fourier Transform in which the magnitude of the first peak was the largest. Since E_0 values cannot be determined exactly from the features in the absorption spectrum, E_0 was treated as an adjustable parameter in the final curve fitting of the data. ΔE_{0j} is defined as the threshold energy difference and was refined for each type of scattering atom j (equation 2).

$$\Delta E_{0j} = E_{0j}^{th} - E_0^{exp} \qquad (2)$$

This allows for discrepancies between empirically chosen energy thresholds, (E_0^{exp}), and theoretical E_0's (E_0^{th}).[107] In the analysis, it was found that the amplitude of the oxygen peak is sensitive to the number of sections of the spline in addition to the choice of E_0.

The $k^3\chi(k)$ of the Fe K-edge for FeOCl and the intercalates are presented in Figures 10-14(b).

A Fourier transformation relates the EXAFS function $k^3\chi(k)$ of the photoelectron wavevector $k(\text{Å}^{-1})$ to its corresponding function $\phi_3(r')$ of distance r'(Å) (equation 3).

$$\phi_3(r') = (2\pi)^{-1/2} \int_{k_{min}}^{k_{max}} k^3\chi(k)e^{i2kr'}dk \qquad (3)$$

The Fourier transform provides a modified radial distribution map of the environment around the X-ray absorbing atom. The Fourier transform peaks are shifted from the true distances due to the effect of a phase shift, which amounts to approximately 0.2 to 0.5 Å, depending principally upon the absorbing and backscattering wave functions. The Fourier transforms of FeOCl and the intercalates are shown in Figures 15 and 16. The first five peaks of the Fourier transforms are assigned as follows: Fe-O; Fe-Cl; Fe--Fe (nearest neighbors); Fe--Fe (c axis); and Fe-Fe (a axis). From the comparison of the Fourier transforms of FeOCl and $FeOCl(TTN)_{1/9}(tol)_{1/21}$ data it is apparent that the FeOCl lattice is largely unperturbed upon intercalation (Figure 17).

A Fourier filtering technique was employed to isolate peaks due to the absorbing atom's near neighbors. The resulting Fourier filtered EXAFS were subsequently truncated at 3.0 Å^{-1} and 13.0 Å^{-1} to eliminate distortion.[109] The Fourier filtered curves were fit using the standard formulation shown in equation 4.

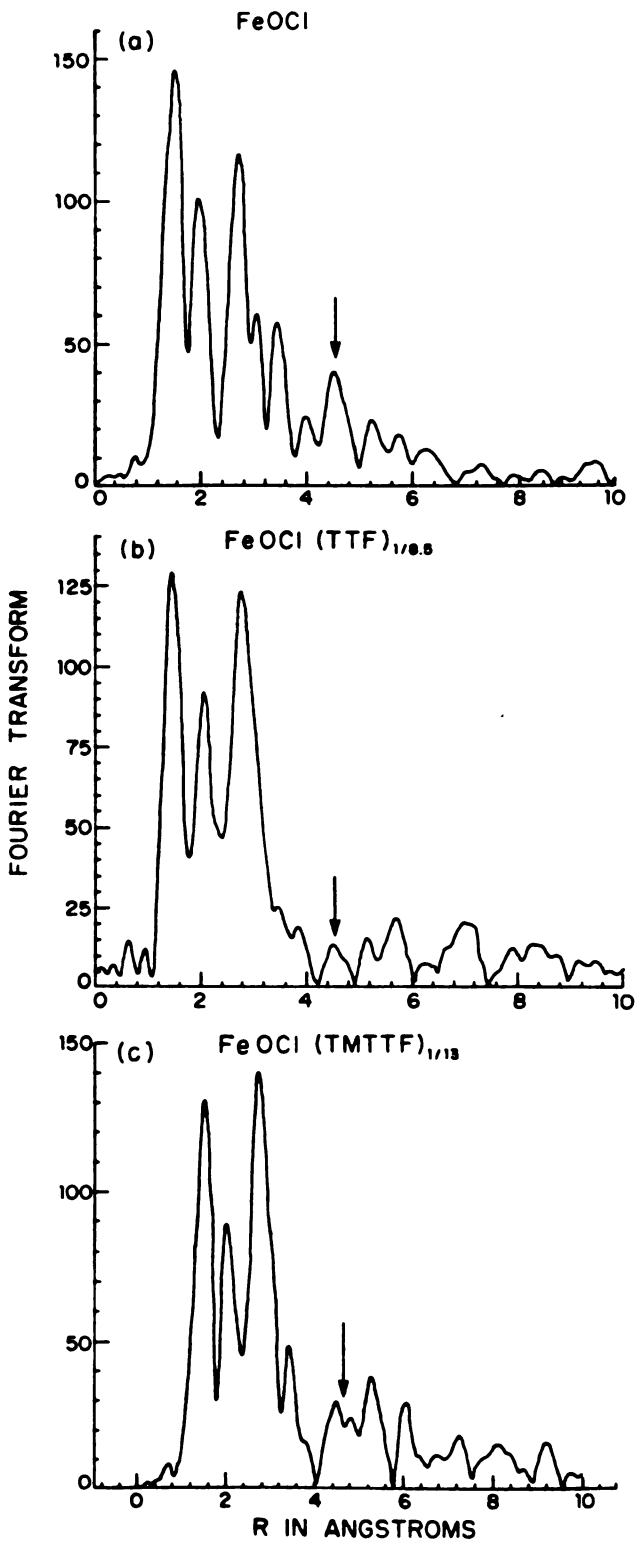

Figure 15. Fourier transforms of the Fe K-edge transmission EXAFS $k^3\chi(k)$ vs r for (a) FeOCl, (b) $FeOCl(TTF)_{1/8.5}$ and (c) $FeOCl(TMTTF)_{1/13}$

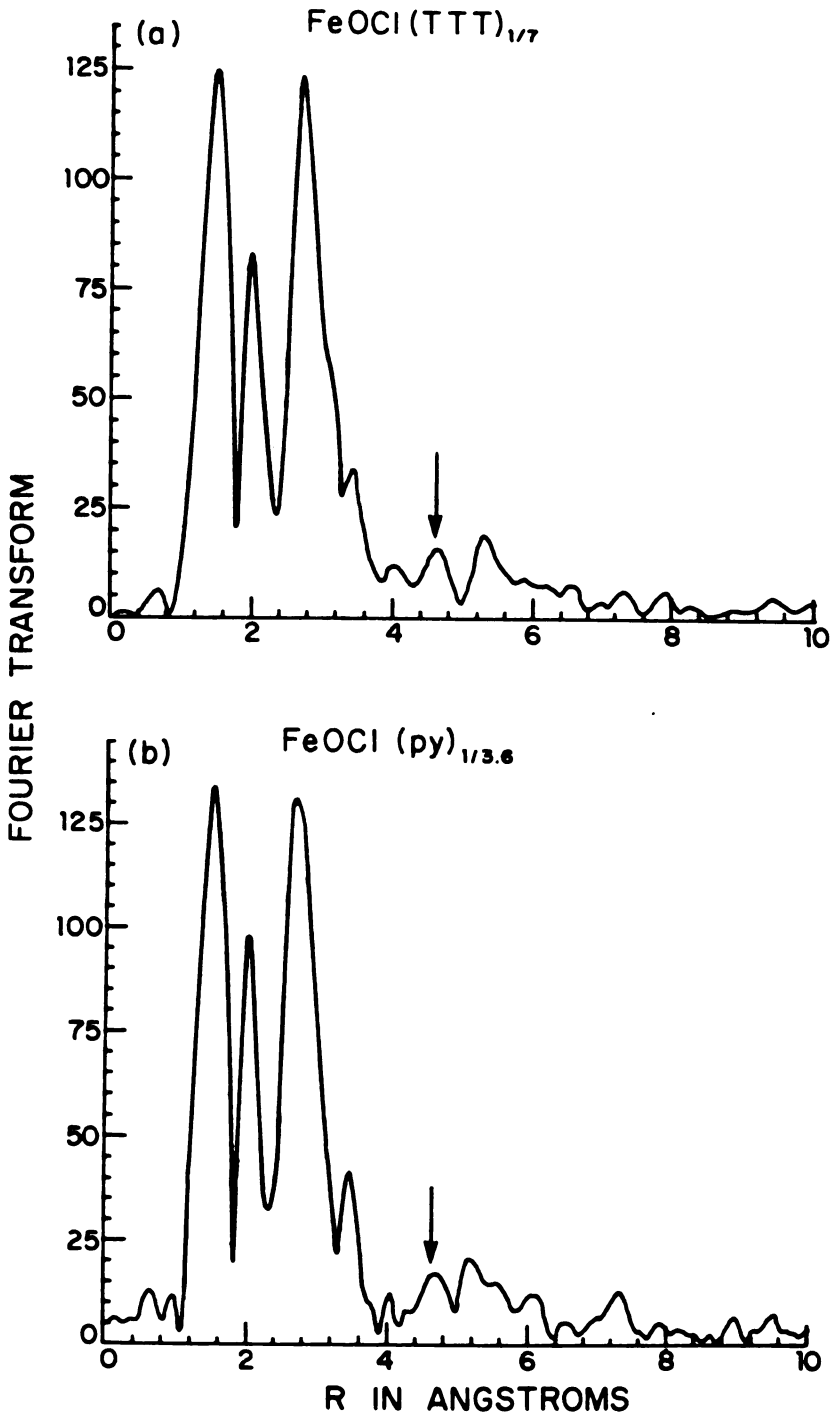

Figure 16. Fourier transforms of the Fe K-edge transmission EXAFS $k^3\chi(k)$ vs r for (a) $FeOCl(TTT)_{1/7}$ and (b) $FeOCl(\overline{py})_{1/3.6}$

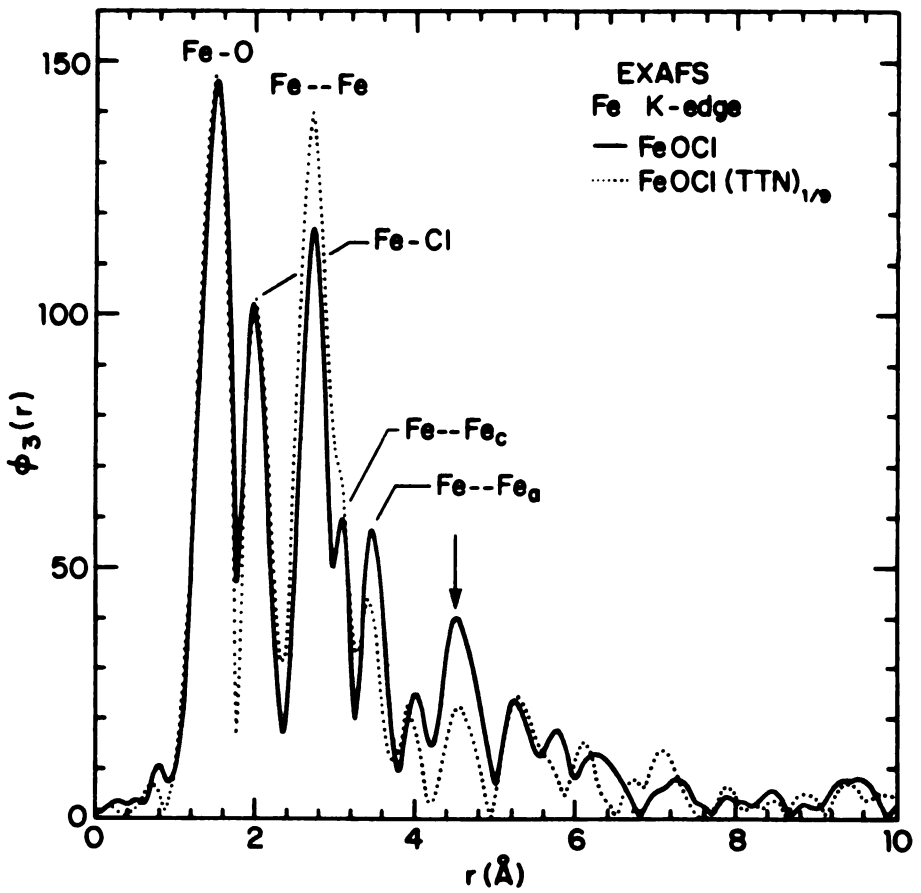

Figure 17. Comparison of the Fourier transforms of the Fe K-edge transmission EXAFS $k^3\chi(k)$ vs r for FeOCl (solid curve) and $FeOCl(TTN)_{1/9}(tol)_{1/22}$ (dotted curve) with peak assignments

$$k^3\chi(k) = \sum_j B_j F_j(k_j) k_j^2 \exp(-2\sigma_j^2 k_j) \cdot \sin(2k_j r_j + \sigma_j(k_j))/r_j^2 \qquad (4)$$

A nonlinear least squares program for iterative estimations of parameters was used to refine the scale factors (independent of the photoelectron wavevector, k_j) for the scattering atoms of the jth type B_j, at a distance r_j from the absorber, and the root-mean square relative displacement σ_j (Debye-Waller factors) along r_j. Theoretical backscattering amplitude $F_j(k_j)$ and phase $\sigma_j(k_j)$ functions, calculated by Teo and Lee,[114] were used in the curve fitting formulation. The scale factor, B_j, is related to the number of nearest neighbors, N_j, of the jth type of atom and to the amplitude reduction factor, S_j, as follows in equation 5.

$$B_j = N_j S_j \qquad (5)$$

The amplitude reduction factors S_j combine into one parameter many effects including the energy resolution of the monochromator[117] and thickness effects.[119,120]

The first two peaks, due to Fe-O and Fe-Cl distances, were filtered using a window of r' = 0.9 - 2.9 Å and fit using Fe-O and Fe-Cl phase and amplitude functions. The next two partially resolved peaks Fe--Fe (near neighbors) and Fe--Fe (c axis interactions) were filtered, r' = 2.0 - 3.6 Å and fit with two terms using Fe phase and amplitude functions while holding the Debye-Waller factors equal. The fifth peak, assigned to Fe--Fe (a axis) was filtered, r' = 3.2 - 3.8 Å,

and fit using one term. Multiple scattering was not a problem for Fe--Fe c interactions due to the small Fe-O-Fe and the Fe-Cl-Fe angles (103.71° and 88.35°, respectively). The Fe-O-Fe angle along the a axis is 149.29°, and the effects of multiple scattering are negligible.[121,122]

The best parameters based on theoretical functions (BFBT) obtained from the curve fitting were adjusted using the fine adjustment based on models (FABM) procedure outlined in the literature.[112,113] Plots of the values obtained for ΔE_0 vs Δr and for B vs σ are shown in Figures 18-20 for FeOCl and the intercalates. In these plots $\Delta r = r - r_{bf}$ (bf = best fit) and ΔE_0, B and σ were defined previously. Pristine FeOCl was used as the model compound for the intercalates. The EXAFS distances and coordination numbers were obtained by fine tuning the parameters obtained from the best fit to the data using theoretical functions as shown in Table 8. Results for different preparations of FeOCl and $FeOCl(TTN)_{1/9}(tol)_{1/21}$ are shown in order to illustrate the reproducibility of the results. Notable trends in the data are (1) the Fe-Cl distances for the intercalate are consistently longer than those for the pristine material; (2) Fe--Fe nonbonded distances are consistently shorter; and (3) in all cases the c axis is elongated compared to that of FeOCl. The c axis has expanded by about 1%, a significant amount for a well-defined extended lattice structure. Debye-Waller factors are given in Table 9 and are consistent with little or no disorder of the FeOCl intercalate lattice, in contrast to EXAFS results on $MnPS_3$ intercalates.[103]

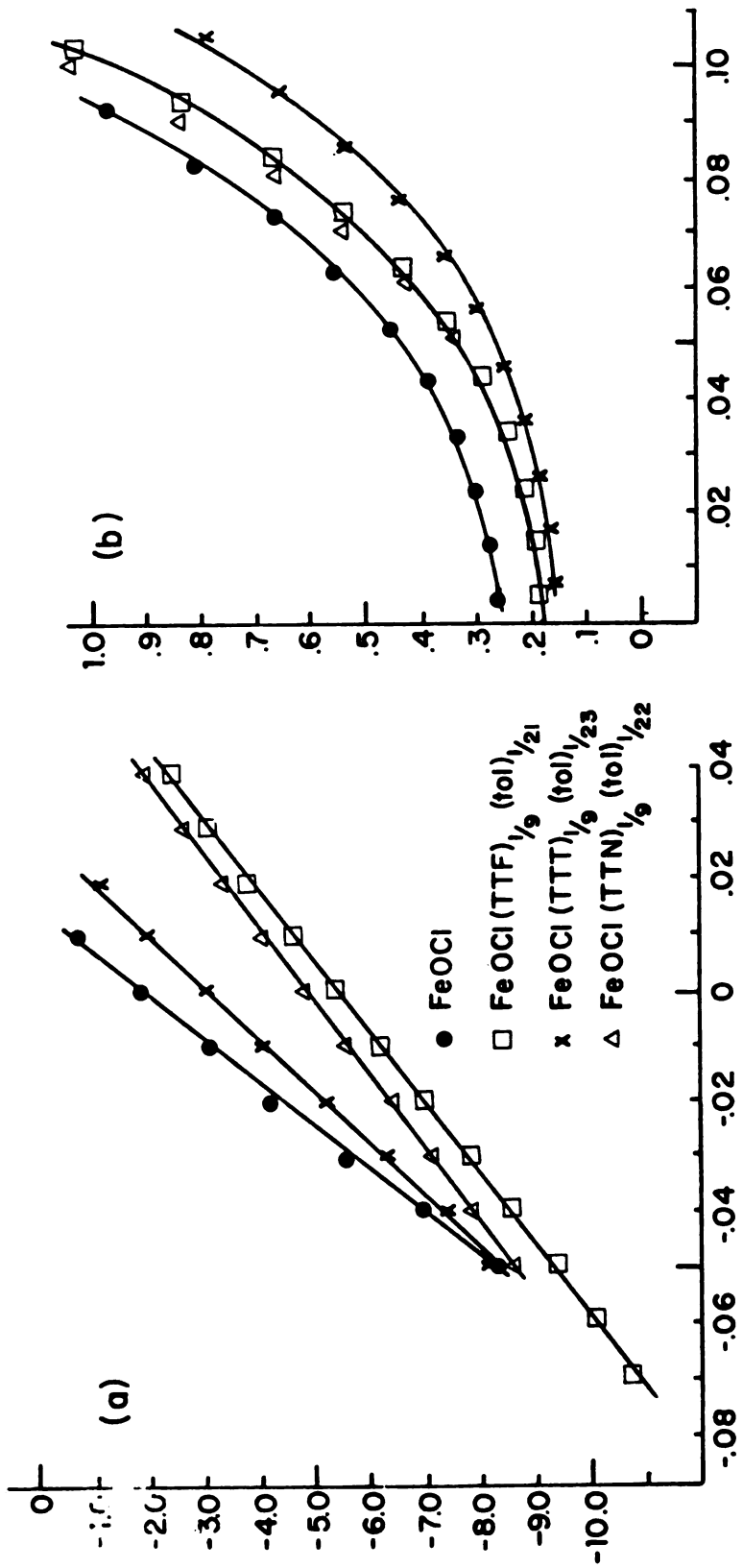

Figure 18. (a) ΔE vs Δr for Fe--Fe nonbonded near neighbors and (b) B vs σ for FeOCl, $FeOCl(\overline{TTF})_{1/9}(tol)_{1/21}$, $FeOCl(TTN)_{1/9}(tol)_{1/22}$ and for $FeOCl\overline{(TTT)}_{1/7}$

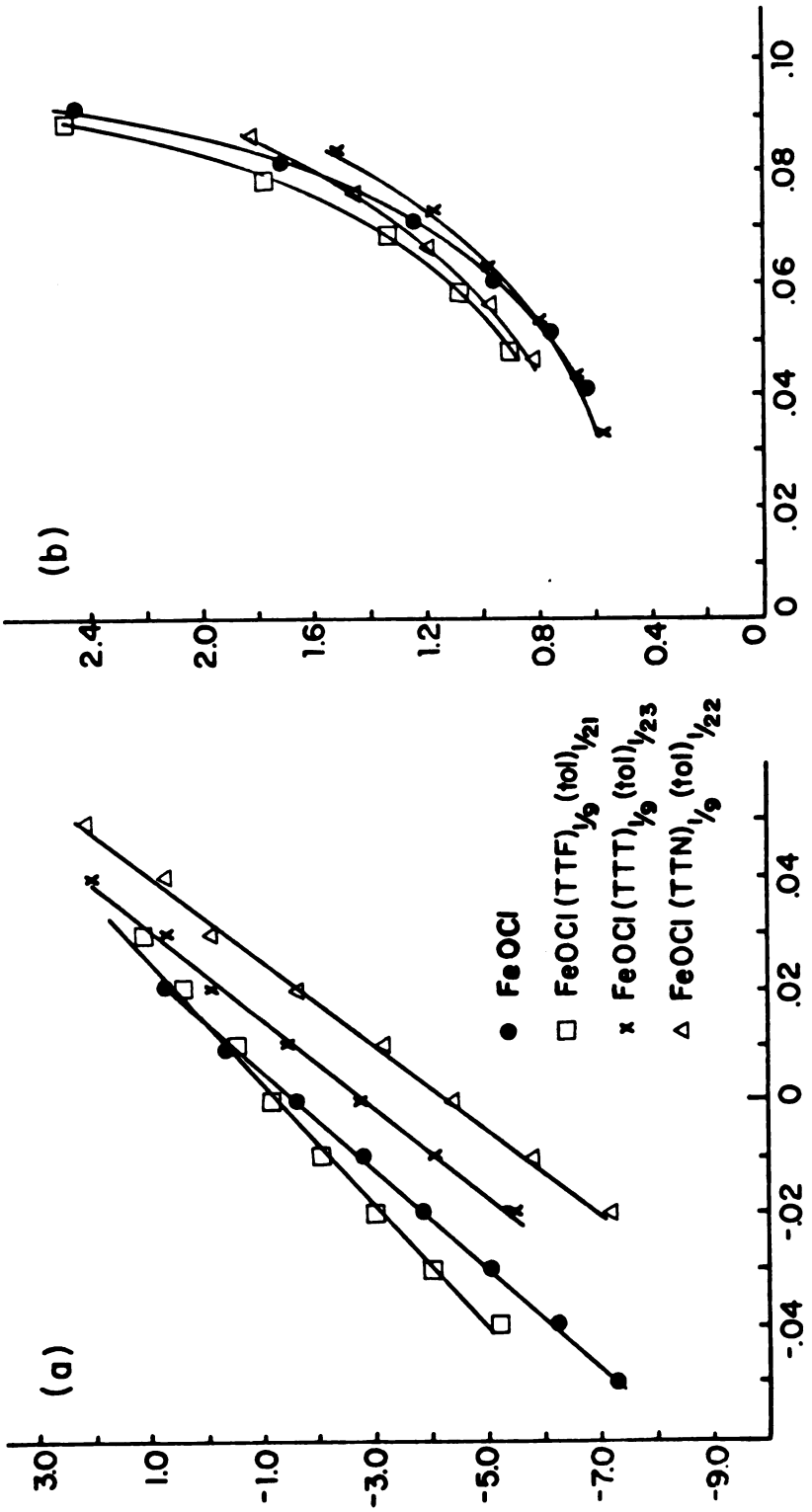

Figure 19. (a) ΔE vs Δr for Fe--Fe (c-axis) and (b) B vs σ for FeOCl, $FeOCl(\overline{TTF})_{1/9}(tol)_{1/21}$, $FeOCl(TTN)_{1/9}(tol)_{1/22}$ and $FeOCl(TTT)_{1/7}$

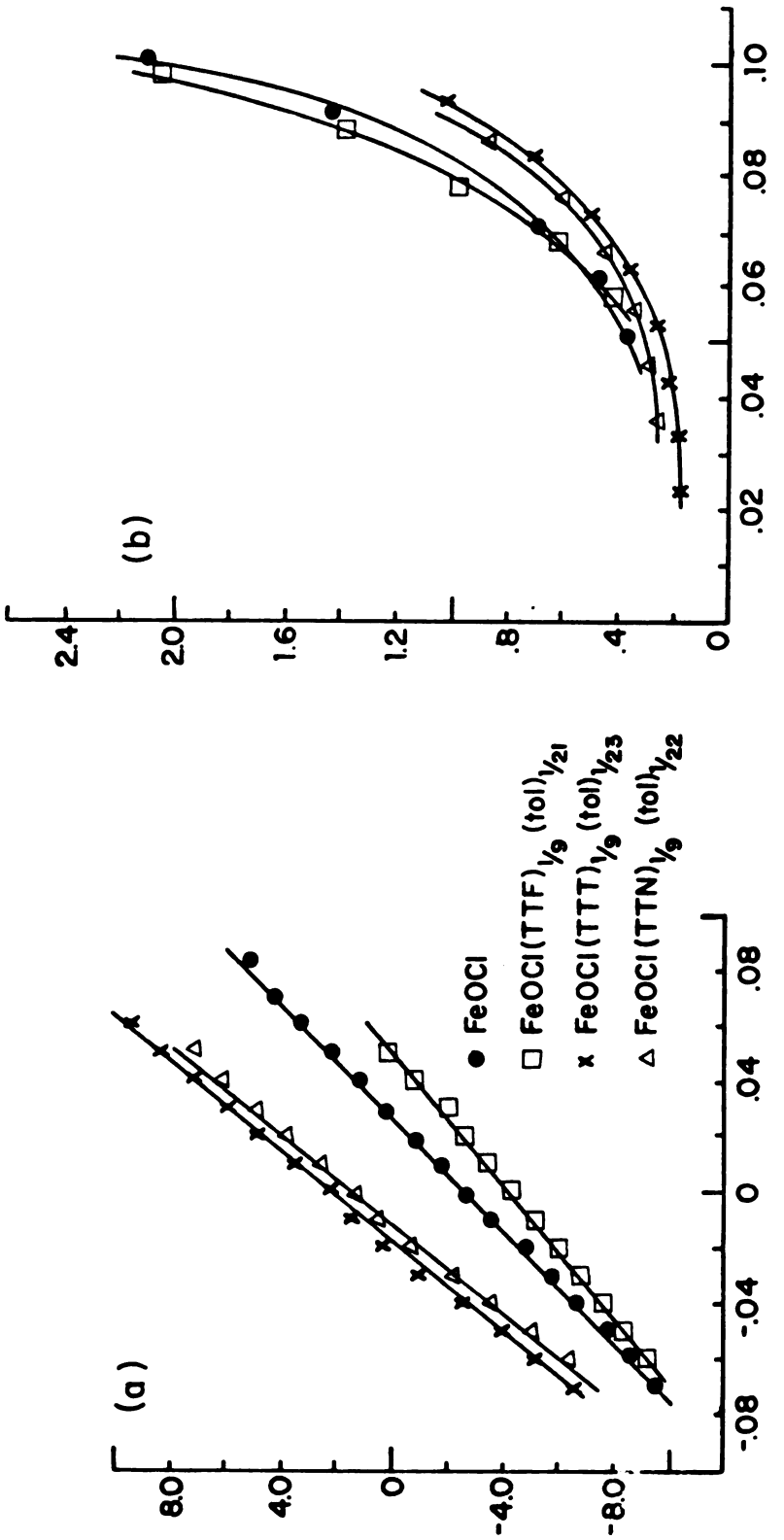

Figure 20. (a) ΔE vs Δr for Fe--Fe (a-axis) and (b) B vs σ for FeOCl, $FeOCl(\overline{TTF})_{1/9}(tol)_{1/21}$, $FeOCl(TTN)_{1/9}(tol)_{1/22}$ and $FeOCl(TTT)_{1/7}$

Table 8. The distances and coordination numbers obtained from the EXAFS analysis for FeOCl and the intercalates

Compound[a]	Fe-O[b] 2.03 A 4.0[c]	Fe-Cl[b] 2.368 A 2.0[c]	Fe--Fe[b] 3.107 A 4.0[c]	Fe--Fe$^{b}_{c}$ 3.302 A 2.0[c] $\perp$	Fe--Fe$^{b}_{a}$ 3.780 A 2.0[c] $\perp$
FeOCl[d]	2.03(2) 4(1)	2.37(5) 2.0(7)	3.11(2) 4(1)	3.30(2) 2(1)	3.78(2) 2.0(8)
FeOCl	2.03(4) 4(1)	2.36(5) 2(1)	3.11(2) 4(2)8)	3.30(2) 2.0(8)	3.78(1) 2(1)
TTF[e]	2.03(4) 3(1)	2.42(5) 2(1)	3.08(2) 4(1)	3.33(1) 3(1)	3.78(4) 1(1)
TTF[f]	2.08(3) 4(1)	2.40(3) 2(1)	3.09(2) 4.5(2)	3.31(2) 2(1)	3.78(2) 2(1)
TTN[d]	2.04(4) 3.1(6)	2.41(4) 1.5(9)	3.08(1) 4(1)	3.34(2) 2(1)	3.80(3) 2.0(5)
TTN	2.03(3) 4(2)	2.40(4) 2(1)	3.08(1) 3.8(6)	3.35(2) 1.5(5)	3.77(3) 2(1)
TTT	2.04(4) 3.8(9)	2.39(5) 1.5(7)	3.07(1) 3.3(5)	3.34(2) 1.3(5)	3.80(2) 1(1)
TMTTF	2.03(3) 4(1)	2.38(4) 2(1)	3.08(1) 5(1)	3.32(1) 3(2)	3.80(2) 1.8(3)

The standard deviation is shown in parentheses

[a]The intercalates are represented by the guest species.
[b]Fe-X distances in A obtained from reference (67).
[c]Coordination number.
[d]A different preparation to illustrate the reproducibility of the EXAFS analysis.
[e]$FeOCl(TTF)_{1/8.5}$.
[f]$FeOCl(TTF)_{1/9}(tol)_{1/21}$.

Table 9. Debye-Waller factors (A^2) obtained from the best fit to the experimental data using theoretical functions

Compound[a]	Fe - Cl[b] Fe - O	Fe - $Fe_{\underline{c}}$[b]	Fe - $Fe_{\underline{a}}$[b]
FeOCl	0.069 0.035	0.069	0.074
TTF[c]	0.050 0.060	0.075	0.074
TTF[d]	0.072 0.040	0.088	0.095
TTN	0.100 0.041	0.073	0.068
TTT	0.078 0.045	0.063	0.061
TMTTF	0.092 0.047	0.075	0.059

[a]The intercalates are represented by the guest species.

[b]Debye-Waller factors for these interactions are listed in A^2.

[c]$FeOCl(TTF)_{1/8.5}$.

[d]$FeOCl(TTF)_{1/9}(tol)_{1/21}$.

It is necessary to consider the interactions between the chloride layer and the organosulfur molecule for the intercalates. The largest increase in Debye-Waller factors is for the Fe-Cl bond (0.069 A^2 for FeOCl vs about 0.100 A^2 for the intercalates). This increase can be attributed to strong interactions between the chloride ions and the intercalant. The $(FeO)_n^+$ sheet is "buried" by chloride ions on either side and the nearest chloride ion in the next layer is at about 4.9 A, which corresponds to the peak at r' = 4.6 in the Fourier transform of FeOCl. Upon intercalation this long distance peak is greatly reduced for all the intercalates as indicated by the arrow in Figures 15 and 16. In the intercalate, each Fe "sees" a different scatterer at this distance, either C, S, or H, thus decreasing the amplitude of this peak.

Hard Sphere Model

There are two interpretations of the X-ray and EXAFS data presented above. One has been presented in the literature[97] and assumes that the chloride ions of FeOCl and the sulfur atoms of the intercalant interact as hard spheres. The other interpretation of the data assumes a nonspherical electronic distribution on the sulfur atoms which allows the TTF molecule to have a "soft" sphere interaction with the chloride ion in the FeOCl lattice. Since the dimensions of the organic intercalants are known,[123-124] and the structure of the host determined from EXAFS and X-ray measurements, adequate information is available to determine the orientation of the intercalant within the host. The hard sphere model will be discussed below; it is based

solely on the X-ray and EXAFS data. The "soft sphere" model will be presented in a later section.

The original hard sphere model took into account a simple expansion of the layers, keeping the FeOCl cell intact. For TTF, it appeared that a monoclinic symmetry provided an adequate interpretation of the X-ray powder diffraction data. For TTN and TTT, doubling of the b axis was not considered. It has been noted[126] that the expansion of the FeOCl layers for amine intercalants is always less than the total van der Waals width of the intercalant. This was observed for all the tetrathiolene molecules in the present work. Before intercalation, a chloride ion in one layer is nested in a hole formed by four pseudo close-packed chloride ions of the layer below. Intercalation results in a large expansion of the FeOCl lattice along the b axis, and a 1% increase in the c axis.

The distance between sulfur atoms in adjacent rings in TTF is 3.4 A.[124] If one sulfur atom rests in a hole formed by four chloride ions of a FeOCl layer, then the sulfur on the adjacent ring must occupy the next hole along the c axis (3.30 A away). This arrangement is based on an excluded volume argument; inspection of orientations shows that the TTF molecule cannot align itself in any other direction without serious disruption of the FeOCl structure. Alignment of TTF along the c axis thus minimizes steric repulsion between the intercalant and the chloride layer, but results in some distortion of the lattice along the c axis. Given the observed increase in interlayer distance (5.7 A), the plane of the TTF molecule (width across the ring = 6.7 A) must be tilted by an angle $\theta = 25 \pm 5^{\circ}$ with respect to the perpendicular to

the chloride layers (Figure 21, top). Equations 6-12 below take into account the "nesting" of the molecule within the layers; r_S and r_{Cl} are the van der Waals radii for sulfur and chloride, respectively. Figure 22 illustrates the geometrical considerations involved in the calculations.

$$y = d_{int} - d_{FeOCl} + g \tag{6}$$

$$g = \sqrt{m^2 - p^2} \tag{7}$$

$$m = r_{Cl} + r_S \tag{8}$$

$$p = \sqrt{(a^2 + c^2)/2} \tag{9}$$

$$h = \sqrt{m^2 - p^2} \tag{10}$$

$$y' = y - g \tag{11}$$

$$\Theta = \cos^{-1}(y'/x) \tag{12}$$

y = distance from center to center of Cl^- plane.

y = g for unintercalated FeOCl.

x = S•••S distance in same ring.

To accommodate the sulfur atoms in TTF, the chloride layers shift laterally with respect to each other. The model predicts a shift in the layers of 25° (β = 115°). This result is consistent with an

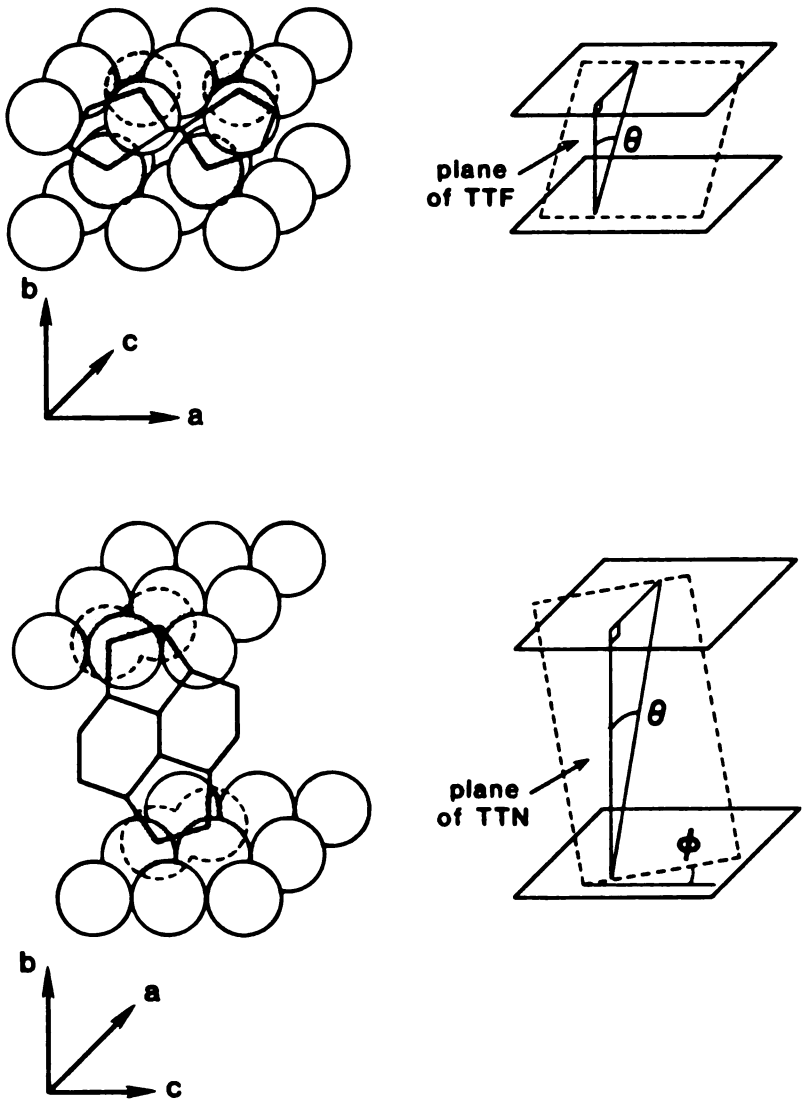

Figure 21. Schematic representation of the orientation of the (top) TTF (bottom) TTT, TTN molecules predicted by the hard sphere model

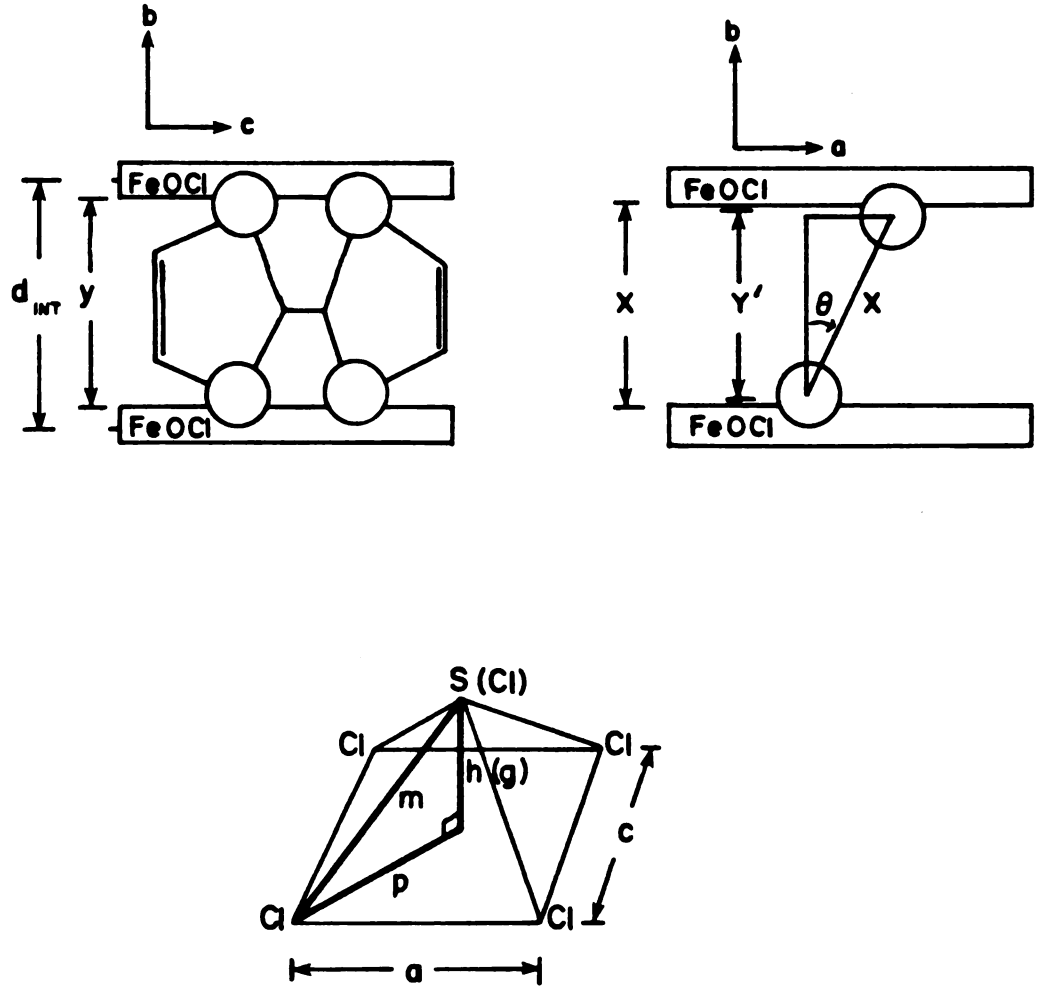

Figure 22. Geometrical basis for equations 6-12 for TTF orientation based on the hard sphere model

interpretation of the X-ray powder diffraction data in which the $FeOCl(TTF)_{1/9}(tol)_{1/21}$ lattice can be considered monoclinic (Table 6).

A slight variation of this model was necessary for TTT and TTN due to the short S-S bonded distance (2.10 Å).[124] If one sulfur of the S-S pair rests in a hole formed by four chloride ions, the bonded sulfur atom cannot occupy an adjacent hole along either the a or c axes. Steric repulsions between the host and intercalant are minimized if TTT and TTN orient themselves along the c axis, with the S--Cl repulsion forcing an elongation of the c axis. As a result, for TTT and TTN there are two angles of importance: $\Theta = 42 \pm 5°$, defined as the angle between the plane of the molecule and the b axis, and $\phi = 14 \pm 5°$, defined as the angle between the S-S bond and the ac plane. Equations 6-12 were used to determine the orientation of TTT and TTN in FeOCl, where x was calculated according to equations 13 and 14 and ϕ calculated according to equation 15. The geometrical considerations involved in the calculations are shown in Figure 23.

$$\phi + 90° = \omega + \delta \qquad (13)$$

$$x = d \cdot \sin \omega \qquad (14)$$

$$\phi = \sin^{-1}((h'-h)/(c/2)) \qquad (15)$$

The variables are defined similarly to those for TTF and Θ is determined by equation 12 using x as defined above. Figure 21 (bottom) illustrates the sulfur interaction with the chloride layer.

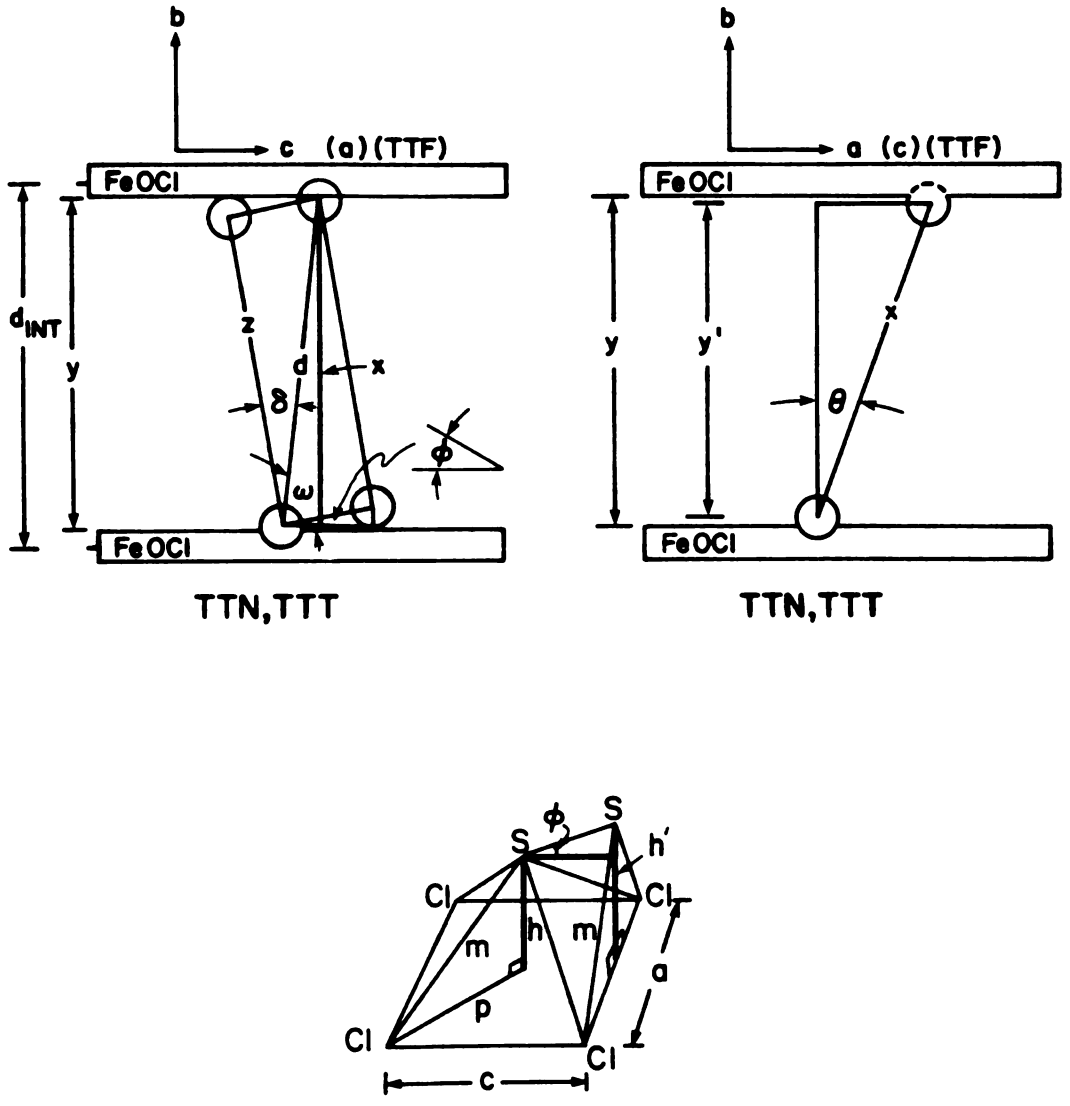

Figure 23. Geometrical basis for equations 13-15 for the TTN and TTT orientation based on the hard sphere model

Neutron Diffraction Results

The method of choice for the structure elucidation of the organosulfur molecule within FeOCl is neutron diffraction. X-ray powder diffraction data are dominated by the FeOCl layers, and give no direct information on the position or orientation of the intercalant. The independence of neutron scattering power upon atomic number, shown in Figure 24, is in contrast with the linear dependence of scattering amplitude with increasing atomic number for X-ray diffraction. Neutron diffraction data are complementary to the X-ray data, and have provided the first indication of long range ordering of the TTF molecule within FeOCl. The study required high neutron flux, a large data collection range (10 - 0.5 A) and resolution comparable to that of an X-ray powder experiment. The GPPD at IPNS has these characteristics and was chosen for the experiment. IPNS uses a proton accelerator and synchrotron to produce high energy neutrons by bombarding a spallation target (uranium). These neutrons are moderated to lower energies before they are used for diffraction. The GPPD is equipped with time-of-flight (TOF) detectors of which there are two sets at 30°, 45°, 60°, 75°, 90°, and 150°. The high resolution data are obtained from the 150° bank of detectors.[127] It should be noted that the only previous reliable structural data on any intercalation compounds were obtained at the ILL (Institute Laue Langevin) by neutron diffraction studies of $MS_2(C_5D_5N)_{0.5}$ (M = Nb, Ta).[34,35]

The experiments measured the neutron diffraction of FeOCl and of $FeOCl(TTF)_{1/8.5}$ and $FeOCl(TTF)_{1/9}(tol)_{1/21}$. The nondeuterated compound contained less than 0.5% H and incoherent scattering by H was

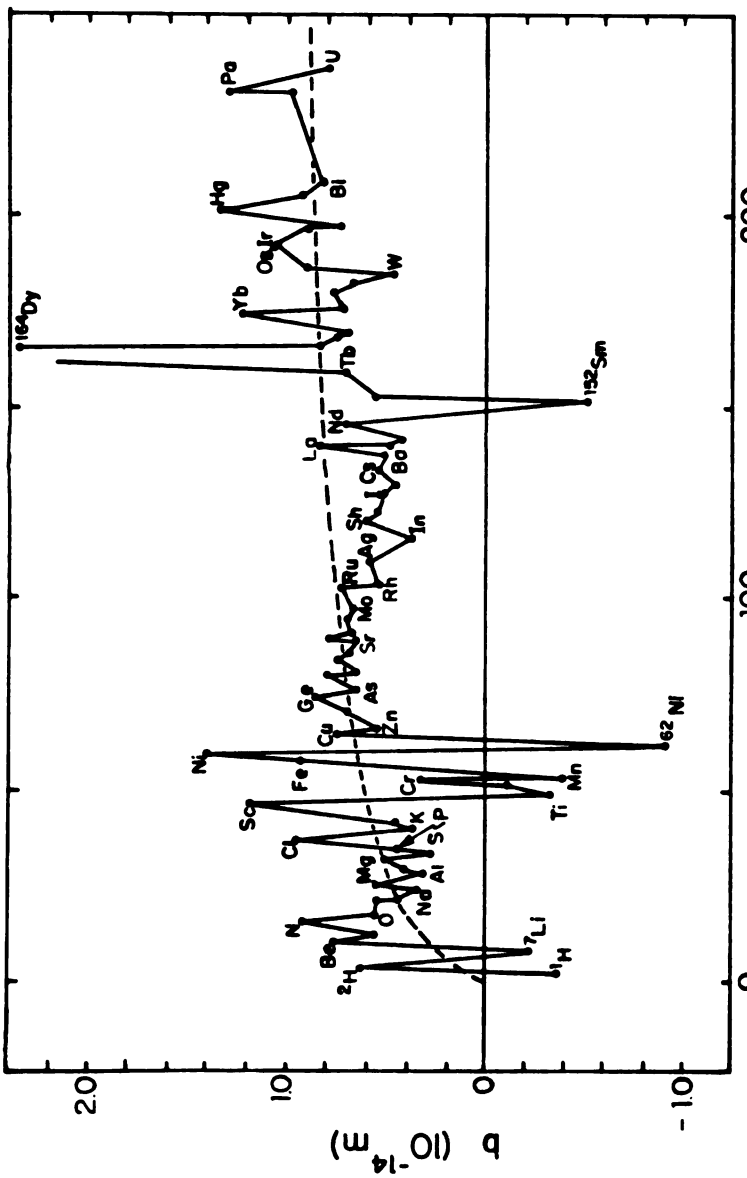

Figure 24. Nuclear scattering (barns) vs atomic weight

not a problem. Subsequent X-ray powder diffraction data on the d_4-TTF intercalate showed that it contains 5-10% pristine FeOCl. The $FeOCl(TTF)_{1/8.5}$. neutron data at both room temperature and 10 K were analyzed for superlattice reflections. No new Bragg peaks were observed in the neutron data compared to the X-ray diffraction data.

The FeOCl structure was refined satisfactorily for both the room temperature and 10 K data, by using the Rietveld technique of refinement.[66] The cell parameters and the atomic positions obtained are given in Table 10 along with the refined parameters. Figures 25 and 26 display the observed and calculated data as well as the difference between the neutron data and the Rietveld refinement for FeOCl at 300 and at 10 K.

The Rietveld refinement with the TOF data was performed by a modified version of a program originally written by Rietveld (1969).[66] Two programs (TOFPRP, TOFLS) fit the background, accounting for frame overlap reflection (TOF zero point, Z), peak shape, and scaling factor, and performed a full-matrix least-squares refinement of the crystal structure. (A frame overlap occurs when reflections generated by slow neutron from a previous pulse have a sufficiently long TOF to appear in the diffraction pattern.) The refinement is achieved by minimizing the sum of the squares of the weighted differences between the observed and calculated intensities for every point in the profile under the Bragg reflections by adjusting the structural and profile parameters.

The Rietveld method is a structure refinement, not a structure determination technique. The basic structure must be known or guessed

Table 10. Cell parameters, final positional, and thermal parameters for FeOCl at 300 and 10 K

	Space group cell constants Pmnm			
		a(Å)	b(Å)	c(Å)
300 K		3.7730(1)	7.9096(1)	3.3010(1)
10 K		3.7666(1)	7.8673(1)	3.2955(1)
	Positional and thermal factors			
		x	y	z
Fe	300 K	0.25	0.11555(8)	0.75
	10 K	0.25	0.11567(9)	0.75
O	300 K	0.25	-0.04795(15)	0.25
	10 K	0.25	-0.04823(16)	0.25
Cl	300 K	0.25	0.32961(7)	0.25
	10 K	0.25	0.33123(10)	0.25
			$B \times 10^3$	
Fe	300 K	13.8(4)	6.2(1)	14.6(5)
	10 K	5.5(4)	2.3(1)	4.5(5)
O	300 K	10.7(6)	7.35(2)	17.6(8)
	10 K	7.2(6)	3.4(2)	11.9(8)
Cl	300 K	43.8(6)	5.6(5)	19.8(1)
	10 K	14.8(4)	2.87(1)	7.93(6)

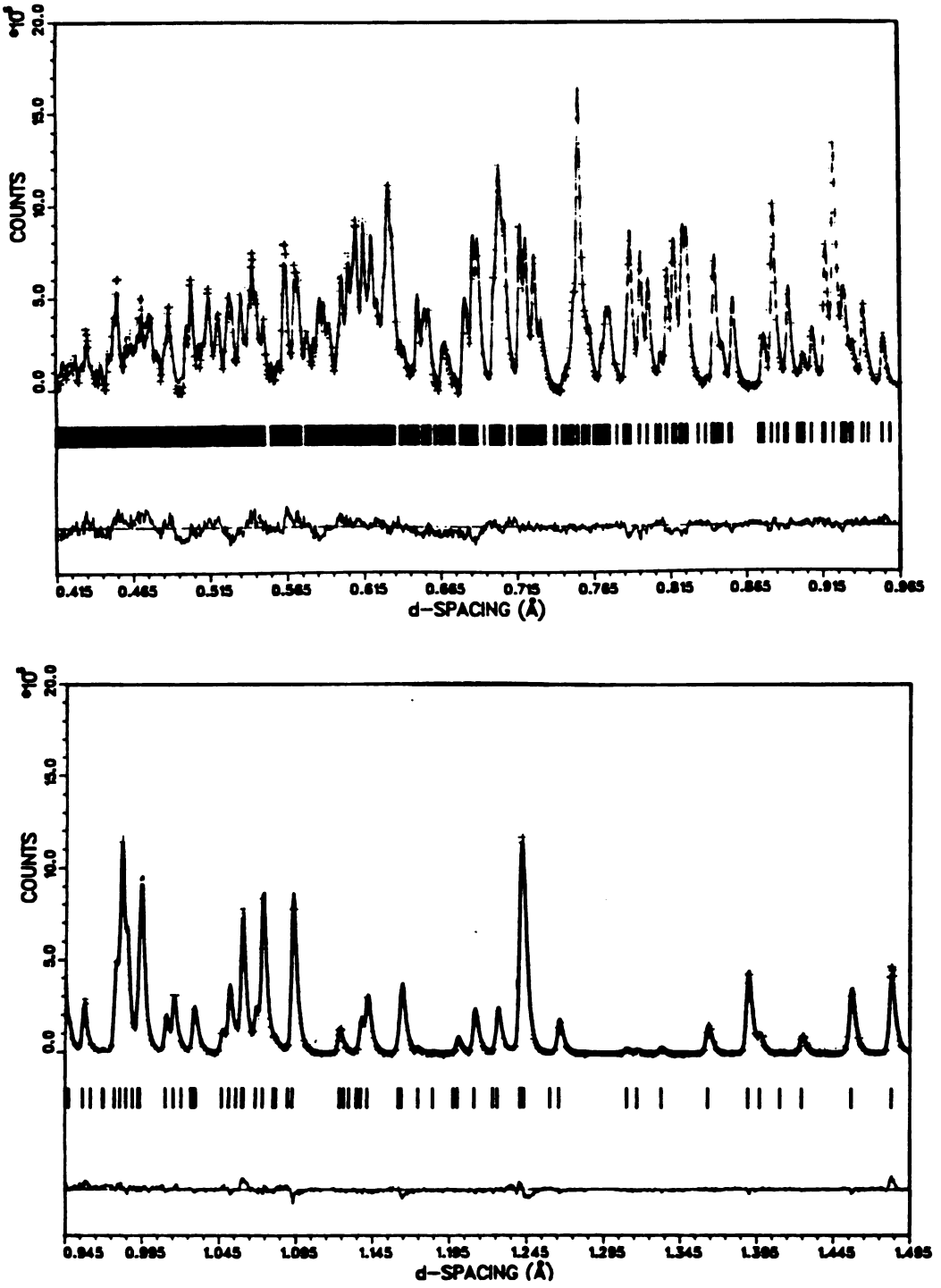

Figure 25. Profile refinement of the 150° TOF detector bank data for FeOCl at 300 K showing the low d region. The observed data are indicated by points and the calculated results by a solid line. Marks directly beneath the pattern indicate the positions of reflections. A difference curve appears at the bottom

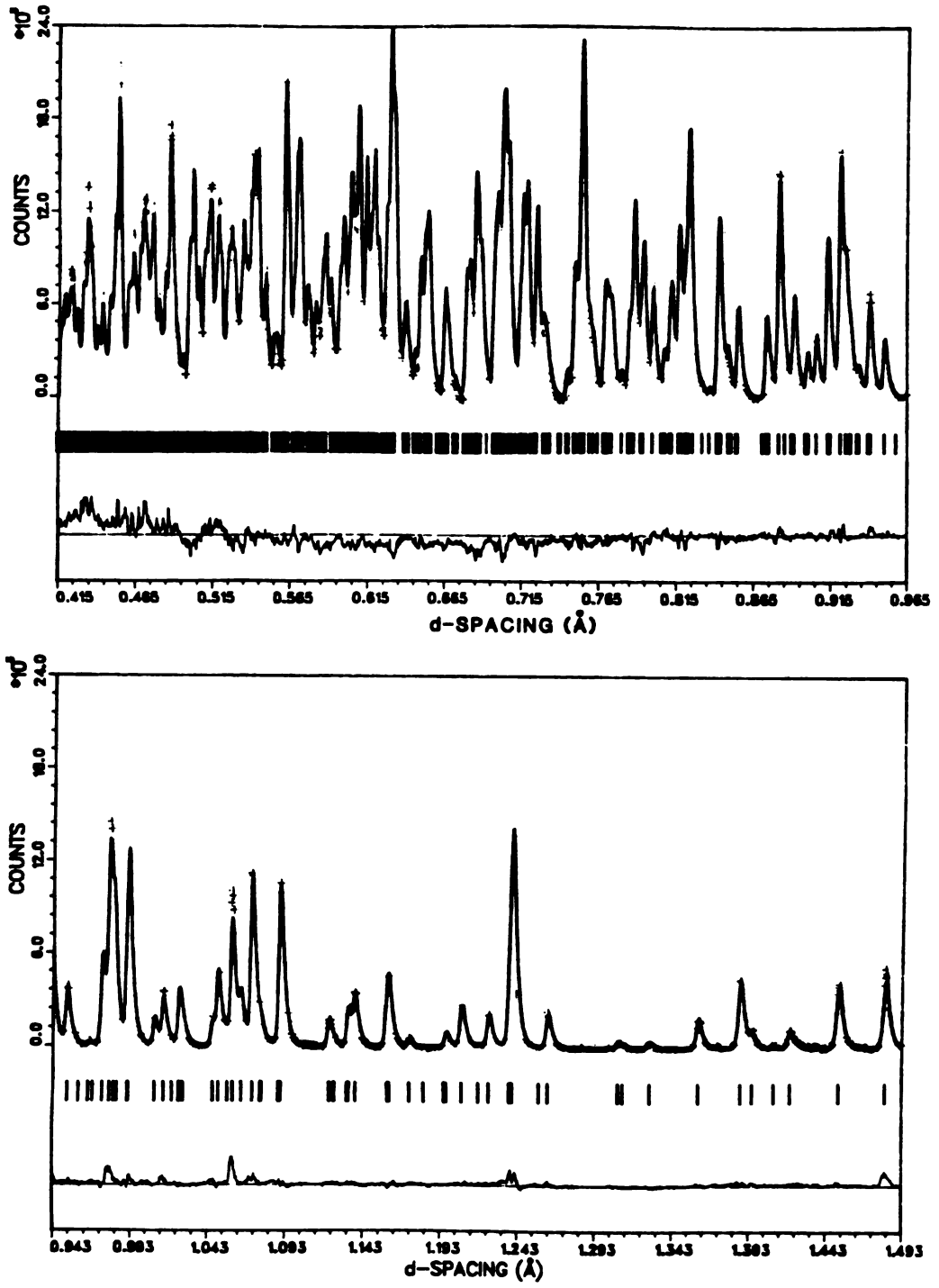

Figure 26. Profile refinement of the 150° TOF detector bank data for FeOCl at 10 K showing the low d region. The observed data are indicated by points and the calculated results by a solid line. Marks directly beneath the pattern indicate the positions of reflections. A difference curve appears at the bottom

at before the data can be fit. The peaks were fit by using TOFMANY, a computer program available at IPNS. This program derives the d spacing from equation 16.

$$tof(i) = difc*D(i) + difa*D(i)^2 + zero(k) \qquad (16)$$

where tof(i) is the time of flight data, difc, difa and zero(k) are instrumental parameters for the GPPD at the time of the experiment and D(i) is the d-spacing. The peak shape is computed from the profile parameters of the diffracted peaks by the convolution of a Gaussian peak with a hypothetical pulse shape composed of a rising exponential leading edge and a decaying exponential trailing edge.[128,129] From the sigma parameter obtained from the fit to the peak shape, full widths at half height could be compared to those of silicon (Figure 27). The diffraction peaks for $FeOCl(TTF)_{1/8.5}$ are not much broader than those for silicon, suggesting that the intercalate is well-ordered crystalline material.

The peaks were indexed by a computer-based method (TOFIDX) available at IPNS. Although there is usually not a unique solution, the program gives figures of merit that discriminate strongly between them. Lists giving apparently good agreement between observed and calculated d-values are of little use as a guide to the correctness of a proposed cell, as was observed for the $FeOCl(TTF)_{1/9}(tol)_{1/21}$ X-ray powder diffraction data. This is because such a comparison can be "improved" to any arbitrary degree simply by making a sufficient increase in the volume of the proposed cell.[130] A minimum of twenty diffraction lines is necessary to obtain reliable results and between 30 and 35 is the optimum number. The principles used in the program

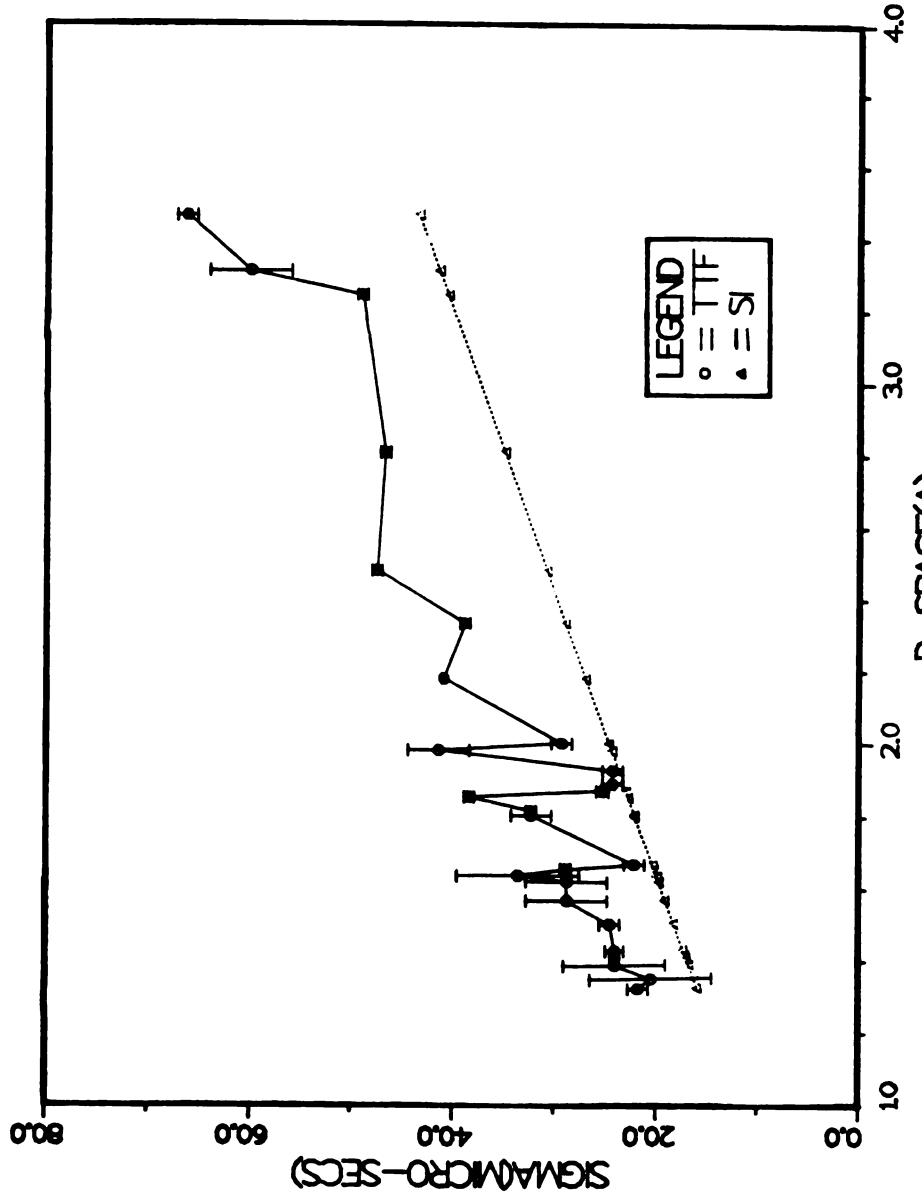

Figure 27. Graph of sigma vs d including error bars obtained from the fit of $FeOCl(TTF)_{1/8.5}$ and Si at 300 K

are discussed in the literature.[131] Twenty experimental reflections whose peak position had been determined from the peak fitting program were used. There were three solutions found by the indexing program (Table 11) for an orthorhombic cell.

Table 11. Cell constants and figures of merit obtained for twenty reflections from neutron powder diffraction data for $FeOCl(TTF)_{1/8.5}$

(a(Å)	b(Å)	c(Å)	Figure of merit	Unit cell volume
3.784	25.961	3.341	1614.9	328.17
10.016	12.986	3.854	14.2	501.31
6.688	25.959	4.585	11.5	796.02

A large figure of merit indicates a good fit: figures of merit less than 4 were disregarded. Although the parameters $\underline{a}$ = 3.784 Å, $\underline{b}$ = 25.961 and $\underline{c}$ = 3.341 Å adequately describe the unit cell (Table 12), it may not be the primitive cell. These parameters are based on the modification of the original host lattice dimensions, and thus provide a reasonable place to start fitting the data.

The model used in the refinement for the FeOCl layers was discussed previously: the alternate layers of FeOCl translate along the

Table 12. Observed and calculated d-spacings (A) of the neutron powder diffraction spectra for $FeOCl(TTF)_{1/8.5}$ with the proposed indexing scheme: $\underline{a}$ = 3.7836(4) A, $\underline{b}$ = 25.9629(3) A and $\underline{c}$ = 3.3410(4) A

d_{obs}(A)	h	k	ℓ	d_{calc}(A)
3.4676	1	3	0	3.4667
3.3128	0	1	1	3.3137
3.2452	0	8	0	3.2452
2.8099	0	5	1	2.8096
2.4827	0	7	1	2.4823
2.3366	1	4	1	2.3365
2.1834	0	9	1	2.1834
2.0029	1	11	0	2.0025
1.9828	1	8	1	1.9826
1.9280	0	11	1	1.9277
1.8918	2	0	0	1.8918
1.8720	2	2	0	1.8720
1.8551	0	14	0	1.8544
1.8157	2	4	0	1.8162
1.8026	1	10	1	1.8024
1.6705	0	0	2	1.6705
1.6566	0	2	2	1.6568
1.6377	1	12	1	1.6372
1.6220	0	16	0	1.6226
1.5701	2	5	1	1.5692
1.5049	1	3	2	1.5049
1.4301	2	9	1	1.4298
1.4164	1	17	0	1.4161
1.4055	0	10	2	1.4048
1.3893	0	12	1	1.3889
1.3509	1	9	2	1.3504
1.3241	0	18	1	1.3242

ac diagonal ((101) direction) by one-half unit cell to accommodate the intercalant.[39] The atomic positions were calculated for the hypothetical unit cell, and the atomic position parameters corresponding to the z coordinate were modified from the crystal structure of FeOCl[67] by multiplying the z parameter of FeOCl by the b axis of FeOCl, dividing by b of the intercalate, $FeOCl(TTF)_{1/8.5}$, and redefining the origin. A fit could be obtained with only Fe, O, and Cl atoms, resulting in a weighted profile of R = 8.9% (Figure 28). Similar fits could be obtained from using either space group Immm or I222 by refining 14 parameters (overall scale factor, cell constants (9), background parameters (2), and half-width parameters (2)). Obvious errors in intensities could not be accounted for by either space group. A Fourier synthesis was performed on the observed and calculated structure factor amplitudes. It was found in the Fourier difference map that there was significant nuclear density within the layers, which corresponds to the TTF molecule.

Upon inclusion of carbons representative of TTF (C has a scattering length of 0.665 barns (10^{-14} m) vs 0.285 barns for S), the R factor was reduced by one-third (R = 5.9%; structure factor reduced from 26.12% to 15.11%). Figure 29 shows the low d region for the observed and the calculated data as well as the difference curve for the Rietveld fit and the neutron data. Large isotropic thermal parameters for the carbon atoms were used to take into account the entire TTF molecule. Negative isotropic thermal parameters were obtained for the oxygen atoms. This could be due to an inadequate data set length or perhaps an error in the position of the oxygen atom.

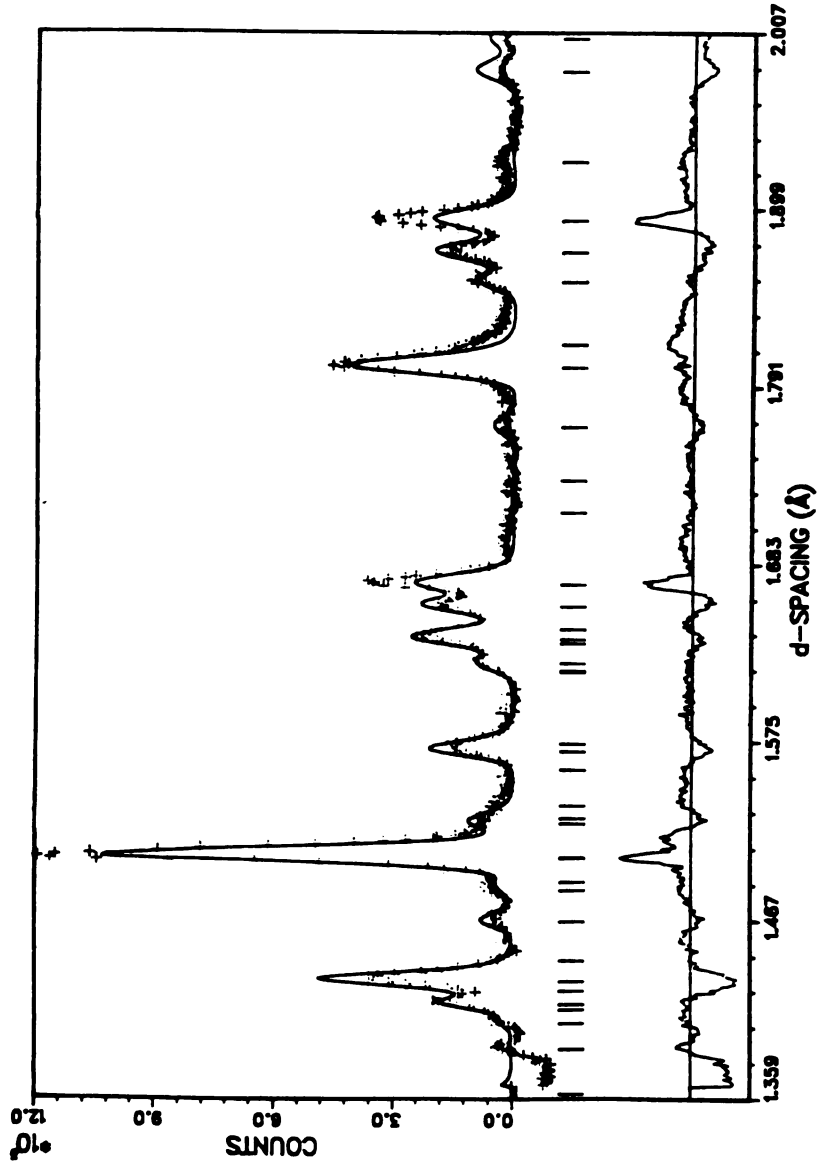

Figure 28. Profile refinement of the 90° bank for $FeOCl(TTF)_{1/8.5}$ using only Fe, O, Cl in refinement (low d region). The observed data are indicated by points, and the the calculated results by a solid line. Marks directly beneath the pattern indicate the positions of reflections. A difference curve appears at the bottom

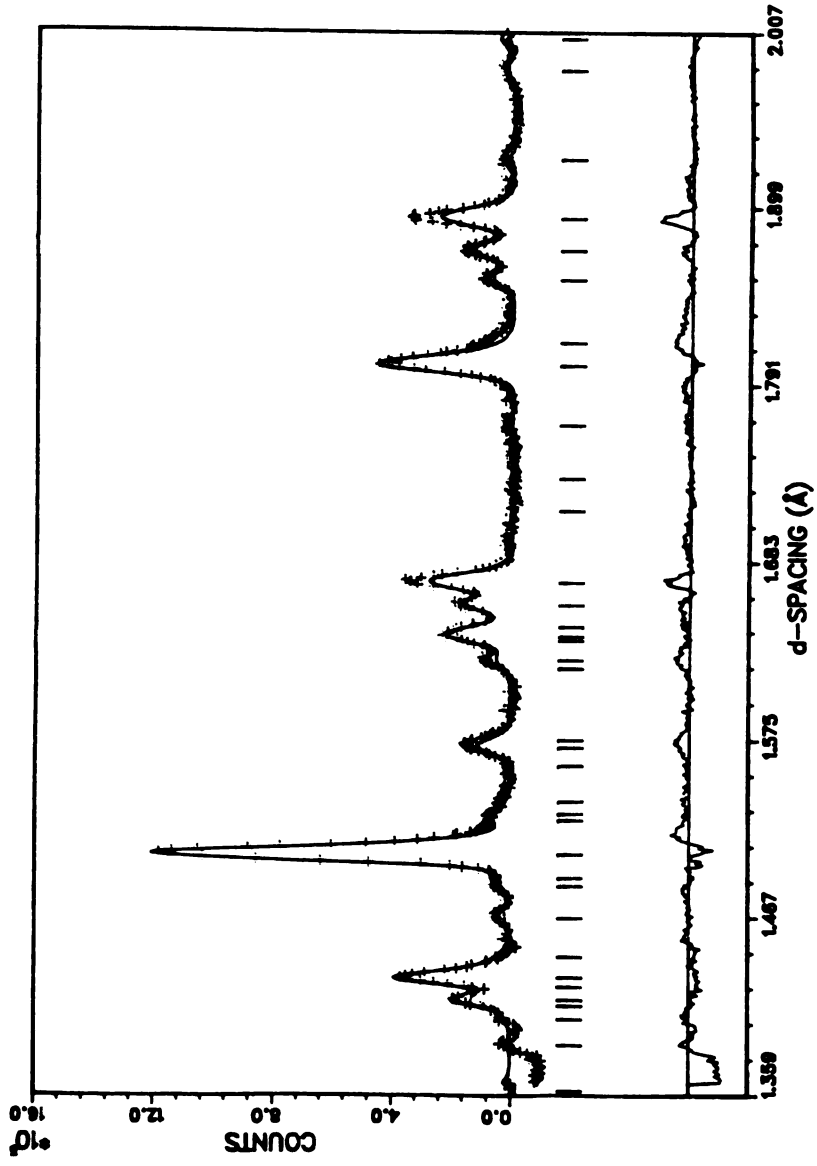

Figure 29. Profile refinement of the 90° bank for $FeOCl(TTF)_{1/8.5}$ including carbons (low d region). The observed data are indicated by points, and the calculated results by a solid line. Marks directly beneath the pattern indicate the positions of reflections. A difference curve appears at the bottom

The data set length was enlarged to about 1 A. The occupational parameters for the carbon atoms were allowed to vary. The data could be refined to a weighted R = 7.2%, which was good considering the incomplete description of the TTF molecule (Figure 30). Atomic positions used in the refinement are listed in Table 13. The data show some discrepancies in fitting the background, which can be attributed either to short range ordering or to incoherent scattering of the hydrogens. The low temperature data were not analyzed.

The $FeOCl(d_4\text{-}TTF)_{1/9}$ sample was run to eliminate the possibility of incoherent scattering, which may be causing the slow oscillation in the hydrogen data background. In the Rietveld analysis, the goodness of fit remained about the same as for $FeOCl(TTF)_{1/8.5}$. The lattice parameters obtained were $\underline{a}$ = 3.7857 (3) A, $\underline{b}$ = 26.016 (3) A and $\underline{c}$ = 3.43375 (4) A. The background deviations are similar to those found in the hydrogen data and indicate that there may be short range ordering contributing to the diffraction. No further analysis was done on this compound due to the presence of 5-10% pristine FeOCl, which affected the peak positions and intensities. IPNS has a program available for multiphase systems, which could be used once an adequate description of the intercalate is obtained.

From these data, it appears as if TTF is aligned along the $\underline{c}$ axis, but the complexity of including the full TTF molecule in the refinement has hindered a more detailed analysis. Once a complete refinement that includes the TTF molecule can be undertaken, the exact structure will be known. At the present stage, the structure of the FeOCl lattice of the intercalate could belong to either a Immm or an

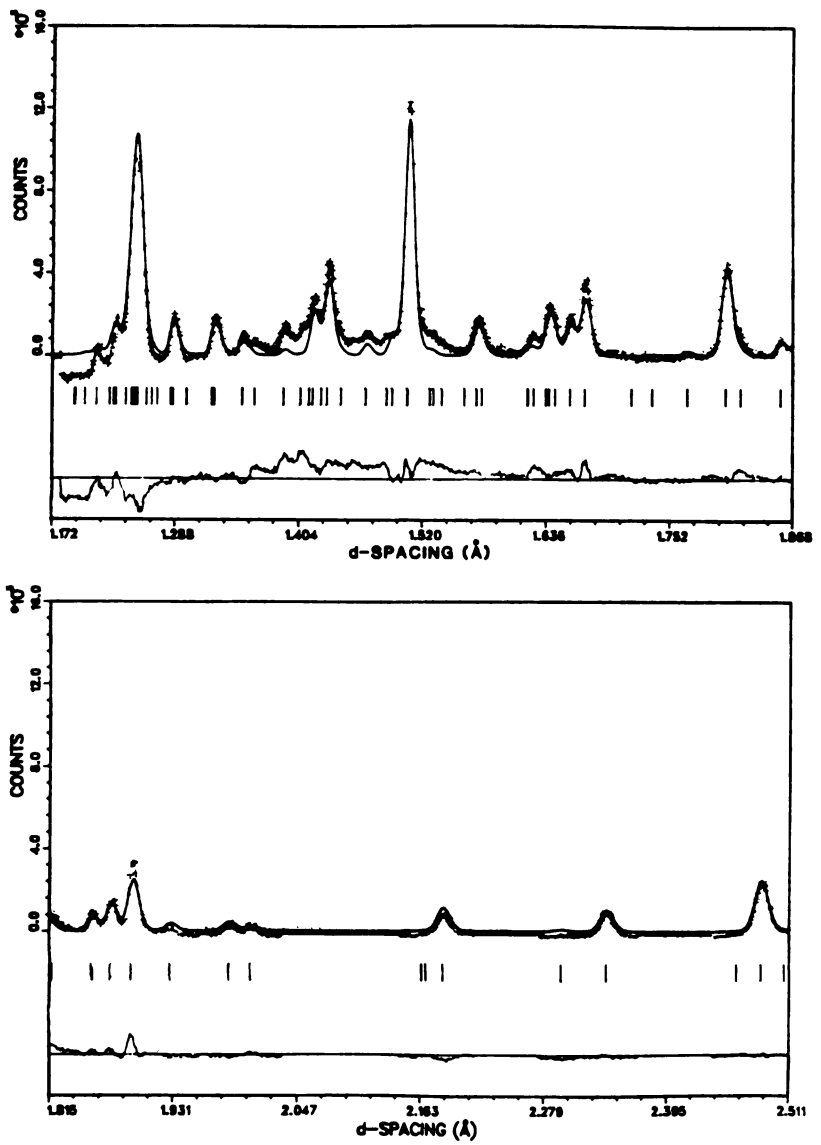

Figure 30. Profile refinement of 90° bank for $FeOCl(TTF)_{1/8.5}$ including data to 1.0 Å. The observed data are indicated by points, and the calculated results by a solid line. Marks directly beneath the pattern indicate the positions of reflections. A difference curve appears at the bottom

I222 space group. The neutron data provide direct evidence for long range ordering of TTF within FeOCl.

Table 13. Atomic positions refined for $FeOCl(TTF)_{1/8.5}$ including carbons, space group = Immm (data set length 3.80 - 1.0 Å, R = 7.2%)

Atom	x	y	z
Fe	0	0	0.2827
O	-0.5	0	0.2655
Cl	0.5	0	0.1509
C	0	0.5	0.0678
C	0	0	0

Soft Sphere Model

The results of the neutron powder diffraction data indicate that the conclusions of the hard sphere model are incorrect. Careful evaluation shows that doubling the b axis reduces the discrepancies between the observed and calculated d spacings of the mixed reflections as was shown in Table 7. The model proposed for the metallocene intercalates, in which the FeOCl layers expand and move laterally along the ac plane, also appears to be valid for the organosulfur intercalates. Tilting the TTF molecule is no longer a valid assumption, since the layers are oriented as shown in Figure 31. Figure 32 shows the ab plane of FeOCl: with the chloride layers eclipsed, tilting of the TTF molecule cannot explain the observed interlayer distance and the relative orientation of the layers. Both the X-ray powder data and the EXAFS data indicate that the intercalates (other than $FeOCl(TTT)_{1/9}(tol)_{1/23}$) are well defined solids with layers that are apparently undistorted. This supports the hypothesis that the layers are "locked" by the intercalant.

The TTF molecule is perpendicular to the layers as shown in Figure 32, locking the layers in place. This places the sulfur atoms of TTF 3.15 A away from a chloride ion, much further than a typical sulfur-chlorine bond (1.99 A for SCl_2 and 2.06 A for S_2Cl_2)[132,133] but well within the sum of the van der Waals radii (3.6 A). It has been determined from electron density maps[134] and from theoretical calculations[135] that the selenium atoms in TMTSF have sp^3 hybridized orbitals arranging the electronic density in a tetrahedral orientation with respect to the selenium. Since sulfur and selenium are similar,

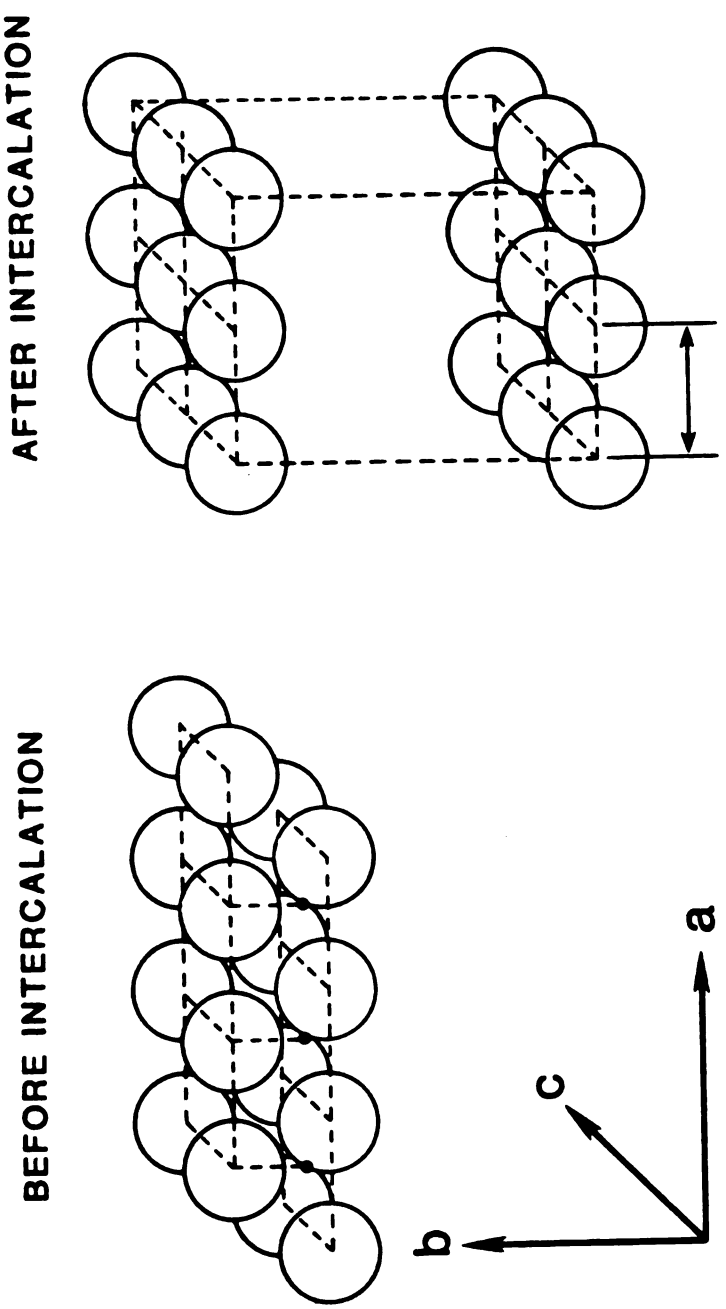

Figure 31. Illustration of the lateral shift of the chloride ion layers of FeOCl upon intercalation

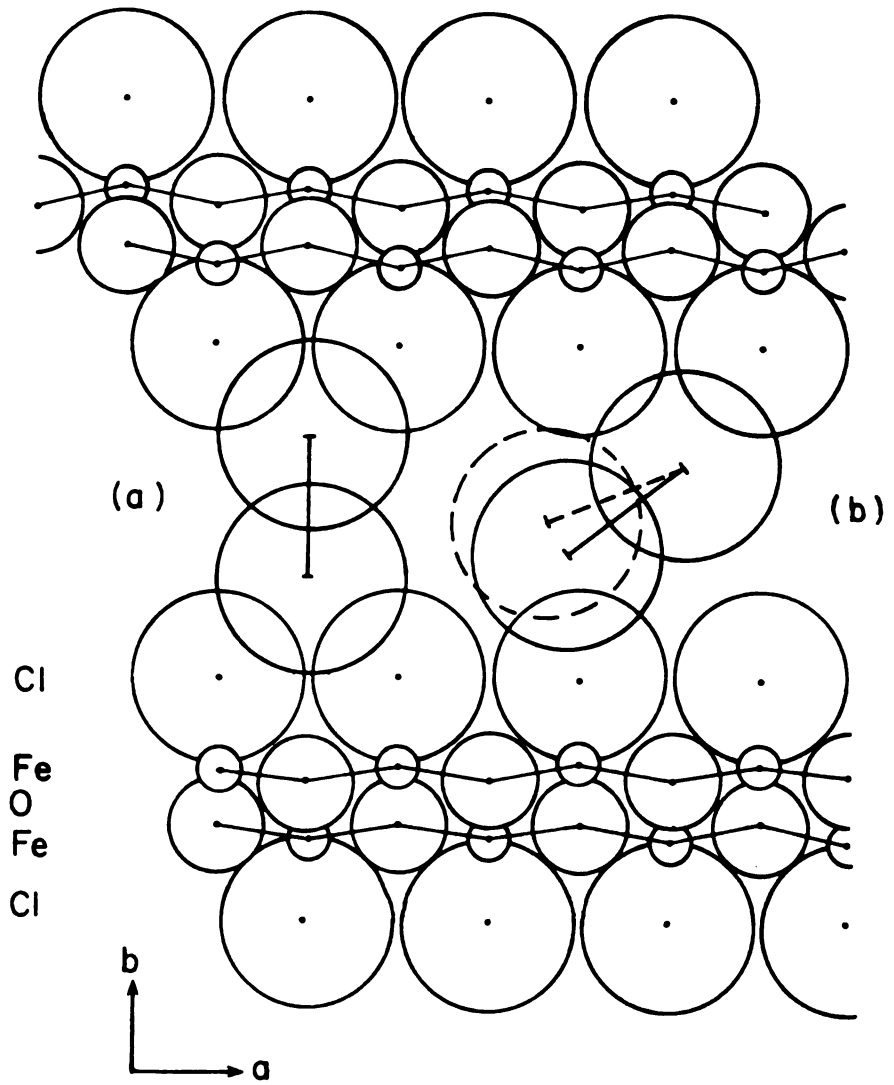

Figure 32. Schematic representation of the possible orientation of TTF taking into account the lateral shift of the layers for both a (a) soft and (b) hard sphere model

the electronic distribution for the sulfur molecule in TTF might be similar to that of TMTSF. Thus, the electronic density of the sulfur atom of TTF is directed between the two chlorides that are along the c axis and further minimizes any type of repulsive interaction between the sulfur of TTF and the chloride ions of the FeOCl layers. This is the first time a model other than the hard sphere model has been considered for any intercalation compound.

For TMTTF, the van der Waals radius of the molecule is estimated to be 2.0 Å. The molecule must be parallel to the layers to account for the observed 3.7 Å interlayer distance. The electronic density on sulfur, if considered to be located in sp^3 hybridized orbitals, again gives minimal interactions between the chloride ions and the sulfur atom in the TMTTF molecule.

The orientations of TTN and TTT are more difficult to predict. As in the hard sphere model, TTN and TTT still must tilt at an angle ϕ (defined in the hard sphere model) to accommodate the short S-S bond (2.10 Å). The molecule must be aligned along the c axis and be tilted at an angle $\phi = 30°$ as shown in Figure 33. TTT, with its bulky naphthacene core, introduces disorder within the layers which may give rise to fewer and broader Bragg peaks.

The maximum stoichiometry is predicted to be $FeOCl(TTF)_{1/8}$ by the hard sphere model; and for the soft sphere model, it is also $FeOCl(TTF)_{1/8}$. The stoichiometry is obtained by simple geometric considerations (Figure 34); the soft sphere model predicts that the TTF molecule occupies a minimum of 4 unit cells along the c axis and

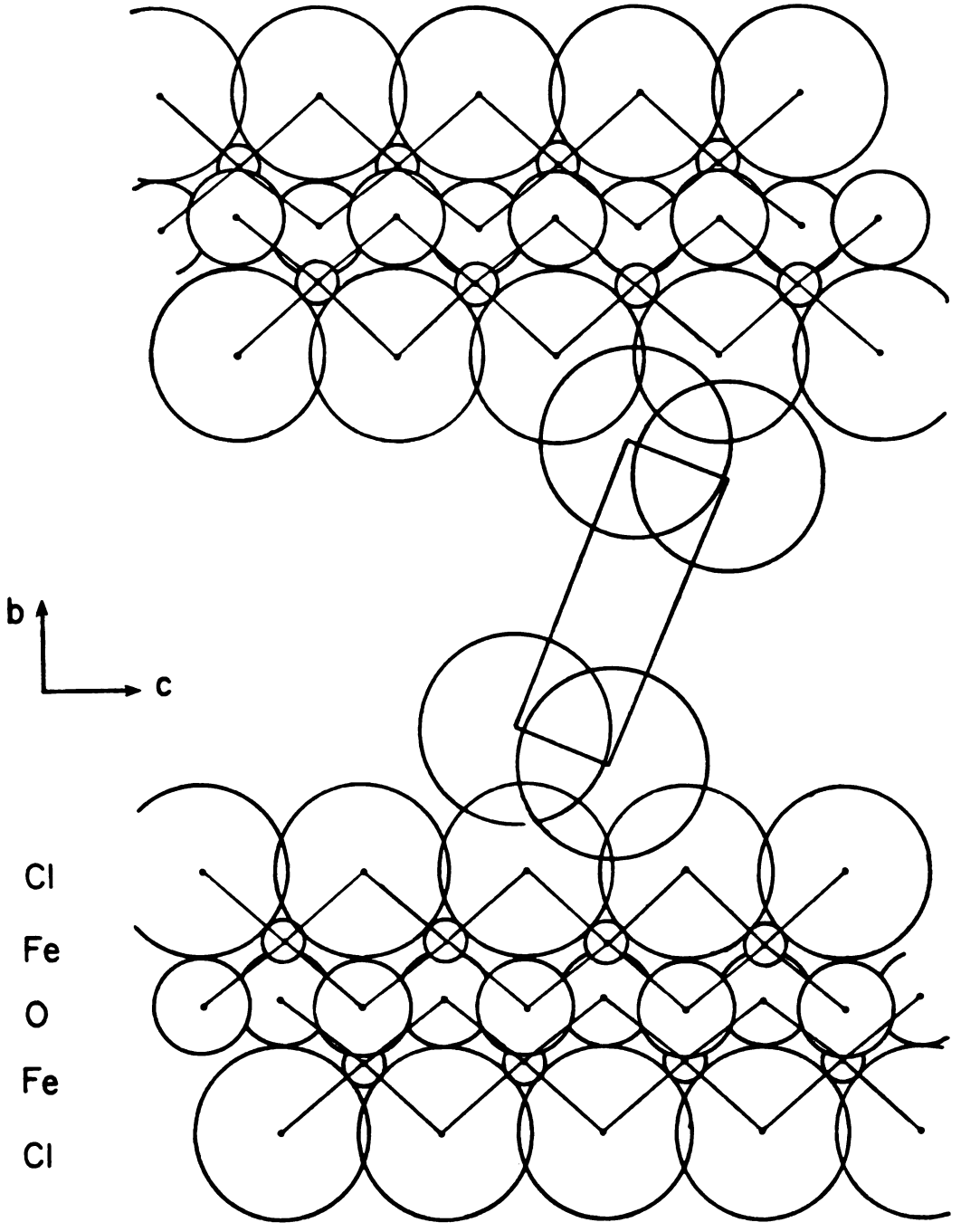

Figure 33. Schematic representation of the orientation of TTN and TTT taking into account the lateral shift of the FeOCl layers

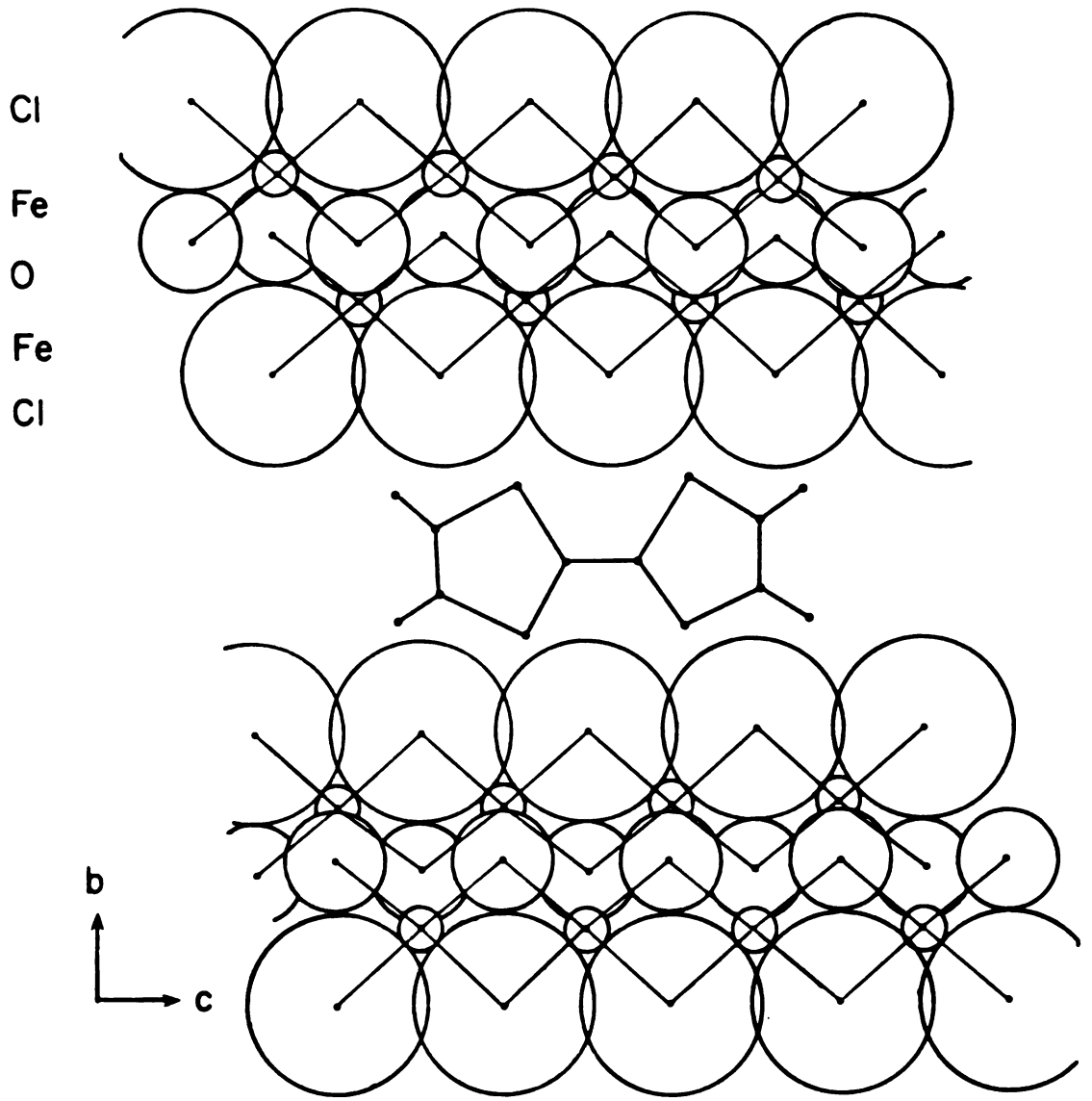

Figure 34. Illustration of the TTF molecule on the bc plane showing the number of cells the molecule spans

one unit cell dimension along the a axis. There are 2 FeOCl units per unit cell. The maximum experimental stoichiometry obtained to date is $FeOCl(TTF)_{1/8.5}$. In the soft sphere model the next TTF molecule is 3.78 A away (one unit cell along a), in the hard sphere model it was assumed the distance between TTF molecules was the sum of the van der Waals radii (3.6 A). Both models indicate that the TTF molecule is approximately close packed within the layers, but only the soft sphere model takes into account the lateral movement of the FeOCl layers.

SOLID STATE NMR STUDIES

Solid state NMR has been used to infer the relative orientations of guest species within a host lattice.[37,100,95,106,136,137] Wideline NMR studies on TaS_2(cobaltocene)$_{1/4}$ provided additional evidence in support of the proposed model based on steric arguments, in which the C_5 symmetry axis of the cobaltocene molecule lies parallel to the TaS_2 layers.[37] NMR spectroscopy provides complementary information to the neutron diffraction studies on FeOCl(TTF)$_{1/8.5}$ and FeOCl(d_4-TTF)$_{1/9}$, thus aiding our understanding of the long and short range ordering of TTF within FeOCl. In addition, NMR can provide information on the molecular dynamics of the intercalant, as well as information on inter- and intramolecular interactions between nuclei in the TTF molecules. Single pulse Fourier transform ^1H NMR spectra were obtained for TTF, FeOCl(TTF)$_{1/8.5}$ and FeOCl(d_4-TTF)$_{1/9}$. ^{13}C-^1H cross polarization, magic angle spinning (CPMAS) spectra were obtained for the samples already mentioned, as well as for the TTF(CA) salts (both the segregated and mixed stack structures) and for $TTF_3Br_2 \cdot 2H_2O$.

The major obstacle in obtaining undistorted wideline spectra of solids is the slow recovery of the receiver, which produces dead-time. This limitation does not allow one to collect the initial part of the free induction decay (FID), which for very broad line spectra causes

substantial distortion of the baseline.[138] Also, more rapid digitization than is commonly used in solution FT NMR is needed. Use of an echo technique overcomes the dead-time problem. Both single pulse and echo experiments will be discussed and compared.

All contributions to an NMR line can be classified as homogeneous or inhomogeneous. High resolution spectra of solutions are homogeneous in general; those of solids may be either. An inhomogeneous line is one in which the separate contributions to the line can be identified. These contributions result from anisotropies in quadrupolar interactions or chemical shifts: crystallites with different orientations with respect to the static magnetic field contribute to different parts of the line.

One method to determine whether the line is broadened homogeneously or inhomogeneously is to irradiate and saturate a specific spot in the line with a large, coherent H_1 field. Immediately after the irradiation, the line is detected either by constant wave or, in this case, pulse FT NMR; an inhomogeneous line will have a "hole" burned into it.[138] This method was used to determine the homogeneity of the spectral line for the $FeOCl(TTF)_{1/8.5}$ sample.

^1H NMR

The ^1H NMR spectrum of solid TTF obtained by Fourier transforming the free induction decay (FID) following a single radio frequency pulse is shown in Figure 35(a,b) (Table 14 defines the abbreviations used in the parameter listing). It consists of a relatively sharp component at about 4 ppm (relative to TMS in deuterated chloroform,

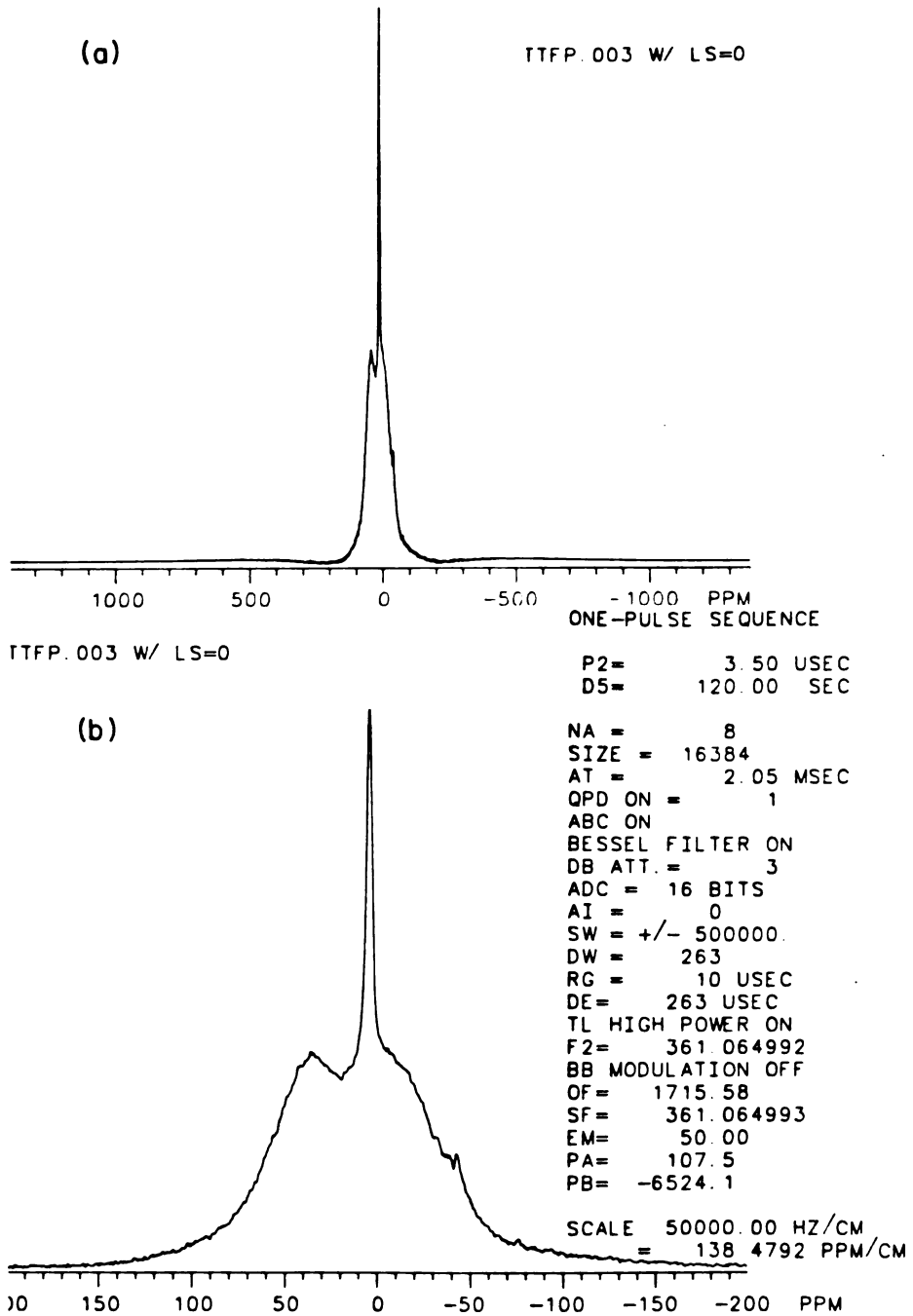

Figure 35. (a) FT ^{1}H NMR of TTF obtained from a single pulse radio frequency, (b) Expanded scale (Table 14 defines the abbreviations used in the parameter listing)

Table 14. Definitions of the abbreviations used in the parameter listing for the NMR spectra

P2	=	tipping pulse time
D5	=	delay between scans
NA	=	number of scans
Size	=	number of points in spectrum
AT	=	time for one scan
QDP ON	=	pulse phase cycling and
ABC	=	data routing
Bessel filter DB ATT.	= }	noise filter
ADC	=	computer word size
AI	=	scaling factor
SW	=	sweep width (Hz)
DW	=	time between points
RG	=	receiver gate (not used)
TL	=	transmitter level
F2	=	decoupler frequency
BB	=	decoupler mode
OF	=	frequency assigned to center of spectrum
SF	=	radio frequency (rf) of tipping pulse
EM	=	apodization function value
PA	=	phase correction
PB	=	phase correction

used as an external standard) on top of a broader doublet. The spectrum of only the sharp component can be obtained by removing the first 100 μs of the FID and Fourier transforming the remainder (Figure 36(a)). The sharp component may then be removed by subtracting its spectrum from the initial single pulse spectrum (Figure 35); a doublet is obtained, which has a splitting of 15 kHz (Figure 36(b)). The line widths and relative intensities of the two components are shown in Table 15. The doublet obtained is referred to as a Pake doublet, which arises when the dipolar interaction between a pair of spin 1/2 nuclei (^1H) is the dominant magnetic interaction.[139] This is most likely the case between the adjacent protons of TTF. This doublet is centered at about 12 ppm (relative to TMS in deuterated chloroform), in contrast to the ^1H spectrum of TTF in solution, which consists of a singlet at 6.2 ppm. The reason for this chemical shift difference between the solid and solution spectra may be the presence of a large ring current effect due to TTF stacking in the solid. Ring current shifts of this magnitude and direction have been seen in large aromatic rings in solution.[140]

Removing the first 100 μs of the FID results in isolating the sharp component, indicating that the decay of the free induction signal associated with this component is much slower than that associated with the broad component. The sharp spectral component may be due to a relatively mobile population of TTF molecules, possibly located at crystal defects, or to absorbed cyclohexane (obtained from the recrystallization), or to water. Assignments based on the solution spectra of cyclohexane or water cannot be applied to the solid,

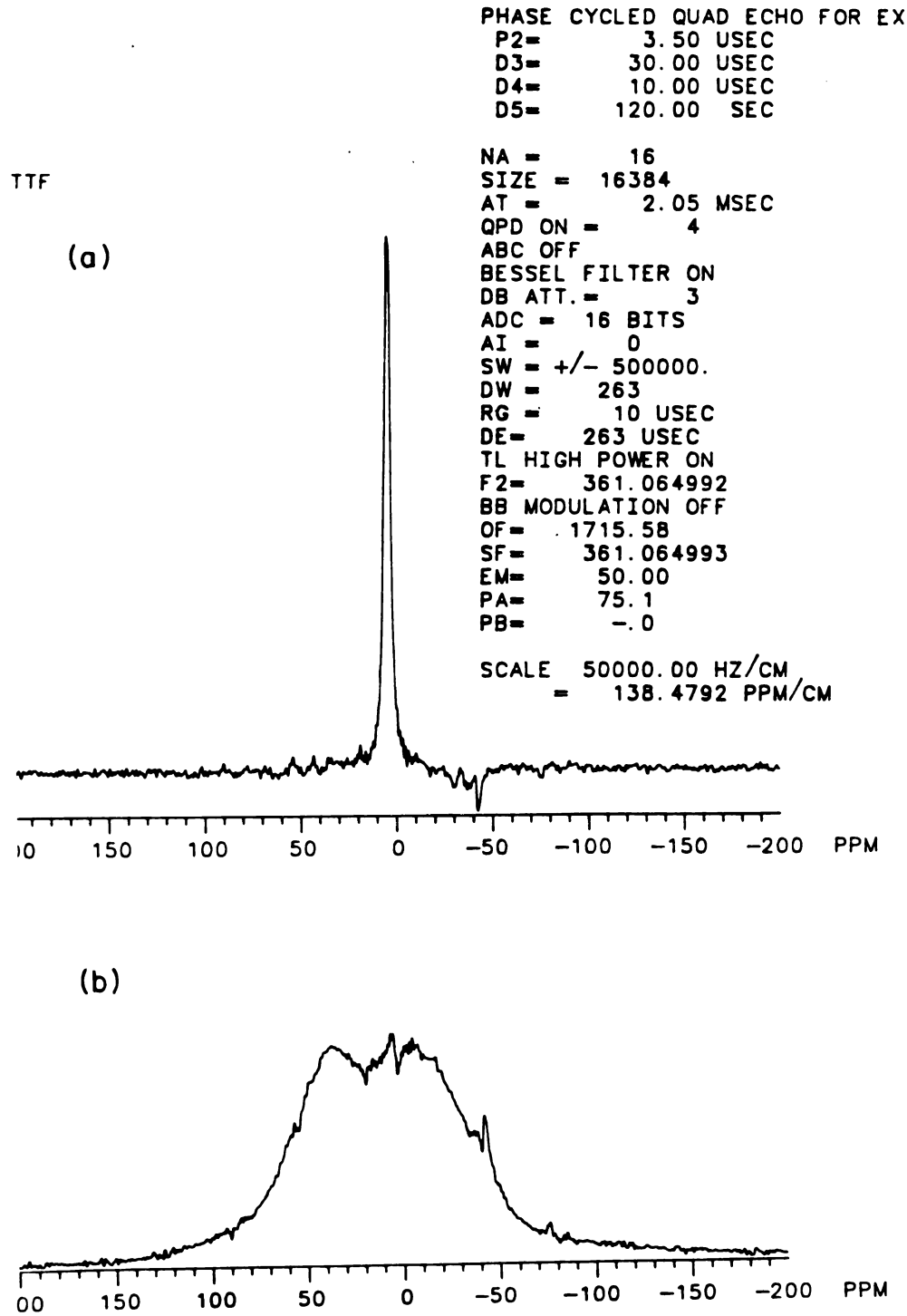

Figure 36. The ^{1}H FT NMR spectrum obtained for TTF (a) after removing the first 100 μs of the FID, (b) by subtraction of (a) from the full FT NMR spectrum of TTF

Table 15. Linewidths and relative areas of the single pulse ^1H spectrum of TTF

Spectral component	Full linewidth at half height (Hz)	% of total spectral area
sharp	1285	7
broad	35×10^3	93

due to experimental uncertainty and the lack of consideration of bulk susceptibility effects.

In an attempt to obtain less distorted spectra, echo experiments were performed. The most common pulse sequence used to produce echoes in solids is Θ_0-τ-Θ_{90}, where Θ is the pulse angle (the subscripts indicate the relative phases of the pulse and τ is the time between pulses).[138,141] Since the Nicolet 360 MHz spectrometer at the University of Virginia is not capable of providing 90° pulses that uniformly excite the entire spectral frequency range of interest, pulse times (and therefore angles) were decreased until distortion was minimized. Figure 37 shows the spectrum of solid TTF obtained with a Θ_0-τ-Θ_{90} sequence. When compared with the single pulse spectrum, the broad component obtained by the echo experiment is narrower and has reduced intensity relative to the sharp component. The linewidths and relative intensities of the two components are shown in Table 16. The

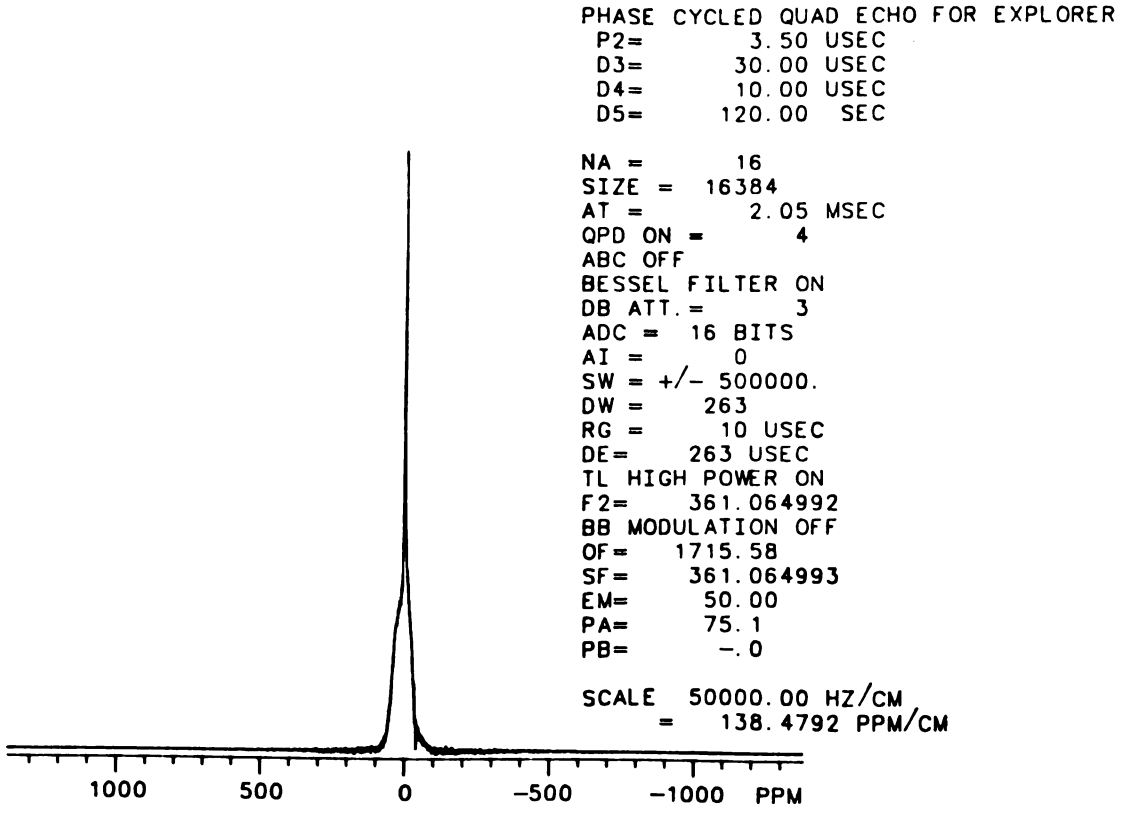

Figure 37. ^1H FT NMR spectrum for TTF obtained by employing a Θ_0-τ-Θ_{90} pulse sequence

Table 16. Linewidths and relative areas of the Θ_0-τ-Θ_{90} ^1H spectrum of TTF

Spectral component	Full linewidth at half height (Hz)	% of total spectral area
sharp	1316	16
broad	23×10^3	84

presence of the sharp component can be used as an internal intensity standard to compare the broad components in the single pulse and echo spectra. Tables 15 and 16 show that the ratio of sharp to broad component intensities is a factor of two greater in the Θ_0-τ-Θ_{90} echo spectrum than in the single pulse spectrum. A considerable portion of the broad component is lost in the echo spectrum due to transverse magnetization decay during the time between the first pulse and the echo peak. The spectrum obtained following a Θ_0-τ-Θ_0 sequence is shown in Figure 38. The spectrum is almost identical to the Θ_0-τ-Θ_{90} spectrum, except that the broad component is 180° out of phase with respect to the same component of the Θ_0-τ-Θ_{90} spectrum. This is expected when strong intra- and intermolecular spin 1/2 homonuclear dipole interactions are present.[142]

One-pulse, Θ_0-τ-Θ_{90} and Θ_0-τ-Θ_0 ^1H spectra of $FeOCl(TTF)_{1/8.5}$ are shown in Figures 39-41. These spectra consist of at least two

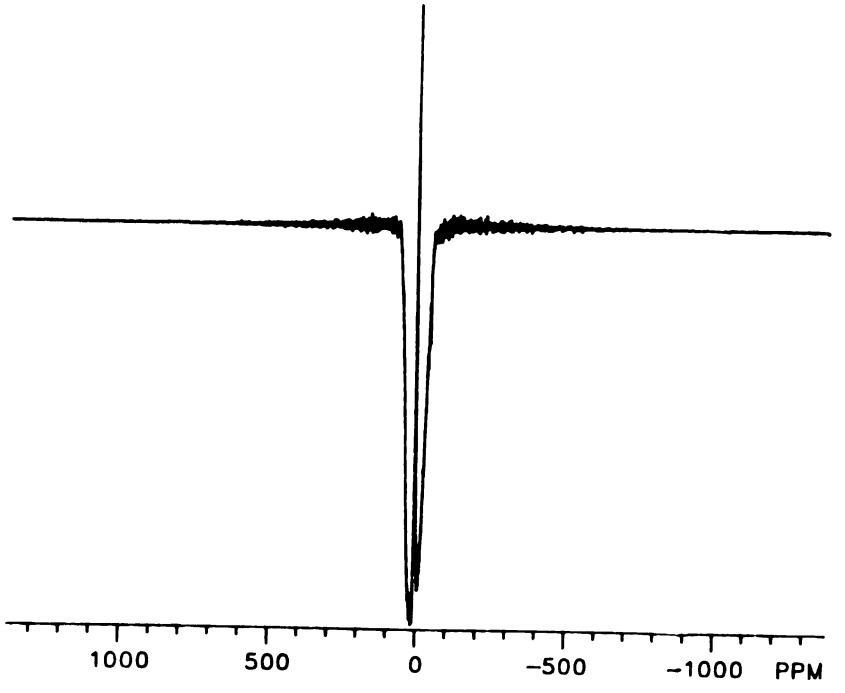


```
90XT90X ECHO FOR EXPLORER
 P2=        3.50 USEC
 D3=       30.00 USEC
 D4=       10.00 USEC
 D5=      120.00  SEC

NA =         16
SIZE =    16384
AT =        2.05 MSEC
QPD ON =       4
ABC OFF
BESSEL FILTER ON
DB ATT.=       3
ADC =  16 BITS
AI =        -1
SW = +/- 500000.
DW =     263
RG =      10 USEC
DE=     263 USEC
TL HIGH POWER ON
F2=     361.064992
BB MODULATION OFF
OF=    1715.58
SF=     361.064993
EM=      50.00
PA=     296.2
PB=         .0

SCALE   14709.47 HZ/CM
      =     40.7391 PPM/CM
```

Figure 38. ^1H FT NMR spectrum obtained for TTF by a Θ_0-τ-Θ_0 pulse

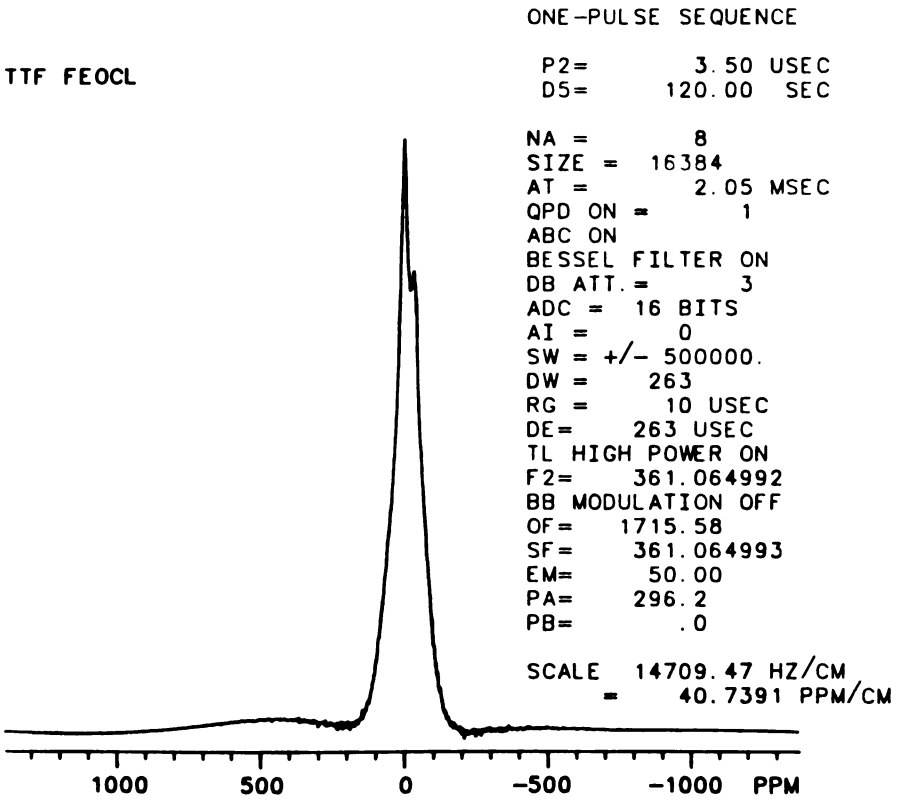

Figure 39. ^{1}H FT NMR spectrum obtained for $FeOCl(TTF)_{1/8.5}$ obtained by a single radio frequency pulse

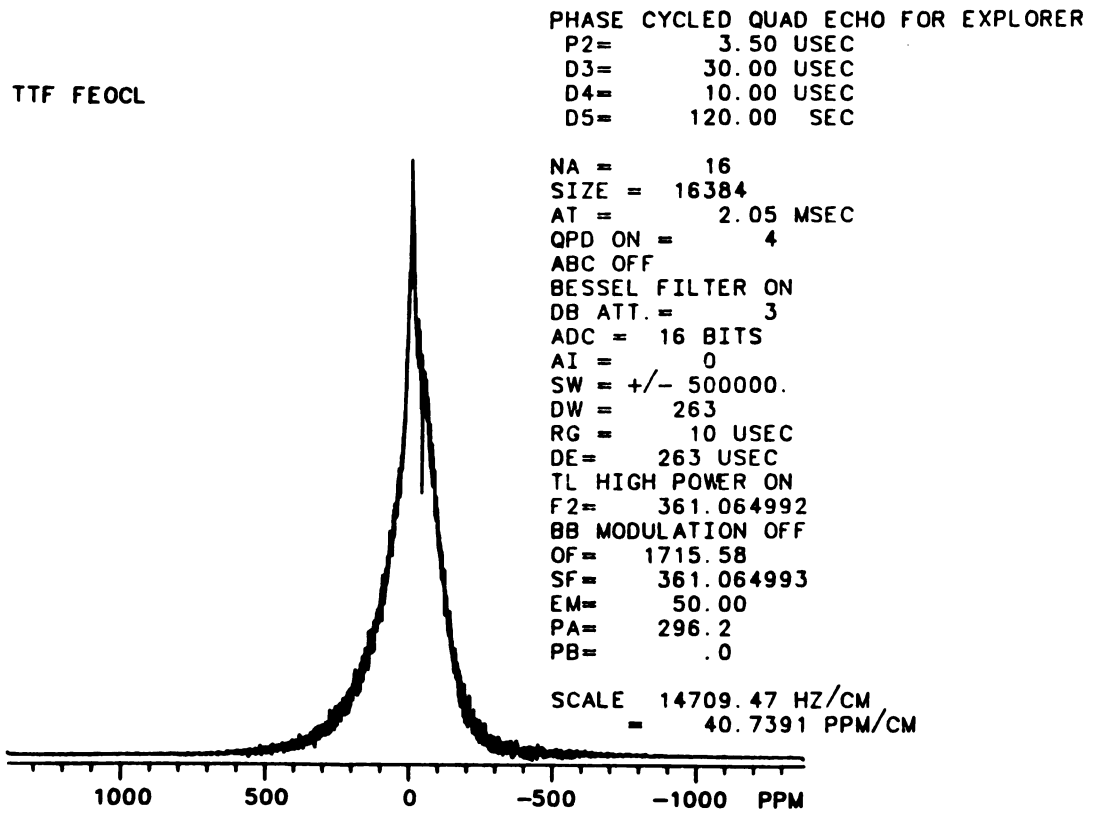

Figure 40. ^1H FT NMR spectrum for $FeOCl(TIF)_{1/8.5}$ obtained by a Θ_0-τ-Θ_{90} pulse sequence

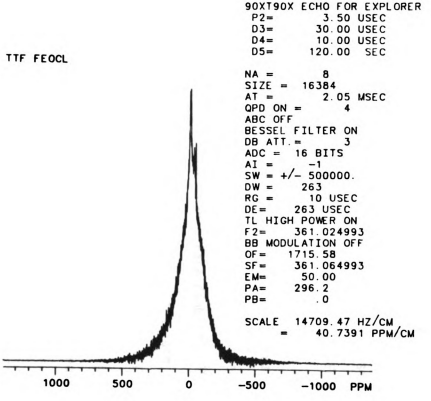

Figure 41. ^1H FT NMR spectrum for $FeOCl(TTF)_{1/8.5}$ obtained Θ_0-τ-Θ_0 pulse sequence

components, as shown by a sharp and broad line. Table 17 lists the relative intensities and linewidths of the two components. The sharp component is at about 1 ppm (relative to TMS in deuterated chloroform) and may be due to mobile TTF or absorbed solvent. Similar ^1H spectra have been observed for pyridine and picolines intercalated into VOCl.[95] In the case of VOCl, the sharp component was attributed to mobile intercalant molecules at crystal defects. The one-pulse spectrum appears to be less broad and somewhat distorted relative to the echo spectra, particularly at the base. The echo spectra are probably closer approximations to the true NMR spectrum of $FeOCl(TTF)_{1/8.5}$, due to the dead-time of the receiver which affects the baseline. The broad component of the $FeOCl(TTF)_{1/8.5}$ echo spectra is considerably broader than its counterpart in the TTF spectrum, and appears to be a single Gaussian line rather than a Pake doublet. This indicates that the magnetic interactions that determine linewidth in $FeOCl(TTF)_{1/8.5}$ and TTF are quite different. Assuming that the TTF molecules in $FeOCl(TTF)_{1/8.5}$ are at best closest-packed, the rigid lattice second moment was calculated using Van Vleck's formula (equation 17). Assuming a polycrystalline sample and accounting for the nuclei of other atoms which are not at resonance with the proton nuclei reduces Van Vleck's equation to the expression shown in equation 18.[143]

$$(\Delta H)^2 = \int_0^\infty (H-H)^2_{av} f(H) dH \qquad (17)$$

Table 17. Linewidths and relative area of echo ^1H spectra for $FeOCl(TTF)_{1/8.5}$

Pulse Sequence	Spectral Component	Full linewidth at half height (kHz)	% of total spectral area	Ratio of $\theta_0-\tau-\theta_0$ to $\theta_0-\tau-\theta_{90}$ spectral area
$\theta_0-\tau-\theta_{90}$	low field sharp	4	3	
	high field sharp		>1	
	broad	61	97	
$\theta_0-\tau-\theta_0$	low field sharp	4	4	
	high field sharp		>1	
	broad	60	96	
				1.2

$$(\Delta H)^2 = (3/5)g_N^2\beta_N^2(1/n)I(I+1)\sum_{j,k} 1/r_{j,k}^6 + (4/15)g'^2_N\beta_N^2(1/n)I'(I'+1)\sum_{j,f} 1/r_{j,f}^6 \quad (18)$$

In equation 18, g_N is the proton g factor, β_N is the nuclear Bohr magneton, n is the number of protons in the unit cell, I is the nuclear spin quantum number, and r is the distance between two nuclei j,k, which is summed over all the intra- and intermolecular interactions (j,k). The sum f runs over all nonresonating nuclei. To calculate second moment by equation 18, the chloride ion of FeOCl was assumed to be 100% Cl^{35} and the shortest H--Cl distance was 2.3 A. The calculated second moment can then be used in equation 19 to obtain the width of the resonance line at half maximum height in units of Gauss.

$$\Delta H_1 = 2.35(\Delta H^2)^{1/2} \qquad (19)$$

Equation 19 is valid assuming that the second moment is not dominated by a single nuclear pair interaction. This appears to be the case for the broad component in the $FeOCl(TTF)_{1/8.5}$ ^1H echo spectrum. The experimental linewidth (60 kHz) is considerably greater than that calculated (ΔH_1 = 29.9 kHz) considering only H--H and H--Cl interactions, indicating that other strong magnetic interactions are important. It has been determined in the ^1H NMR study of pyridine and picolines intercalated into VOCl that dipolar interactions between the unpaired spin density on the chloride ions and the protons provide a large contribution to the line widths at high magnetic field (4.7 T).[95] A similar situation is expected for $FeOCl(TTF)_{1/8.5}$. Line broadening due to the presence of unpaired spin density on the protons (hyperfine exchange broadening) of the radical cation of TTF would be small compared to the dipolar mechanism.[144] Broadening by the dipolar mechanism will contribute to inhomogeneous lines, while the hyperfine mechanism will contribute to homogeneous lines.

In order to learn more about the interactions causing the line broadening in the $FeOCl(TTF)_{1/8.5}$ spectra, a series of hole-burning experiments were performed. In these experiments, a portion of the spectrum was irradiated with a continuous radio frequency field and then the entire spectrum was recorded (Figures 42-44). Field strengths ($\gamma B_2/2\pi$) of 145 and 43 Hz were applied during the delay between the end of the acquisition and the echo pulse sequence for the spectra shown in Figures 41 and 42, respectively. Irradiation of a

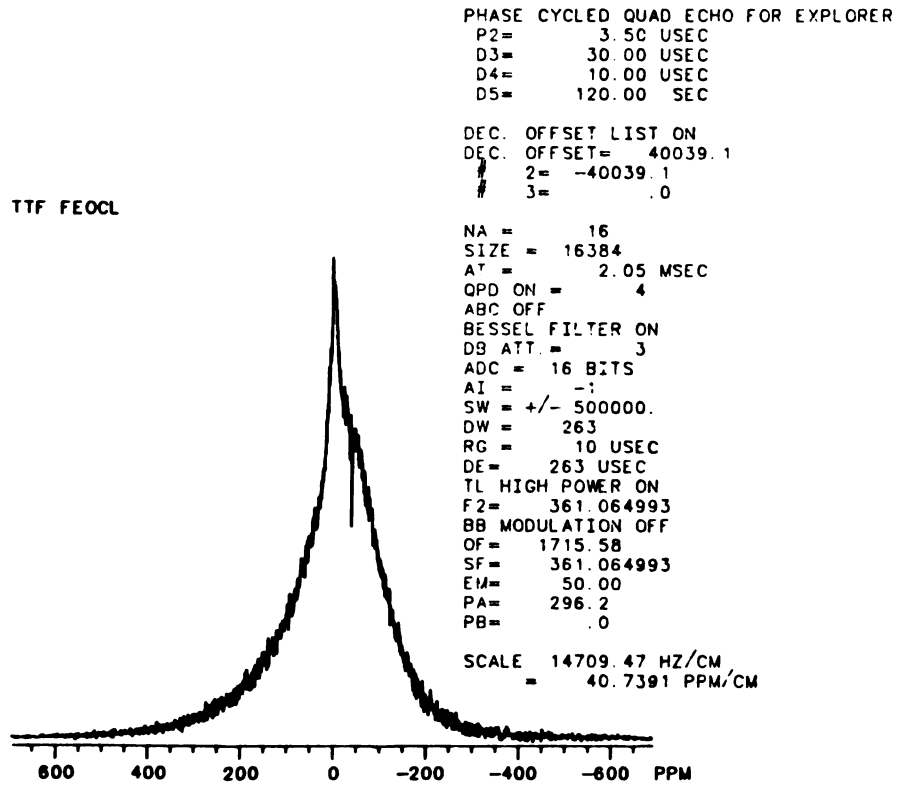

Figure 42. ^{1}H FT NMR using the same parameters as those shown in Figure 37, drawn to the same scale as Figures 43 and 44

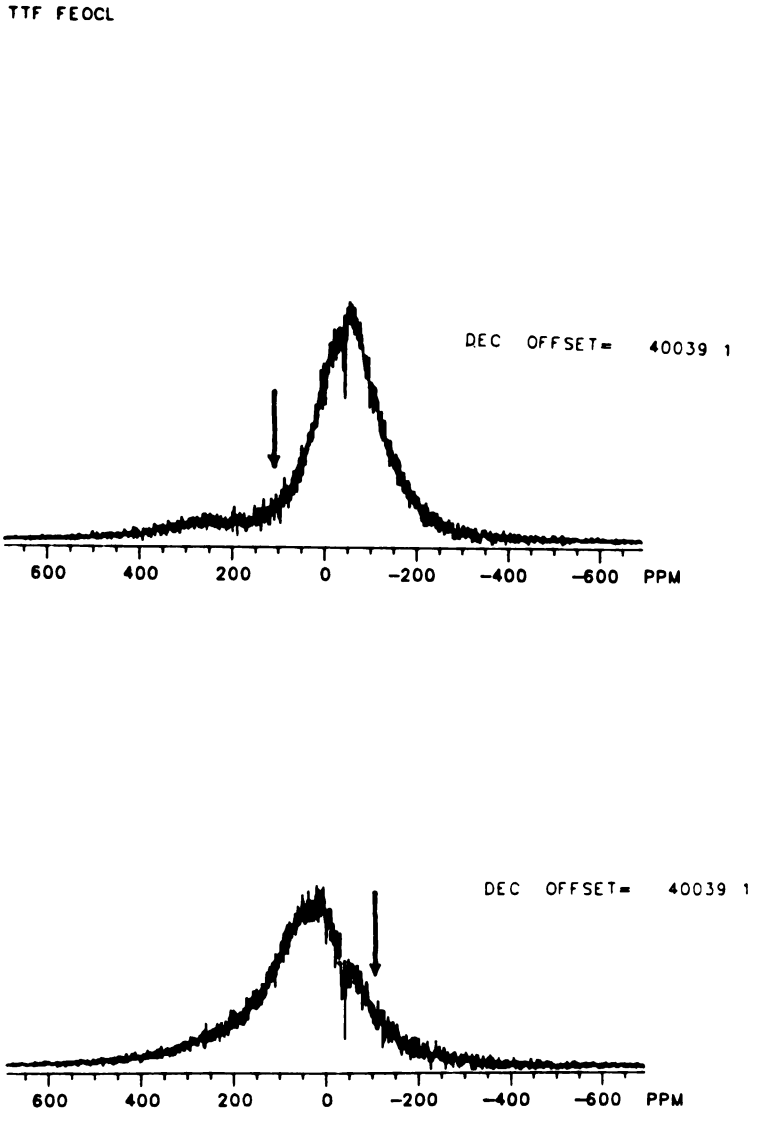

Figure 43. (a and b) ^{1}H FT NMR for $FeOCl(TTF)_{1/8.5}$ hole burning experiments using a field strength of 145 Hz. Arrows indicate location of preirradiation

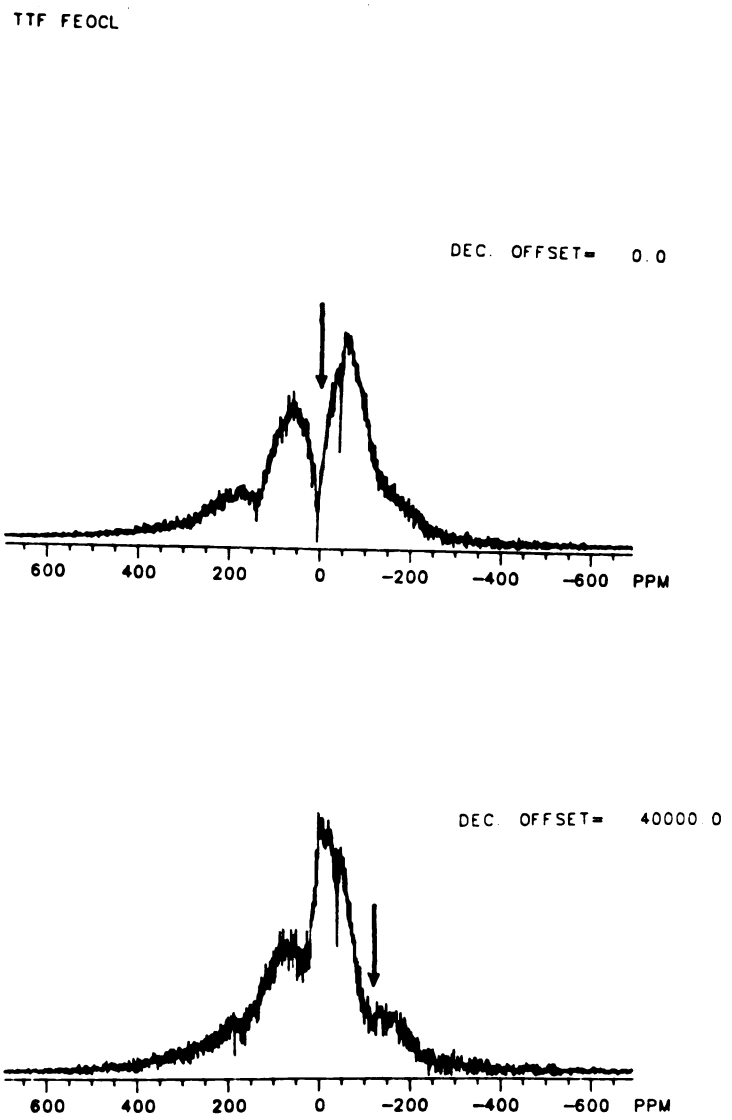

Figure 44. (a and b) ^{1}H FT NMR for $FeOCl(TTF)_{1/8.5}$ hole burning experiments using a field strength of 43 Hz. Arrows indicate location of preirradiation

portion of the spectrum prior to the observation pulses clearly changes the spectral lineshape. This indicates that the lines are inhomogeneous and that dipolar interactions are important in determining the linewidth. It should be noted that the relatively small fields which were used for preirradiation affected a rather large spectral width. This may be due either to magnetization transfer by molecular motion or spin diffusion, or to hyperfine exchange broadening. The discontinuities evident in the spectra at large distances from the preirradiation frequency (i.e., 140 and -140 ppm in Figure 44(b)) indicates that more than one broad spectral component is present, and the preirradiation has different effects on the component amplitudes. The presence of multiple broad components is most simply interpreted as evidence for molecular domains with different structural and/or dynamic characteristics.

^{13}C NMR

The splitting pattern of the ^{1}H-coupled ^{13}C spectrum of TTF in deuterated chloroform ($CDCl_3$) (Figure 45(a and b)) allows one to unequivocally assign the two peaks in the decoupled spectrum of the solid (Figure 46). The spectrum of TTF shows lines at 119.0 and 110.0 ppm, due to carbon in the ring double bonds and to the bridged carbons, respectively. The triplet at 77.0 ppm is due to $CDCl_3$. The 110.0 ppm line, due to the bridging carbons, is split into a 1:2:1 triplet by the nearest pair of equivalent protons. The 119.0 ppm signal due to the carbons in the ring double bonds is split into two by the adjacent protons, and this doublet is further split by the proton two bonds away. The ^{13}C spectrum of solid TTF obtained by

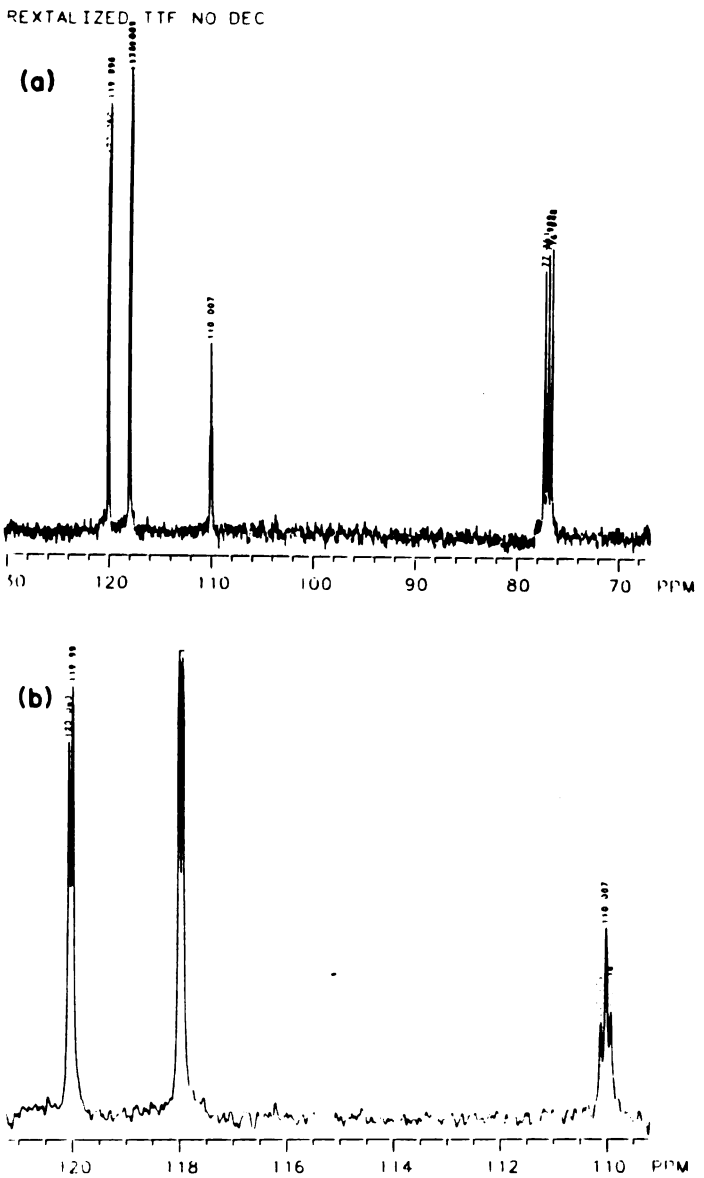

Figure 45. (a) ^{1}H-coupled-^{13}C FT NMR spectrum of TTF in $CDCl_3$, (b) The expanded scale showing the peaks corresponding to TTF

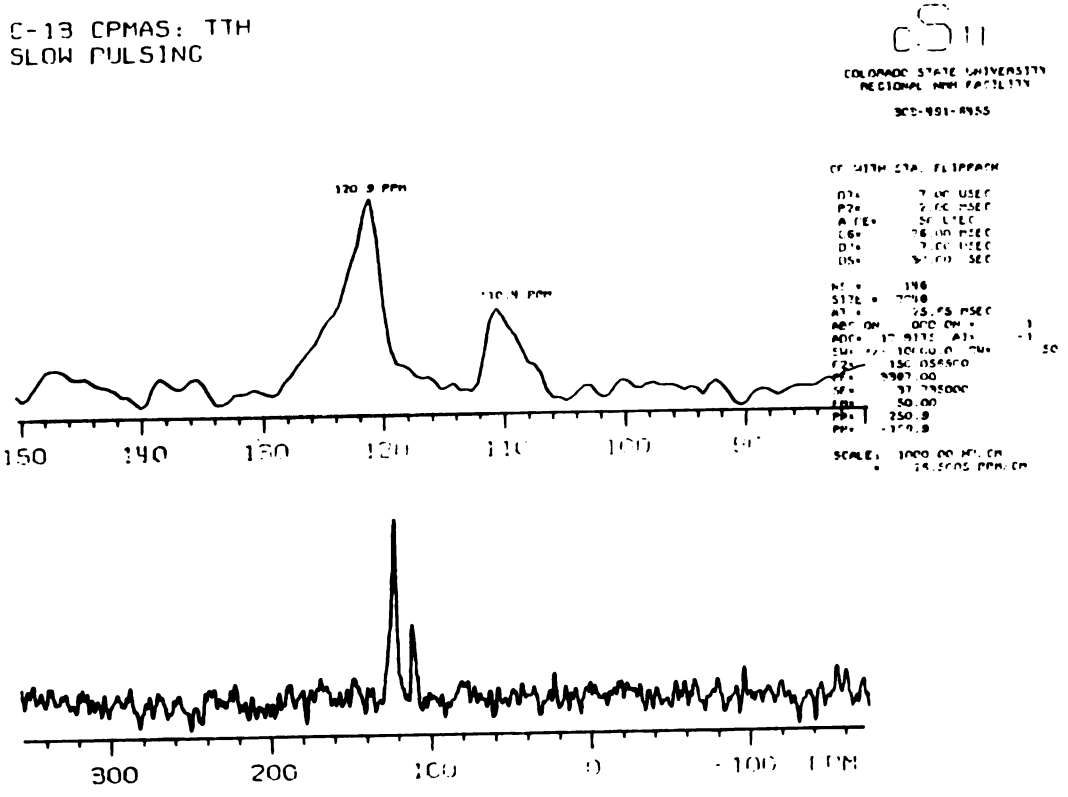

Figure 46. ^{13}C CPMAS spectrum for TTF

using ^{13}C-^{1}H cross polarization high power ^{1}H decoupling and magic angle spinning (CPMAS) is shown in Figure 46. The spectrum is very similar to the solution spectrum except for the linewidths, indicating that the conformation of solution and solid TTF are very similar.

^{13}C CPMAS spectra of $TTF_3Br_2 \cdot 2H_2O$, and TTF(CA), both segregated stack (ss) and mixed stack (ms) structures, are shown in Figures 47-49. These compounds are models for TTF in $FeOCl(TTF)_{1/8.5}$. The $TTF_3Br_2 \cdot 2H_2O$ and TTF(CA) (ss) spectra are very similar (Figures 47 and 48), consisting of single lines at 136 and 138 ppm, respectively. Two overlapping resonances at 121 and 128 ppm are seen for the TTF(CA) (ms) spectrum (Figure 49). ^{1}H-^{13}C cross polarization results in an enhancement of peaks due to the transfer of polarization from the hydrogen to the carbon. No peaks were observed by CPMAS for the chloranil molecule, in which all the carbons are bonded to nonhydrogen atoms. Assuming relative peak intensities are approximately the same for TTF and TTF(CA) (ms), the peaks in the TTF(CA) (ms) spectrum can be assigned. The TTF(CA) (ms) low field resonance (128 ppm) is due to the bridging carbons, and the high field resonance (121 ppm) is due to the ring double bond carbons. Thus, the bridging carbons of TTF(CA) (ms) are shifted 18 ppm downfield from those of TTF, while the ring double bond resonance occurs at the same position in both materials. The large downfield shift is consistent with ESR studies of TTF^{+},[145] which indicate that the majority of the unpaired spin density is located on the bridging carbon. $TTF_3Br_2 \cdot 2H_2O$ has a spectrum similar to that of TTF(CA) (ss). It has been shown that in both these compounds the TTF rings are stacked immediately adjacent to each other,

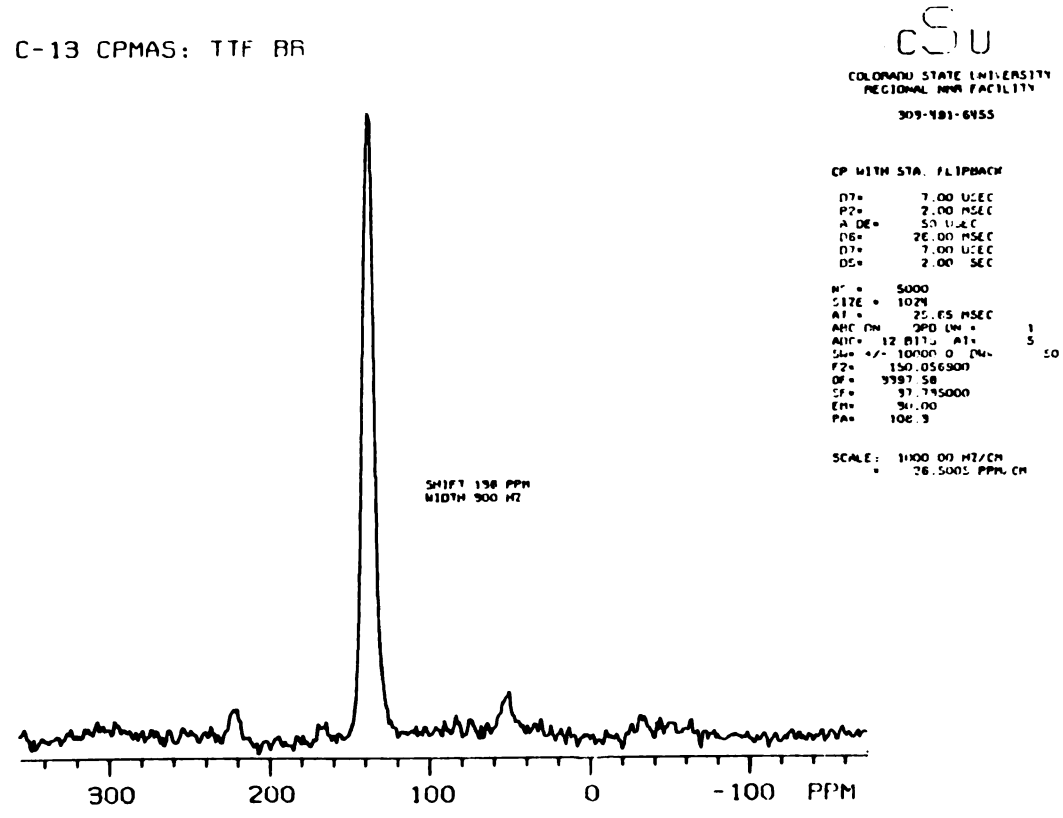

Figure 47. ^{13}C CPMAS spectrum for $TTF_3Br_2 \cdot H_2O$

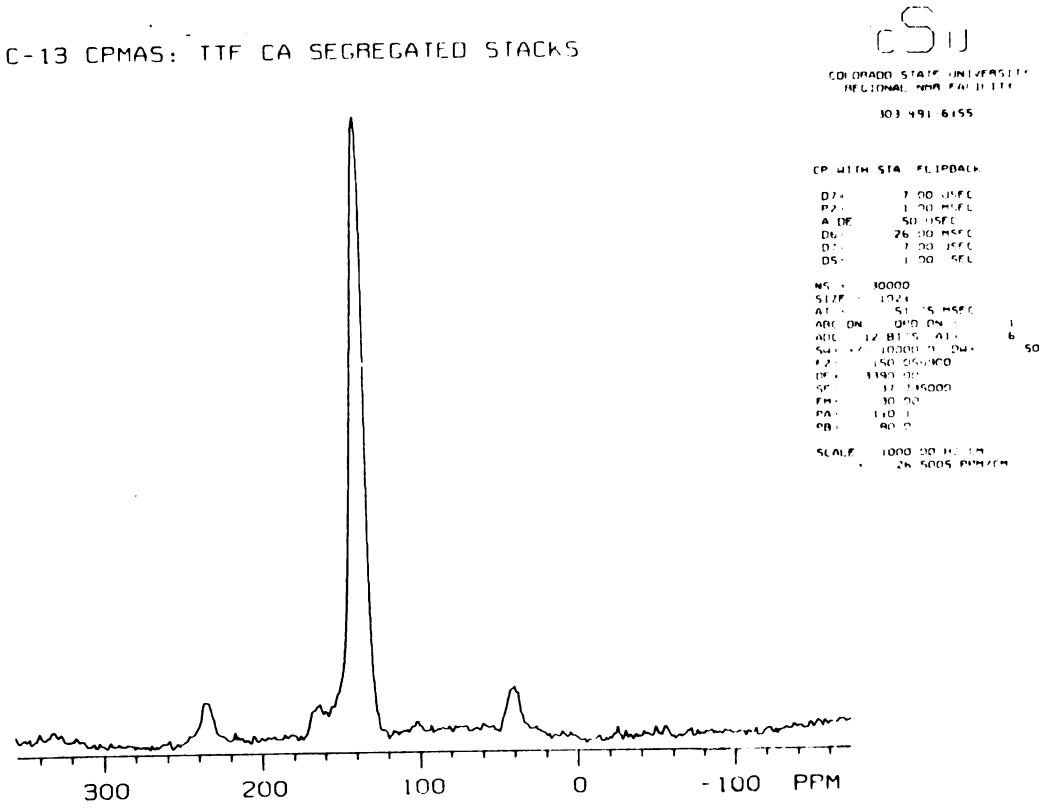

Figure 48. ^{13}C CPMAS spectrum for TTF(CA) (ss)

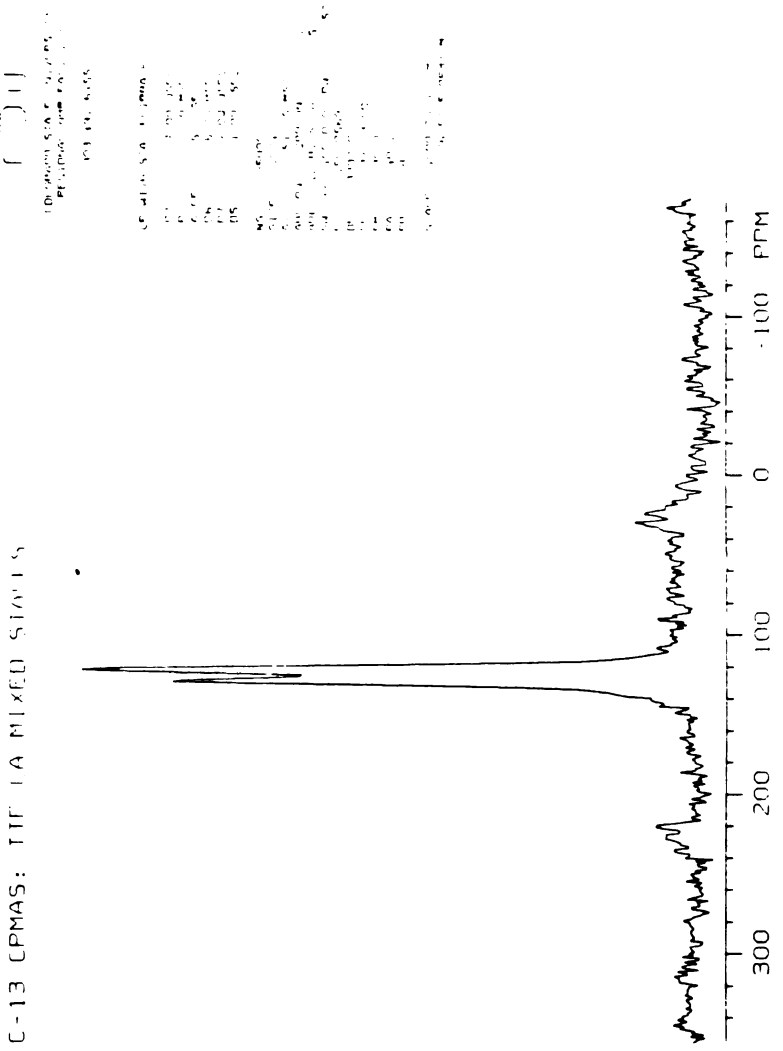

Figure 49. ^{13}C CPMAS spectrum for TTF(CA) (ms)

as opposed to TTF(CA) (ms) in which the stacks consist of alternating TTF and CA moieties.[48,146] The single peaks observed in TTF(CA) (ss) and $TTF_3Br_2 \cdot 2H_2O$, are probably overlapping, unresolved resonances due to the bridging carbons and the ring double bond carbons of the TTF molecule. Thus, the bridging carbons have been shifted about 26 ppm downfield and the double bond carbons have shifted 17 ppm downfield relative to neutral TTF. Because the TTF in all three salts is fully ionic, the difference in spectra of the compounds must be due to the difference in stacking (mixed stacks vs segregated stacks).

No ^{13}C spectrum could be observed for $FeOCl(TTF)_{1/8.5}$ under either of the following conditions: (1) CPMAS with high power ^1H decoupling, (2) direct excitation of carbons with MAS and ^1H decoupling. The fact that no spectrum was observed indicates the presence of strong magnetic interactions that are not present in the simple TTF salts used as models. Just as the chloride-proton interactions appear to have a large effect on the linewidth of the ^1H $FeOCl(TTF)_{1/8.5}$ spectrum, chloride unpaired spin density-^{13}C nuclear dipolar interactions probably cause the ^{13}C CPMAS spectrum to be too broad to observe. The electronic configuration of the TTF molecule in $FeOCl(TTF)_{1/8.5}$ is expected to be similar to that of TTF(CA) (ss) and $TTF_3Br_2 \cdot 2H_2O$, based on the IR data.[147] These salts yield high resolution ^{13}C CPMAS NMR spectra in contrast to $FeOCl(TTF)_{1/8.5}$, suggesting that the electronic structure of TTF in $FeOCl(TTF)_{1/8.5}$ is probably not responsible for the severe line broadening.

^2H NMR

Deuterium NMR provides spectra that should be more readily interpretable than those discussed previously, because the chloride unpaired spin density-nuclear interaction is expected to be less important than in the ^1H and ^{13}C cases. Since the linewidths due to dipolar interactions are approximately proportional to the product of the gyromagnetic ratios of the two dipoles involved, the paramagnetic dipolar contributions to the ^2H spectra should be about seven times smaller than to the ^1H spectrum. The ^2H spectrum is usually dominated by the electric quadrupole interaction of the I = 1 spin, which is due almost entirely to intramolecular contributions.[148] A deuterium NMR spectrum of a motionless or motionally restricted C-D bond would consist of two overlapping asymmetric lines. The separation between the line maxima, $\Delta\nu_q$, is related to the quadrupole coupling constant and to the angle, Θ, that the C-D bond makes with respect to the magnetic field. With powders, there is a random orientation of the C-D bonds with respect to the magnetic field. A quadrupole powder pattern arises due to the different frequencies for each orientation of the C-D bond (Figure 50). The average line shape is very sensitive to molecular motion and its analysis can distinguish between types of motion within a solid. Therefore ^2H NMR spectra are usually amenable to analysis of molecular orientation and dynamics.

The ^2H NMR of d_4-TTF obtained following a single 90° pulse is shown in Figure 51. The intensity of the quadrupole echo signal for d_4-TTF (Θ_0-τ-Θ_{90} pulse sequence) was about 100 times smaller than the free induction decay following the first pulse. The absence of a

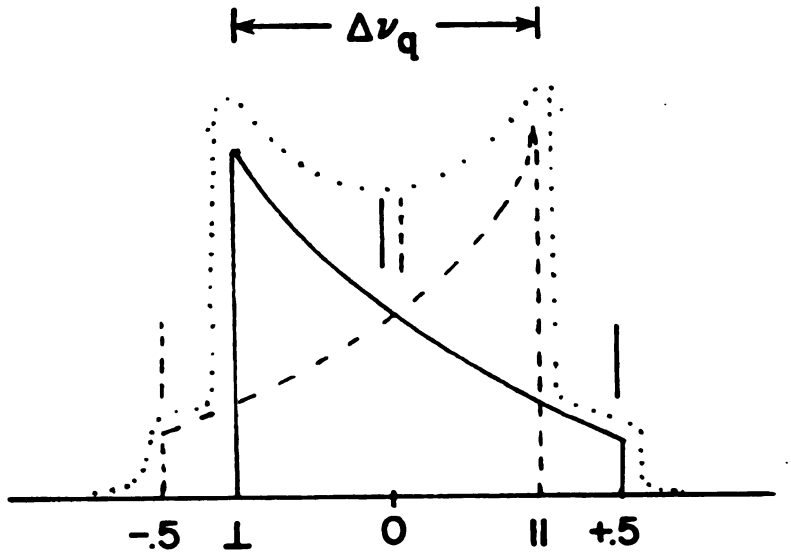

Figure 50. A schematic representation of a quadrupolar powder pattern resulting from a sterically rigid C-D bond

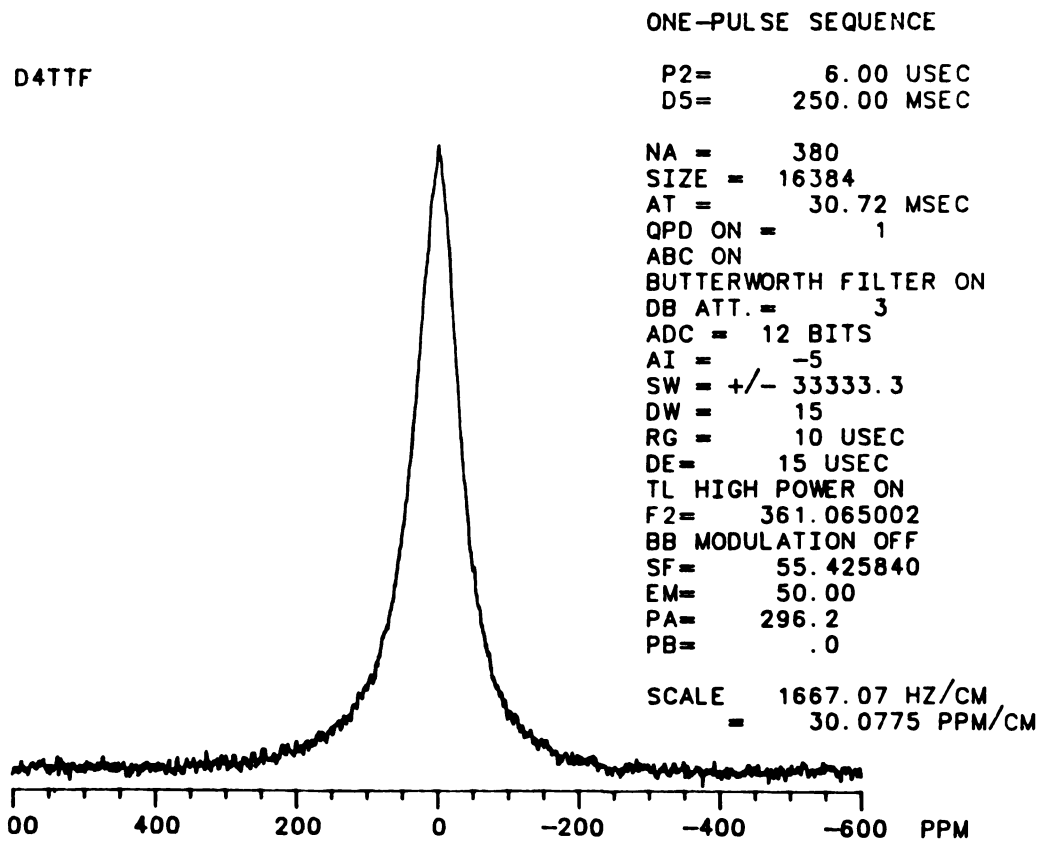

Figure 51. ^{2}H FT NMR of d_4-TTF obtained from a single 90° pulse

quadrupole echo signal has been observed for isotropic, but not for an anisotropic, molecular reorientation when the pulse separation (τ) in the echo experiment becomes larger than the molecular rotational correlation time (τ_c), unless $\Delta_0\tau_c >> 1$ where $\Delta_0 = (3/8)e^2Qq/h \sim 4 \times 10^5\ s^{-1}$.[147] This indicates that d_4-TTF undergoes isotropic reorientation with a correlation time that is less than 30 μs (which is the pulse separation, τ). If, in fact, the reorientation is anisotropic, then the longest correlation time must be 30 μs and the shortest must be greater than 2.5 μs ($1/\Delta_0$).

The quadrupole echo spectrum of $FeOCl(d_4\text{-TTF})_{1/9}$ (obtained with a Θ_0-τ-Θ_{90} sequence) is a broad, featureless line (Figure 52). The width at half height is 100 kHz. When the strength of dipolar interactions becomes a significant fraction of the quadrupolar interaction and $\omega_D\tau \geq 1$ ($\omega_D = 2\pi\nu_D$, where ν_D is the line broadening due to dipolar interactions and τ is the time between pulses), it has been shown that the spectra are no longer symmetric about their center. If the spin dephasing due to dipolar interactions is not refocussed, the echo spectra are distorted.[150] The ^1H spectra indicate that the dipolar interactions between the unpaired electron density on the chloride and the ^1H nucleus is a significant fraction of the electronic quadrupolar interaction; it is, therefore, expected to be present in the $FeOCl(d_4\text{-TTF})_{1/9}$ spectrum. The pulse sequence Θ_0-$\tau/2$-180_{90}-$\tau/2$-Θ_{90}-$\tau/2$-180_{90}-$\tau/2$-echo has been shown to refocus both quadrupolar and dipolar interactions,[150] reducing echo distortion due to spin dephasing resulting from dipolar interaction. The echo spectrum obtained from this pulse sequence is shown in Figure 53. This

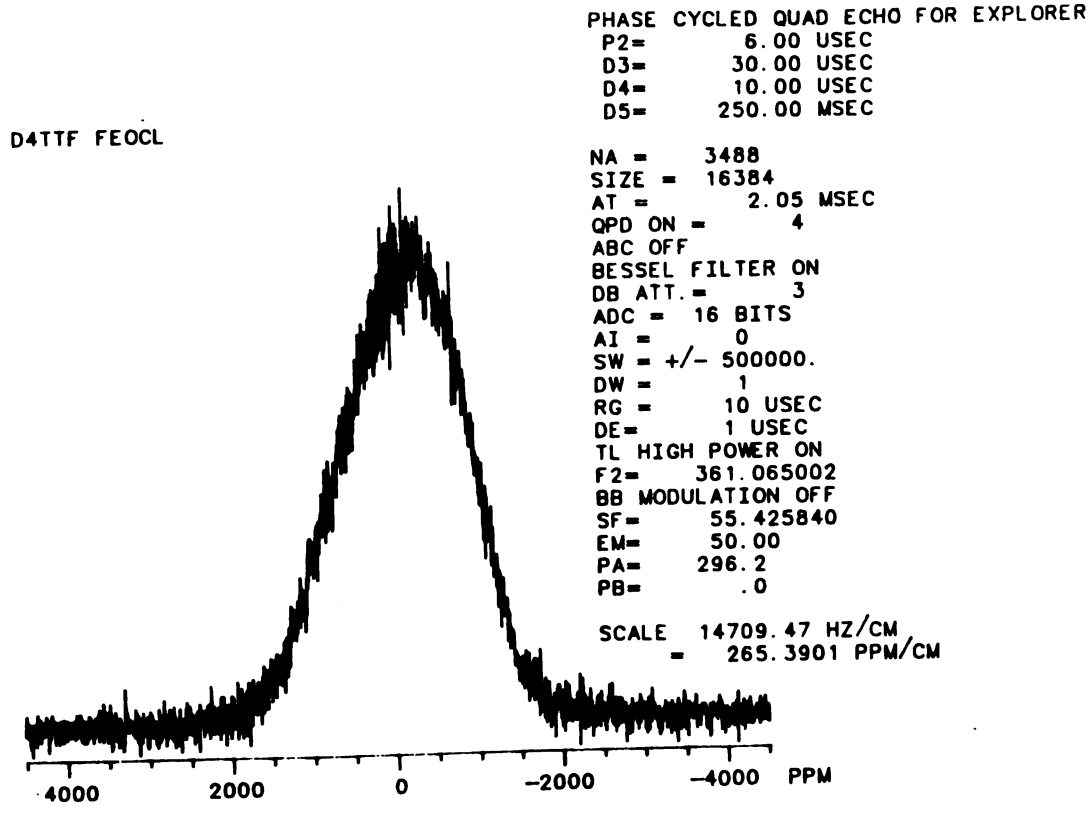

Figure 52. The ^{2}H quadrupole echo spectrum for $FeOCl(d_4\text{-}TTF)_{1/9}$

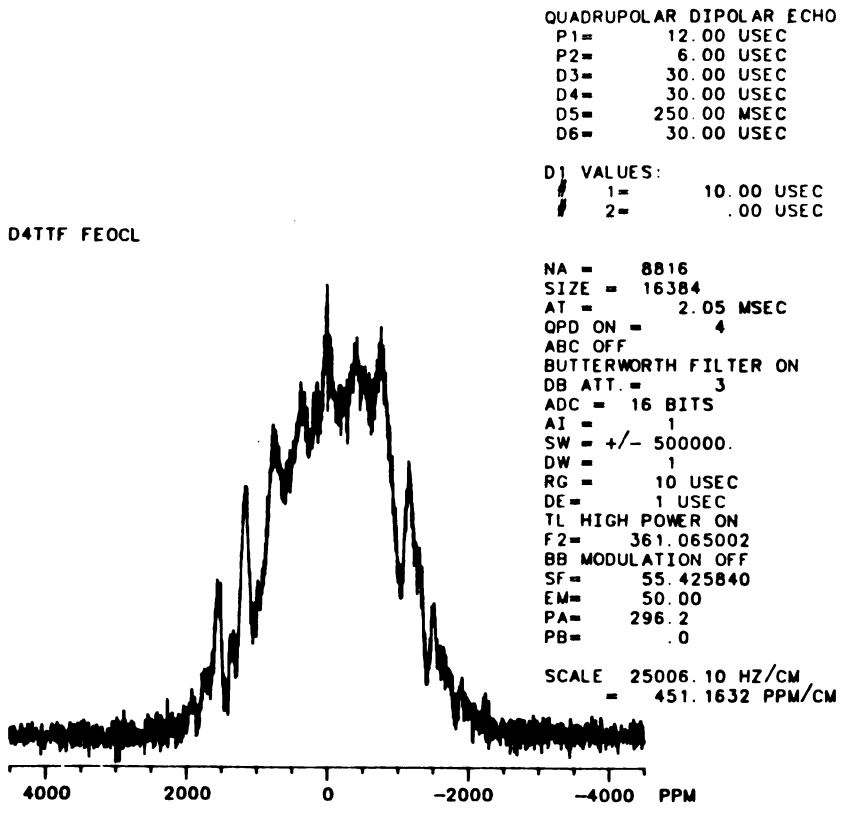

Figure 53. The ^{2}H quadrupolar-dipolar echo spectrum for $FeOCl(d_4\text{-}TTF)_{1/9}$

echo spectrum has considerably better spectral resolution than in the quadrupole echo spectrum shown in Figure 52; four splittings appear to be present.

Although the ^2H NMR studies of $FeOCl(d_4\text{-TTF})_{1/9}$ are still at a preliminary stage, the large difference between the simple quadrupolar echo spectrum (Figure 52) and the quadrupolar-dipolar echo spectrum (Figure 53) is reproducible, and multiple splittings are always present in the latter spectrum. A central peak and several quadrupole splittings appear to be present. The central peak appears at the same frequency as the d_4-TTF line (Figure 51), and the splittings are 42, 84, 128, and 169 kHz for peaks A, B, C, and D, respectively. The quadrupole coupling constant e^2qQ/h and C-D bonds in aromatic rings is about 185 kHz.[149] If no detectable motion took place (i.e., $\tau_c > 1 \times 10^{-3}$ s) then the C-D bonds oriented at 0° and 90° with respect to the magnetic field would give resonance components that had splittings of 278 and 139 kHz, respectively. Orientations between 0° and 90° would give intermediate splittings. The relatively sharp peaks often seen in powder ^2H NMR specvtra are usually due to C-D bonds oriented at 90° with respect to the field. The peaks in Figure 53, which have a splitting of 169 kHz, cannot be due to 90° orientations because of the magnitude of the splitting. In order to obtain an understanding of complex ^2H NMR spectra such as these, detailed simulation will be necessary.

The work to date indicates that a strong dipolar interaction, probably between the unpaired electronic density on the chloride ion and the ^2H nuclei, is present and must be refocused in order to avoid

spectral distortion. Initial comparison of the quadrupolar-dipolar echo spectrum of $FeOCl(d_4\text{-}TTF)_{1/9}$ with well characterized ^2H echo spectra of other solids indicates that more than one component is present in the $FeOCl(d_4\text{-}TTF)_{1/9}$ spectrum. The presence of more than one spectral component suggests that d_4-TTF domains in $FeOCl(d_4\text{-}TTF)_{1/9}$ have different degrees of motional freedom and/or an average orientation with respect to their axes of motional averaging. The fact that an echo spectrum is not observed for $FeOCl(d_4\text{-}TTF)_{1/9}$ indicates that the d_4-TTF reorientation is anisotropic and/or has a correlation time which is between 2.5 μs and 30 μs. Factors such as pulse spacing, spectrometer frequency and pulse power have a large effect on the spectra, and so details such as spectral asymmetry and exact splittings should not be considered final. More complete ^2H NMR studies, which include variation of the parameters mentioned above, spectral simulations, relaxation measurements and spectra of oriented samples, will provide information on the dynamics of d_4-TTF in $FeOCl(d_4\text{-}TTF)_{1/9}$ and aid the neutron data analysis by providing complementary information on the relative orientation of d_4-TTF within the FeOCl layers.

ELECTRONIC PROPERTIES OF THE INTERCALATES

A combination of spectroscopic and physical methods has been applied to characterize FeOCl and the tetrathiolene intercalates. Differences in intercalant content (as much as 1%) appear to have little effect upon the data obtained from the techniques described below.

Infrared Spectroscopy

Extensive molecular vibration studies of charge transfer compounds with TTF,[152] TMTTF,[153] and TTT[154] as the electron donor molecule have been reported. There has been very little work on any TTN salt, presumably due to the difficulties in the synthesis of TTN.[155,156] The infrared spectrum of pristine FeOCl shows only a single strong vibrational band at 485 cm^{-1}, which is assigned to the Fe-O stretch (Figure 54). Consequently, direct information on the guest species can be obtained by infrared spectroscopy.

On the time scale of vibrational spectroscopy (10^{-13}-10^{-14} sec), electronic distribution in charge transfer compounds can be studied. For one-dimensional organic metals, vibrational spectroscopy provides evidence for partial charge transfer if the electronic transition does not introduce too much background absorption. The infrared spectrum for a compound having localized electronic charge distribution would exhibit frequencies of both neutral and ionized molecules, whereas

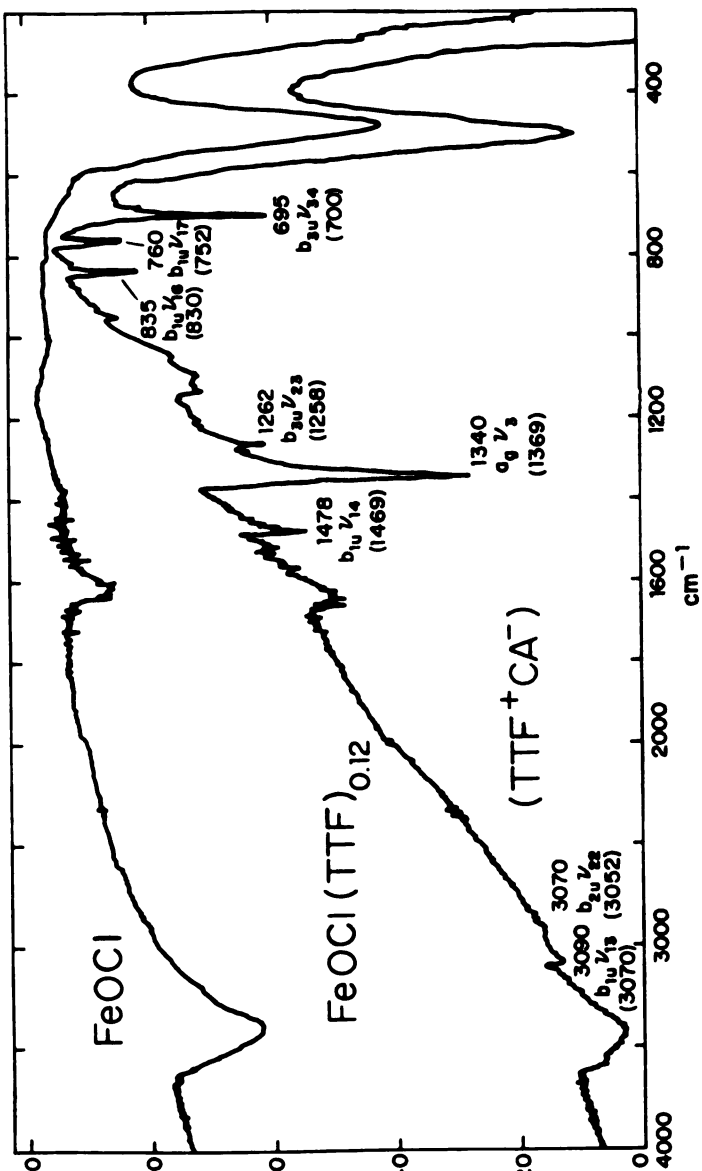

Figure 54. Infrared spectra of FeOCl and FeOCl(TTF)$_{1/8.5}$ with assignments. Values for TTF(CA) are in parenthesis

delocalized distributions would be characterized by single frequencies of average values.[157] Radicals participating in strong intermolecular interactions exhibit new vibronic absorptions in the infrared which are due to a mechanism of intensity borrowing from the charge transfer transition.[152]

In order to help identify the infrared spectra of $FeOCl(TTF)_{1/8.5}$, $FeOCl(d_4\text{-}TTF)_{1/9}$ and $FeOCl(TTF)_{1/9}(tol)_{1/22}$, salts of TTF with chloranil, TTF(CA), were prepared and the vibrational spectra confirmed.[48] TTF(CA) crystallizes in two phases (depending upon the synthetic procedure), a black crystalline phase consisting of segregated stacks in which the TTF stack is made up of $(TTF^+)_2$ dimers[48] and a green crystalline phase containing mixed stacks of TTF and CA.[68] The a_g modes are the only ones allowed by symmetry to couple with electrons in TTF resulting in electron-intramolecular vibrational modes.[48] The $a_g\nu_3$ mode consists of the simultaneous stretching of the ring and the ethylenic C=C bonds.[158] It is this vibration that has been used to designate the degree of charge transfer, usually for the Raman data. The $a_g\nu_3$ mode in the Raman spectrum for the salts $TTF(I)_{0.71}$, $TTF(Br)_{0.76}$, and $TTF(Cl)_{0.80}$, which exhibit partial charge transfer,[157] and for $FeOCl(TTF)_{1/9}(tol)_{1/21}$[65] are listed in Table 18. Linear dependence of vibrational frequencies <u>vs</u> charge transfer should not be assumed for all organic charge transfer compounds, but the experimental values obtained for the TTF salts are in approximate agreement with a linear correlation. From the values listed in Table 18, it is clear that the TTF moiety in $FeOCl(TTF)_{1/9}(tol)_{1/21}$ is present as the radical cation.

Table 18. Position of the $a_g\nu_3$ band observed in the Raman data with the values for the charge transfer

Compound	$a_g\nu_3$	Charge Transfer[a]
TTF•	1518	0
TTF-TCNQ	1456	0.63
$TTF(I)_{0.71}$	1452	0.67
$TTF(Br)_{0.76}$	1448	0.71
$TTF(Cl)_{0.80}$	1441	0.79
TTF	1420	1.00
$FeOCl(TTF)_{1/9}(tol)_{1/21}$	1404	1.00[b]

Frequency in wave numbers

[a]Reference 157.
[b]Reference 65.

Raman spectroscopy is preferred to infrared for determining charge transfer, since the spectrum obtained is generally simpler and dominated by totally symmetric modes. Infrared spectra are complicated by low lying electronic absorptions[159] and interference effects.[160,161]

Complete characterization of both the neutral and fully ionic TTF molecule[158] by infrared spectroscopy has overcome the complexities in the analysis of the infrared data. Information on the degree of charge transfer can be ascertained from the infrared data, which complement the Raman data. The infrared data for $FeOCl(TTF)_{1/8.5}$

and $FeOCl(d_4\text{-}TTF)_{1/9}$ intercalates and for TTF(CA) and d_4-TTF(CA), segregated stack structure,[48] (ss) are shown in Tables 19 and 20. The frequencies corresponding to CA have been omitted for clarity. Comparison of the bands for the TTF and d_4-TTF intercalates shows that these molecules are fully ionic radical cations. The strong infrared absorption at 1340 cm^{-1} can be assigned to the $a_g\nu_3$ mode (Figures 54 and 55) based on the comparison of the infrared spectrum of $FeOCl(TTF)_{1/8.5}$ and $FeOCl(d_4\text{-}TTF)_{1/9}$ with that of the CA salt (ss).[48] This had been predicted by a theoretical model[160] applied to dimerized segregated stack systems.[152] This was also observed in the infrared spectrum for $FeOCl(TTF)_{1/9}(tol)_{1/22}$,[86] suggesting that TTF is present as isolated dimers within the layers of FeOCl for both the toluene and the dimethoxyethane preparation.

$FeOCl(TMTTF)_{1/13}$ exhibits very weak vibrational bands due to the intercalant compared with the Fe-O stretch at 485 cm^{-1}, and the background absorption is much greater than that observed for $FeOCl(TTF)_{1/8.5}$. The infrared data for $FeOCl(TMTTF)_{1/13}$ can be compared to those obtained for $TMTTF^+$ in $(TMTTF)_2X$ where $X = BF_4^-$, ClO_4^-, PF_6^- and Br^-[162] and are listed in Table 21. All the strong peaks observed for $TMTTF_2Br$ and $TMTTF_2ClO_4$ are also observed for $FeOCl(TMTTF)_{1/13}$, except for the $a_g\nu_3$ band indicative of dimeric units (1361 cm^{-1}), which is absent. Since the TMTTF radical cations are lying parallel to the FeOCl layers, the absence of dimeric units is not surprising.

Table 19. Infrared spectral features of $FeOCl(TTF)_{1/8.5}$ and the TTF infrared absorptions of TTF(CA), (ss)

$FeOCl(TTF)_{1/8.5}$	$FeOCl^{a}(TTF)_{1/9}(tol)_{1/21}$	TTF(CA)	Assignment[b]
		482(m)	$a_g\nu_6$
		629(w)	$b_{2u}\nu_{26}$
695(m)	684(s)	700(w)	$b_{3u}\nu_{34}$
		710(w)	
760(m)	745(m)	752(mw)	$b_{1u}\nu_{17}$
835(mw)	820(m)	830(w)	$b_{1u}\nu_{16}$
	1080(w)	1105(mw)	$b_{1u}\nu_{15}$
1262(w)	1250(w)	1258	$b_{2u}\nu_{23}$
1340(s)	1332(s)	1364(s)	$a_g\nu_3$
1478(m)	1465(w)	1469(sh,s)	$b_{1u}\nu_{14}$
3070(w)		3052(m)	$b_{2u}\nu_{22}$
3090(w)	3070(vw)	3070(m)	$b_{1u}\nu_{13}$

Frequencies in wave numbers, relative intensities are indicated in parentheses

[a]Reference 86.
[b]Reference 48.

Table 20. Infrared spectral features of $FeOCl(d_4\text{-TTF})_{1/9}$ and the d_4-TTF infrared absorptions of d_4-TTF(CA), (ss)

$FeOCl(d_4\text{-TTF})_{1/9}$	d_4-TTF(CA)[a]	Assignment[a]
525(w)	540(w)	$b_{3u}\nu_{34}$
740(mw)	740(mw)	$b_{2u}\nu_{25}$
	795(w)	$b_{1u}\nu_{16}$
830(mw)	832(mw)	$b_{1u}\nu_{15}$
1335(s)	1370(s)	$a_g\nu_3$
1428(w)	1432(sh,s)	$b_{1u}\nu_{14}$
2269(w)	2268(m)	$b_{2u}\nu_{22}$
2310(w)	2310(w)	$b_{1u}\nu_{13}$

Frequencies in wave numbers

[a]Reference 48.

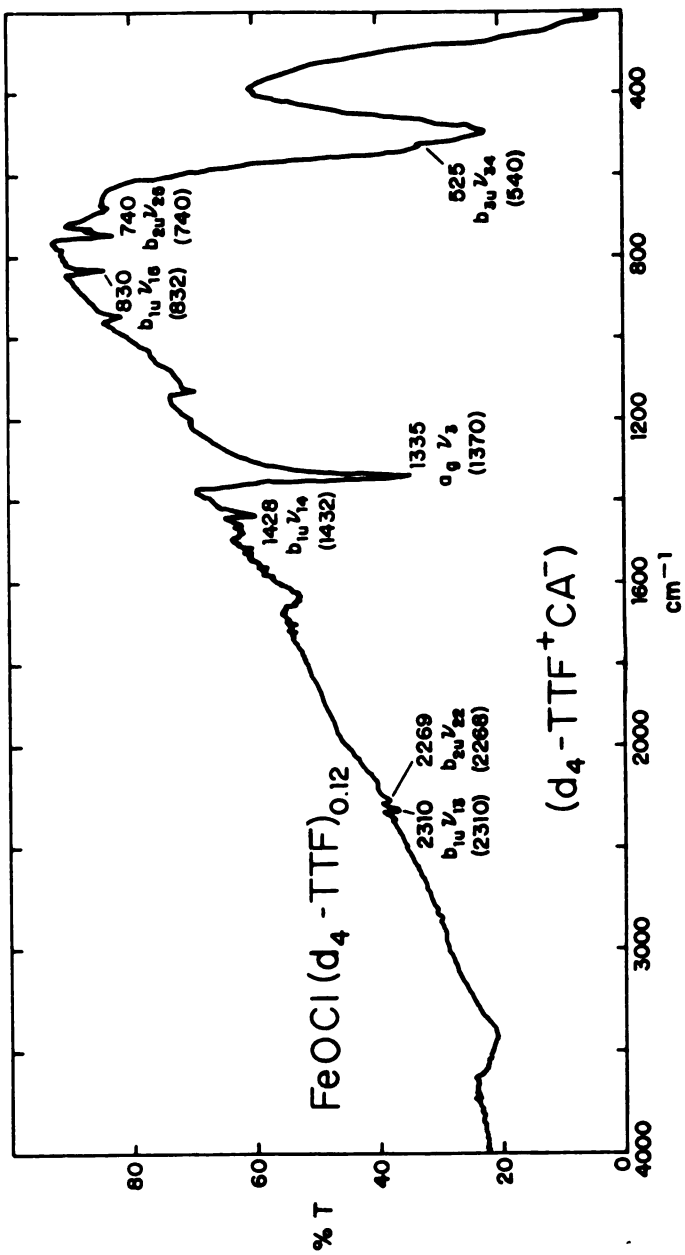

Figure 55. The infrared spectrum for FeOCl(d_4-TTF) with assignments. Values for d_4-TTF(CA) are in parenthesis

Table 21. Infrared spectral features for $FeOCl(TMTTF)_{1/13}$ and the TMTTF infrared absorptions of $(TMTTF)_2X$ ($X = BF_4^-$, ClO_4^-, and PF_6^-)

$FeOCl(TMTTF)_{1/13}$	$(TMTTF)_2X$[a]	Assignment[a]
690(m)		
940(sh,m)	935(ms)	CH_3
1332(m)	1340(vs)	$a_g\nu_4$
	1361(s)	$a_g\nu_3$
1470(m,br)	1438(mw,br)	CH_3 asymm
1560(m)	1560(sh)	$b_{1u}\nu_{28}$ ($a_g\nu_3$)
2920(vw)	2923	CH_3 asymm
2960(vw)	2973	

Frequencies in wave numbers

[a]Reference 162.

The infrared data for $FeOCl(TTT)_{1/9}(tol)_{1/23}$ are listed in Table 22 and compared with values for TTT^+ in TTT(X), where X = Cl^-, Br^-, I^- and SCN^-.[69] With some samples of the intercalate, certain peaks could be assigned to neutral TTT: these may be due to the presence of small amounts of unintercalated TTT on the surface of the intercalate. Otherwise, the data correspond to that of the TTT cation.

Infrared data for TTN salts are nonexistent. The only salt whose synthesis has been published to date (TTN•TCNQ) is metallic and thus has no discernable infrared spectrum.[156,163] The infrared data for $FeOCl(TTN)_{1/9}(tol)_{1/21}$ are listed in Table 23 and compared with those for those of the neutral compound. Most of the peaks are red shifted with respect to neutral TTN, as are those of the other intercalants, and may be assigned to the radical cation.

The broad absorption (4000-1600 cm^{-1}) observed in the infrared spectra (Figures 54 and 55) for $FeOCl(TTF)_{1/8.5}$ and for $FeOCl(d_4\text{-}TTF)_{1/9}$ is present in all the spectra of the intercalates and appears to be due to an electronic transition. Sample preparations with various grinding times and suspension of the solid in mineral oil as well as KBr had little effect upon the presence of this absorption. Organic charge-transfer compounds with conductivities on the order of 10^{-4} to 10^{-2} $(ohms\text{-}cm)^{-1}$ exhibit a similar broad absorbence in this region of the spectrum (4000-1600 cm^{-1}), which has been attributed to the continuum of electronic transitions.[164]

Infrared spectroscopy of the tetrathiolenes is consistent with the guest species being fully ionic. The presence of the broad absorption at about 0.6 - 0.3 eV is similar to that observed in all

Table 22. Infrared spectral features for $FeOCl(TTT)_{1/9}(tol)_{1/23}$ and the infrared absorptions of TTT(X), X = Cl^-, Br^-, and SCN^- and $TTT^\bullet$

$FeOCl(TTT)_{1/9}(tol)_{1/23}$	TTT(X)[a]	$TTT^\bullet$[a]
683(s,br)		685(w)
738(m)		733(vs)
752(m,sh)	751(m)	742(s)
761(m)		
949(w)		
973(m)	972(m)	968(m)
998(m)	998(vs)	
1008(m)		1010(w)
1059(m)	1058(s)	
1167(m)	1163(m)	1148(w)
1273(w,sh)	1274(vs)	1248(w)
1284(s)	1286(vs)	
1311(s)	1313(s)	1305(vs)
1361(m)	1361(s)	1319(s)
1429(m)	1432(m)	
1452(m)		
1463(s)	1463(s)	
1504(w)	1504(w)	1522(w)
1552(m)	1550(m)	
1598(m)	1599(m)	1612(m)

Frequencies in wave numbers

[a]Reference 69.

Table 23. Infrared spectral features for $FeOCl(TTN)_{1/9}(tol)_{1/21}$ and the infrared absorptions of TTN°

$FeOCl(TTN)_{1/9}(tol)_{1/21}$	TTN°[a]
623(m)	623(s)
695(m)	670(m)
740(s)	725(w)
810(s)	797(s)
962(w)	815(w,sh)
975(w)	965(w)
1100(w,br)	1070(m)
1185(m)	1185(s)
	1200(w)
1260(m,sh)	1260(s,sh)
1280(m)	1280(s)
1388(s)	1362(s)
	1370(s)
1495(w)	1455(s,sh)
1570(w)	1540(s)

Frequencies in wave numbers

[a]Reference 156.

the mixed valence compounds of TTF which are conductors[155] and suggests that the intercalates should exhibit an increase in conductivity over that of FeOCl. From the infrared and Raman data of $FeOCl(TTF)_{1/8.5}$, $FeOCl(d_4\text{-}TTF)_{1/9}$, and $FeOCl(TTF)_{1/9}(tol)_{1/21}$, the TTF^+ molecules within the host layers appear to exist as dimerized units. Although the steric interactions of TMTTF are different from the TTF intercalant, the electronic structure deduced from the infrared data is consistent with TMTTF also being a fully ionic cation. Similar conclusions can be drawn for the TTN and the TTT intercalates. Charge transfer has occurred, presumably from the guest to the host lattice.

Optical Spectra

The optical spectra of the intercalates are shown in Figures 56 and 57. The band gap reported for FeOCl is 1.9 eV.[99] The value of the band gap corresponds to a "break" in the absorption curve.[165] Both Figures 54 and 55 both show the spectrum for FeOCl, but at different concentrations. The intercalates have a greater absorption at low energy (0.5 eV) and more structure in their spectra at high energy (3.5 - 1.5 eV) compared to FeOCl.

$FeOCl(TTF)_{1/8.5}$ and $FeOCl(TTF)_{1/9}(tol)_{1/21}$ exhibit a broad absorption centered at about 1200 nm (1.03 eV) (Figure 56). A possibly related transition is observed in the spectra of salts such as TTF(CA) (ss) at 833 nm (see Figure 56). This corresponds to charge transfer between the $(TTF^+)_2$ ions as illustrated below.[166,152]

$$(TTF^+)(TTF^+) \longrightarrow TTF^0TTF^{2+} \qquad \text{(a)}$$

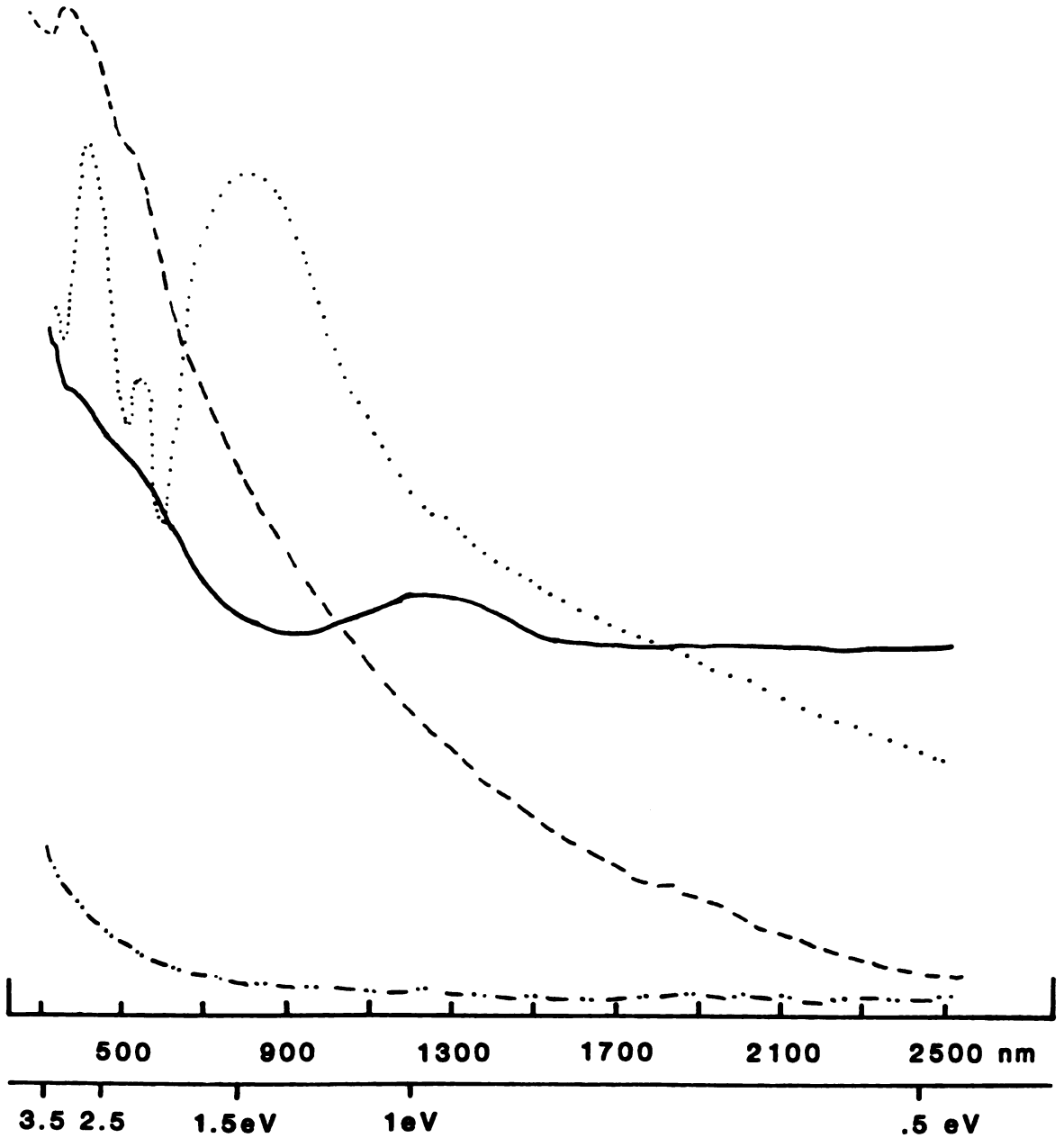

Figure 56. Optical spectra of (flurolube mulls between NaCl plates) for FeOCl(---), FeOCl$(TTF)_{1/8.5}$ (——), and TTF(CA)(ss)(•••••). The baseline is indicated also (-•-•-•-). Absorption is an arbitrary scale

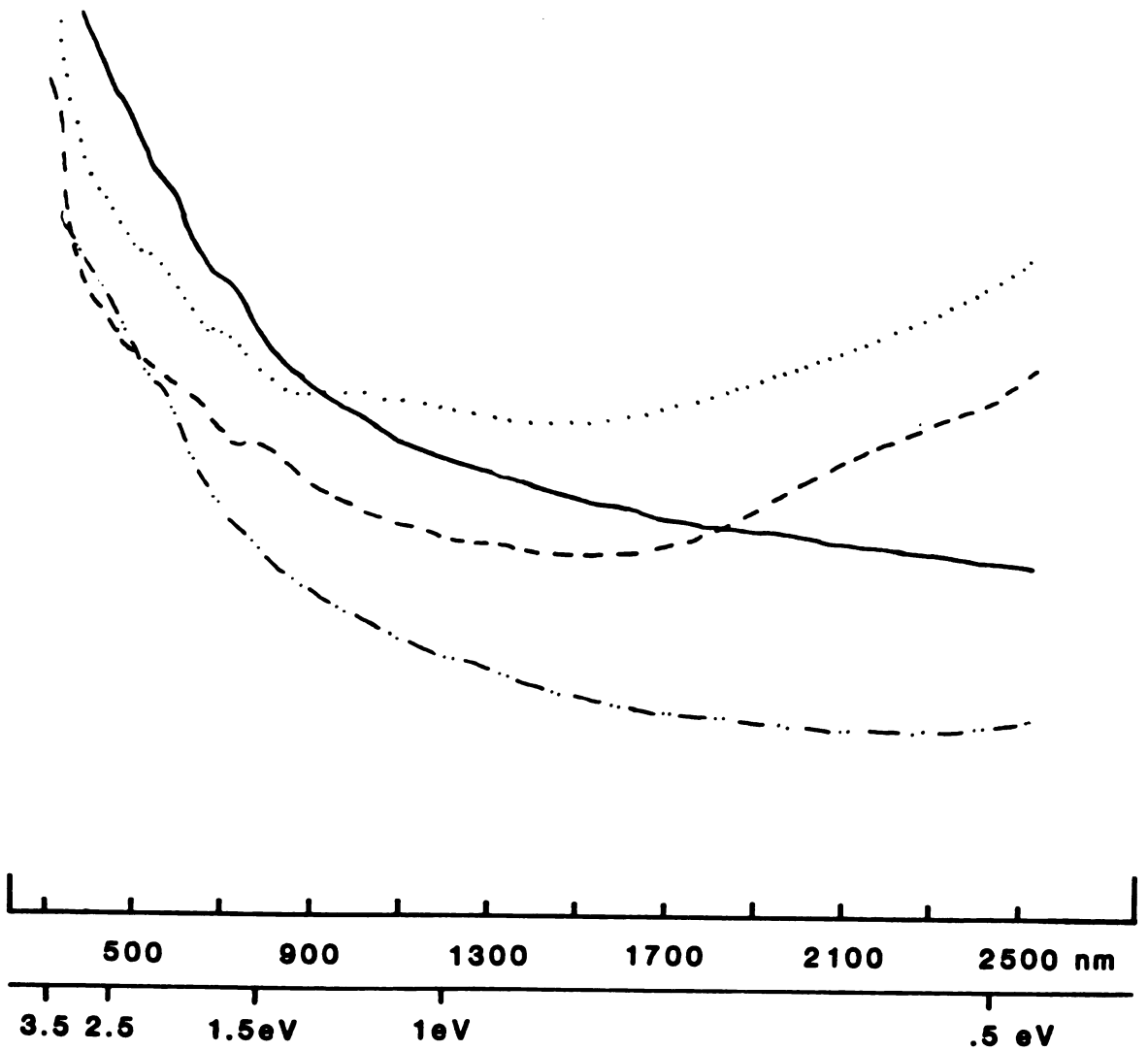

Figure 57. Optical spectra (flurolube mulls between NaCl plates) for FeOCl(-·-·-·-), $FeOCl(TMTTF)_{1/13}$(——), $FeOCl(TTN)_{1/9}(tol)_{1/21}$(·····) and $FeOCl(TTT)_{1/9}(tol)_{1/23}$ (---). Absorption is an arbitrary scale

For mixed valence salts, there is an additional, stronger, charge transfer band, which is located at 1110 nm for $TTF(Br)_{0.71}$ and 1250 nm for $TTF(SCN)_{0.57}$,[166] corresponding to the transition shown below.

$$(TTF)^{+}(TTF)^{0} \longrightarrow (TTF)^{0}(TTF)^{+} \qquad (b)$$

Although the absorption in $FeOCl(TTF)_{1/8.5}$ is centered at 1250 nm, the mechanism of charge transfer shown in (b) is unlikely due to the absence of evidence for partial charge transfer in the infrared data. The probable explanation is that the charge transfer observed for the fully ionic TTF(CA) (ss) compound has shifted to lower energy in the intercalate.

Alternatively, the absorption at 1250 nm could be attributed to an intervalence charge transfer band. The existence of intervalence charge transfer ($Fe^{3+} \rightarrow Fe^{2+}$) has been proposed based on the evidence from Mössbauer spectroscopy for charge transfer between the guest and host.[36] Most intervalence bands are broad, intense absorptions.[167] Typically they obey the relation

$$\Delta = (\nu_{IT} \times 2310)^{1/2} \qquad (20)$$

at 300 K, where ν_{IT} is the frequency of the absorption maximum in wavenumbers and Δ is the width at half height of the absorption. Using this formulation the half width value obtained (4299 cm^{-1}) is about four times larger than an estimation of the experimental value (1288 cm^{-1}) of the absorption peak at 1250 nm for $FeOCl(TTF)_{1/8.5}$. Because of the underlying absorption present in the spectrum, the peak

is not well resolved and could correspond to an intervalence charge transfer band, but due to the absence of this peak in any of the other intercalates this explanation seems highly unlikely. The visible region exhibits bands that have been attributed to TTF^{+}.[86]

The poor intensity and resolution of these spectra (Figures 56 and 57) are similar to that observed for the layered compound $FePS_3$ and its intercalates.[168] Although infrared data for the FeOCl intercalates indicate that charge transfer has occurred, no intervalence charge transfer band could be identified. The TTF intercalates have a band centered at 1250 nm which is attributed to charge transfer between the dimeric units of TTF.

Conductivity

The conductivity obtained from "single crystals" was of the same order of magnitude as the powder samples,[169] indicating that the "crystals" were probably aggregates. The anisotropy of the "crystal" could be measured by using a standard four-probe technique for the ac plane and a two probe conductivity apparatus for the b axis.[63,70] Conductivity values of 4.4×10^{-4} and 4.1×10^{-7} $(ohms\text{-}cm)^{-1}$, for the ac plane and the b axis, respectively, of $FeOCl(TTF)_{1/9}(tol)_{1/21}$, show the anisotropy to be ca. 10^3.

While single crystals are desirable, the problems in obtaining X-ray diffraction quality single crystals by the reaction procedure described have been insurmountable thus far. This has made it necessary to measure two probe pressed powder conductivities. Using an apparatus described elsewhere,[63,70] temperature dependent conductivity data for FeOCl and the tetrathiolene intercalates have been

obtained (Figure 58). Multiple samples were examined and data from samples which did not obey Ohm's law were disregarded. The variation of conductivity over the temperature range of -60 to 80°C indicates that both FeOCl and its intercalates behave as semiconductors. Band gaps listed in Table 24 were obtained from the least squares fit to the relationship,[171] $\ln \sigma = -E_g/2k_BT$, where E_g corresponds to the band gap and k_B is Boltzmann's constant. It should be noted that although a band gap could not be identified in either the infrared or the near-infrared region, there was a significant background in the optical and vibrational spectra of all the intercalates compared to FeOCl, which suggests an electronic transition.

The pressed powder conductivity increases from ca. 10^{-7} for pristine FeOCl to ca. 10^{-2} for $FeOCl(TMTTF)_{1/13}$ (Table 24). The similarity in the slopes for the variable temperature measurements suggests that the eletronic conductivity is due to the host lattice.[172] $FeOCl(TMTTF)_{1/13}$ exhibits the highest room temperature conductivity, further corroborating this hypothesis. It has been shown that to obtain high conductivity of the type seen in the organic metals the electron donor molecules must be stacked one on top of the other. This requirement is obviously not met by the TMTTF intercalate in which the plane of the tetrathiolene is parallel to the FeOCl layers, rather than perpendicular.

X-Ray Absorption Near Edge Structure

As a result of the physical methods employed thus far, an interesting question arises as to whether the electron from the intercalant is in the host layers, and if so, where. Interpretation of

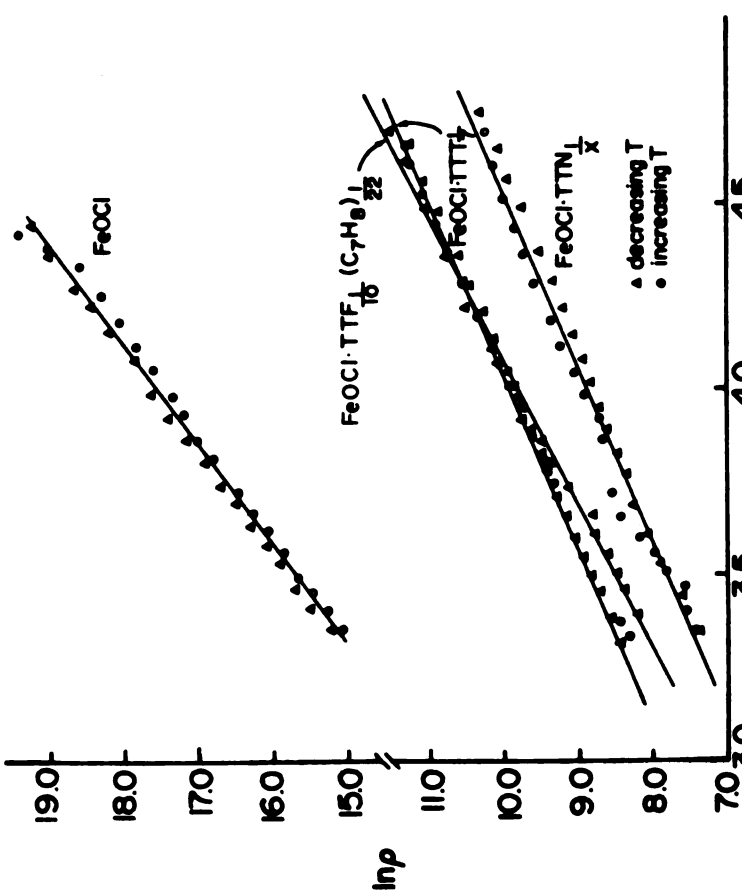

Figure 58. $\ln\rho$ vs 1/T for two probe pressed powder conductivity measurements

Table 24. Two-probe pressed powder conductivity measurements for FeOCl and the intercalates

Compound	E_g(eV)	$\sigma_{RT}(\Omega\text{-cm})^{-1}$
FeOCl	0.61	4.4×10^{-6} 2.0×10^{-7}
$FeOCl(TTF)_{1/9}(tol)_{1/21}$	0.36	3.5×10^{-3}
$FeOCl(TTF)_{1/8.5}$	0.45	7.8×10^{-4}
$FeOCl(TMTTF)_{1/13}$		1.6×10^{-2}
$FeOCl(TTF)_{1/9}(tol)_{1/22}$	0.35	2.1×10^{-3}
$FeOCl(TTF)_{1/9}(tol)_{1/23}$	0.38	2.3×10^{-3}

Mössbauer data has led to various charge transfer models,[173-175] including an electron hopping model proposed for Lewis base intercalates.[36] The Mössbauer spectra of $FeOCl(py)_{1/3}$ and related amine intercalates, analyzed using the electron hopping model, are consistent with the presence of 10-13% ferrous iron sites within the FeOCl lattice.[176]

Without access to Mössbauer spectroscopy (until our very recent collaboration), X-ray Absorption Near Edge Structure (XANES), spectroscopy provided an alternate method to probe the electronic state of the iron. XANES comprises the pre-edge, edge, and about 10-20 eV of the post-edge region of the X-ray absorption spectrum. Figure 59

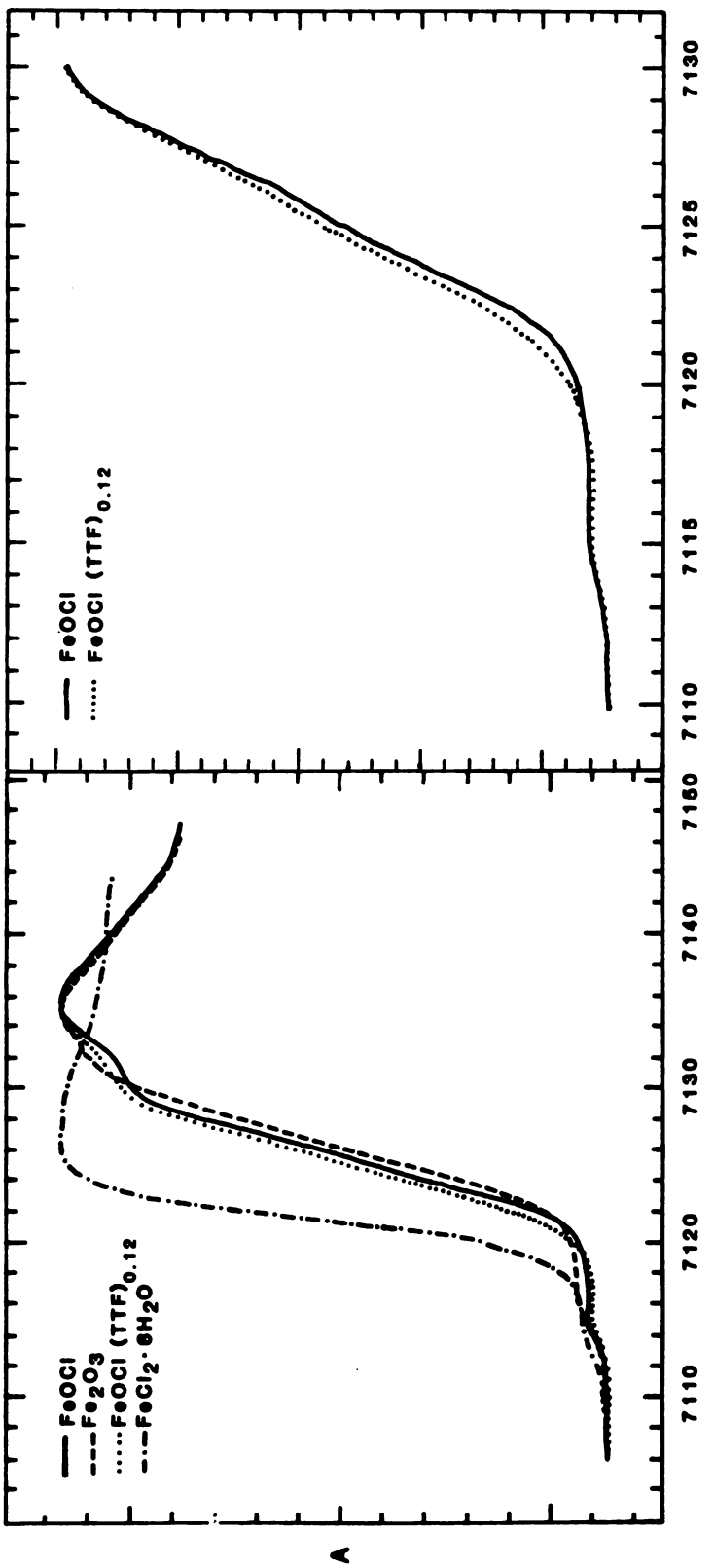

Figure 59. The Fe K-edge X-ray absorption edge spectrum for (a) FeOCl and various materials (b) and FeOCl and $FeOCl(TTF)_{1/8.5}$

shows the edge shifts for various iron +3 and +2 compounds. The spectra of the materials containing ferrous iron are shifted to lower energy with respect to those of materials containing ferric iron. The Fe K-edge XANES spectra for FeOCl and for $FeOCl(TTF)_{1/8.5}$ are shown in Figure 5. For all the intercalates the edge is shifted to lower energy, indicative of the presence of Fe^{+2}. Small shifts such as seen in Figure 57 have also been observed for MTS_2 (M = first row transition metal, T = Ti, Zr, V, Nb).[177] Unfortunately, XANES is not a quantitative technique, and although the data indicate that charge transfer to FeOCl has occurred, the edge shift cannot provide a measure of the percentage of ferrous sites within the lattice. Preliminary Mössbauer data on the tetrathiolene intercalates verify the presence of 8-10% ferrous sites, but further work is necessary before these results can be considered conclusive.

Magnetic Studies of FeOCl and the Intercalates

Variable temperature magnetic susceptibility

The molar susceptibility of powdered FeOCl and the intercalants between 5 and 300 K is shown in Figures 60 and 61. The data are interpreted as due to strong antiferromagnetic coupling. The room temperature magnetic moments were calculated using the spin-only relationship ($\mu_{eff} = 2.828 \sqrt{\chi T}$) and are low compared to the spin only value for high-spin iron +3 (see Table 25).

A considerable amount of information on the magnetic interactions has been obtained from Mössbauer spectroscopy,[36,40,70,100,178] and very little by variable temperature susceptibility.[41,179] It has been suggested that the $\chi(T)$ data below about 350 K reflect short

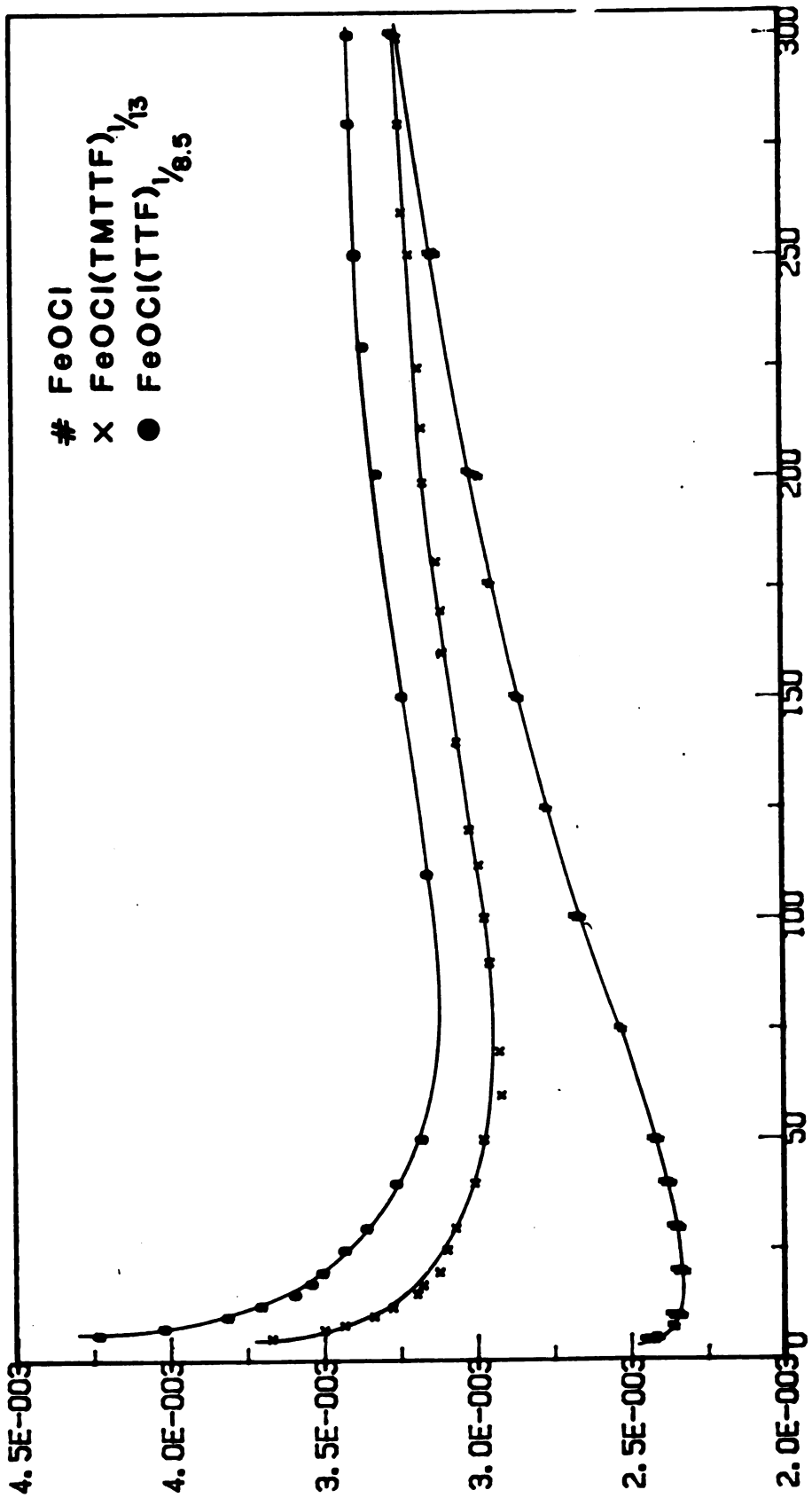

Figure 60. χ molar vs T for FeOCl, $FeOCl(TMTTF)_{1/13}$ and $FeOCl(TTF)_{1/8.5}$ with lines drawn through the points

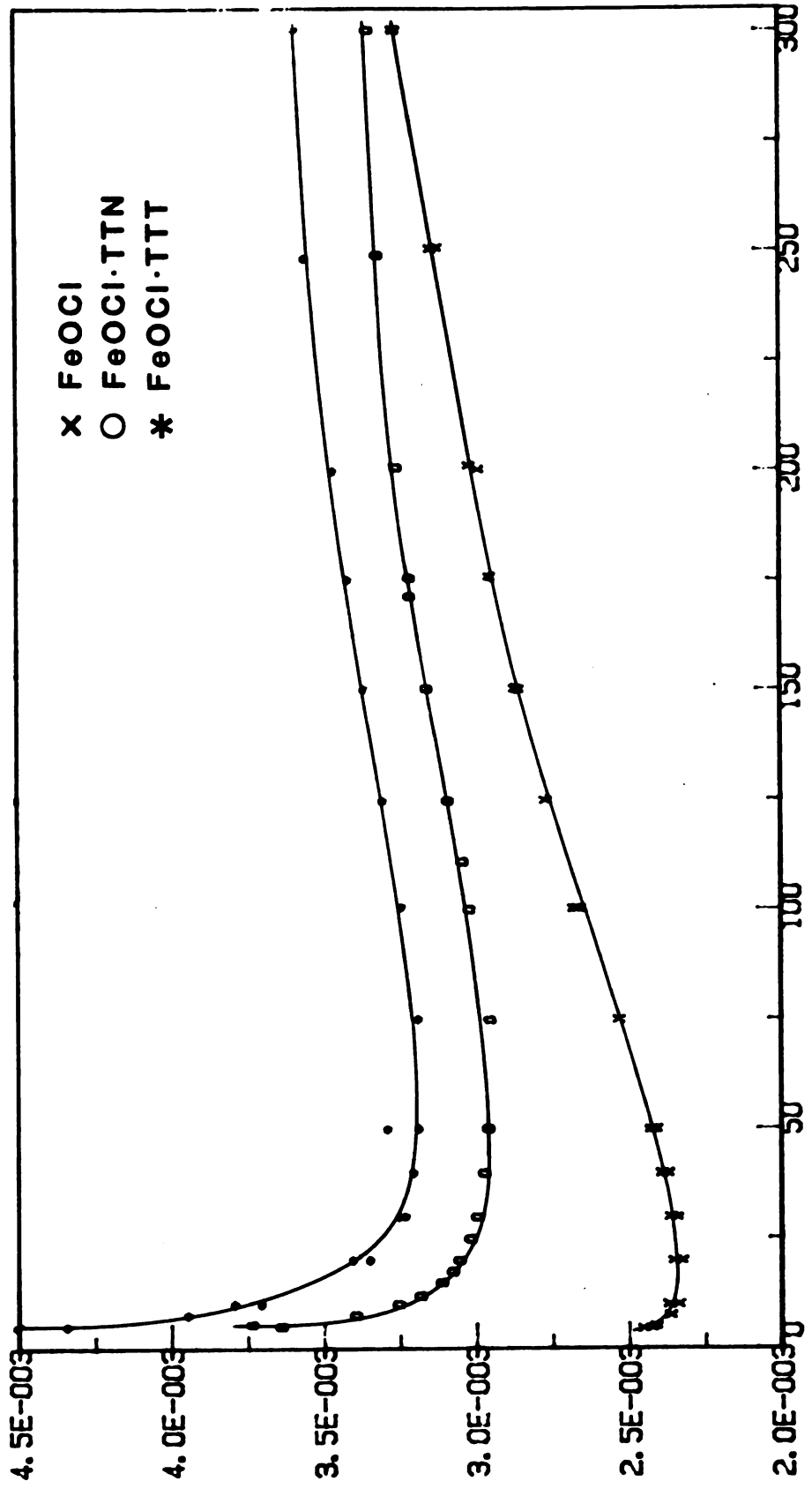

Figure 61. χ molar vs T for FeOCl, $FeOCl(TTN)_{1/9}(tol)_{1/21}$ and $FeOCl(TTT)_{1/9}(tol)_{1/23}$ with lines drawn through the points

Table 25. Effective moments calculated for high spin Fe^{+3}, FeOCl, and the intercalates at 300 K using spin-only formula

Compound	μ_{eff}
Fe^{+3}	5.9
FeOCl	2.76
$FeOCl(TTF)_{1/8.5}$	2.8
$FeOCl(TMTTF)_{1/13}$	2.8
$FeOCl(TTF)_{1/9}(tol)_{1/22}$	2.8
$FeOCl(TTF)_{1/9}(tol)_{1/23}$	2.9

range antiferromagnetic ordering of FeOCl.[41] The Mössbauer data show no evidence for magnetic ordering at 300 K for this sample.[180] After investigating various models employing linear chain theories,[181] two-dimensional theories and other models which considered extended chains,[182,183] it was found that the model that best describes the data so far is based on short range interactions.[184] The model consists of a system of three spins interacting in the form of a linear chain. It has been proposed that the short range magnetic interactions are fluctuating on a time scale faster than can be resolved by Mössbauer spectroscopy.[41] The short range interaction model provides a reasonable fit to the data, indicating that the hypothesis of short range magnetic order is basically correct.

The variable temperature susceptibility data for the intercalates (shown in Figures 60 and 61) are very similar to those of FeOCl. There is a low temperature Curie tail in the intercalates, which may be due to impurities in the intercalates, otherwise the curves are almost temperature independent between 90 and 300 K. The similar slopes for the susceptibility curves between 90 and 300 K for FeOCl and the intercalates suggest that the short range magnetic interactions observed for FeOCl are also present in the intercalates.

Neutron diffraction

Mössbauer spectra of both single crystal and powder show the onset of a magnetic hyperfine interaction at 92 ± 3 K for FeOCl.[40,76,178] Analysis of the spectra shows that more than one set of crystallographically equivalent Fe^{+3} sites is present and that all the Fe^{+3} spins cannot be parallel to either the a, b, or c axis.[177] This is in agreement with preliminary Mössbauer data in which the two different lattice sites can be resolved for pristine FeOCl.[184]

AT 10 K the neutron diffraction data show the presence of new peaks (Figure 62), compared to the 300 K data, which are attributed to the magnetic lattice of FeOCl.[185] The magnetic structure which was proposed for FeOCl by Adam and Buisson from the analysis of the neutron data is shown in Figure 63. This structure has a doubled crystallographic lattice along both the a and b axis and the spins turned by 99° from one unit cell to the next in the c direction.

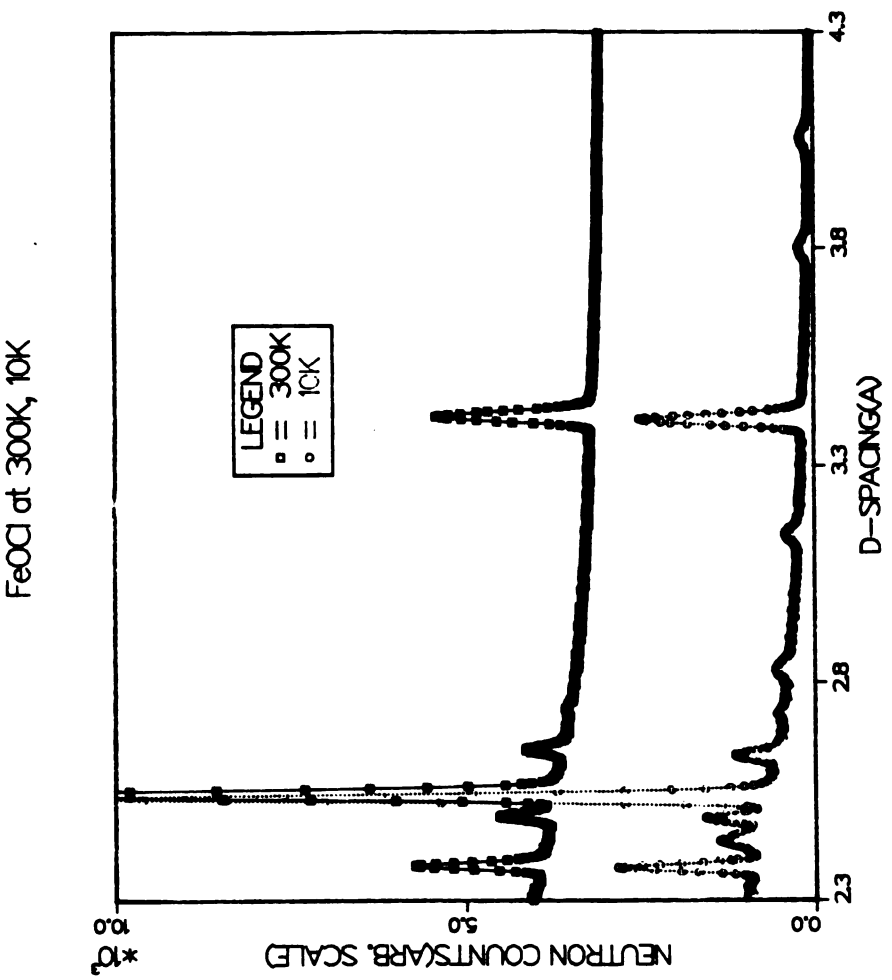

Figure 62. Neutron powder diffraction for FeOCl 300 K (top) and 10 K (bottom) data

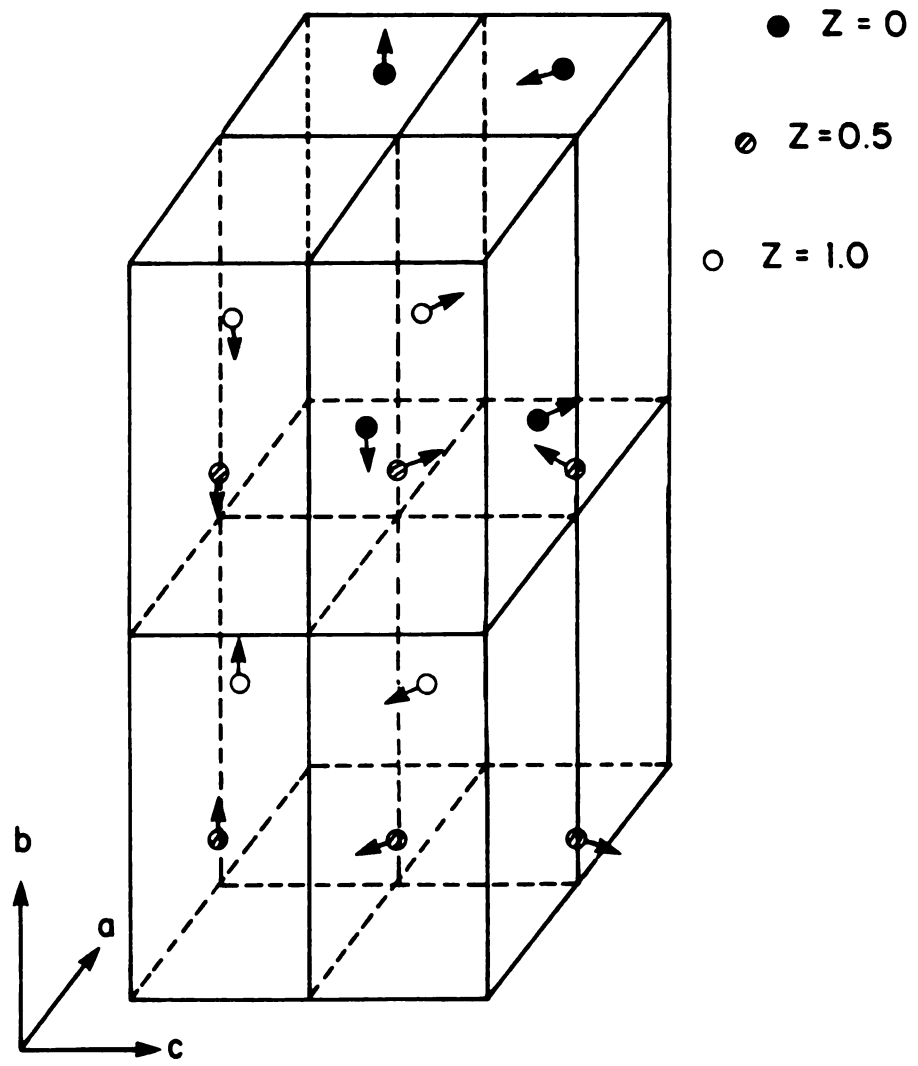

Figure 63. Magnetic lattice for FeOCl (8 unit cells) showing the direction of spins proposed by Adam and Buisson

The low temperature neutron data for $FeOCl(TTF)_{1/8.5}$ (Figure 64) show no new peaks, thus indicating that the long range magnetic order has been abolished upon intercalation. Considering the antiferromagnetic coupling across the b axis (Figure 63), it is not surprising that intercalation abolishes the long range order.

Variable magnetic susceptibility measures bulk effects and no Neel temperature is observed for either FeOCl or for the intercalates over the available temperature range. Fitting the magnetic susceptibility of the intercalants will provide information on the changes in the short range magnetic interactions. More direct information can be determined from Mössbauer spectroscopy, and those experiments are currently underway.

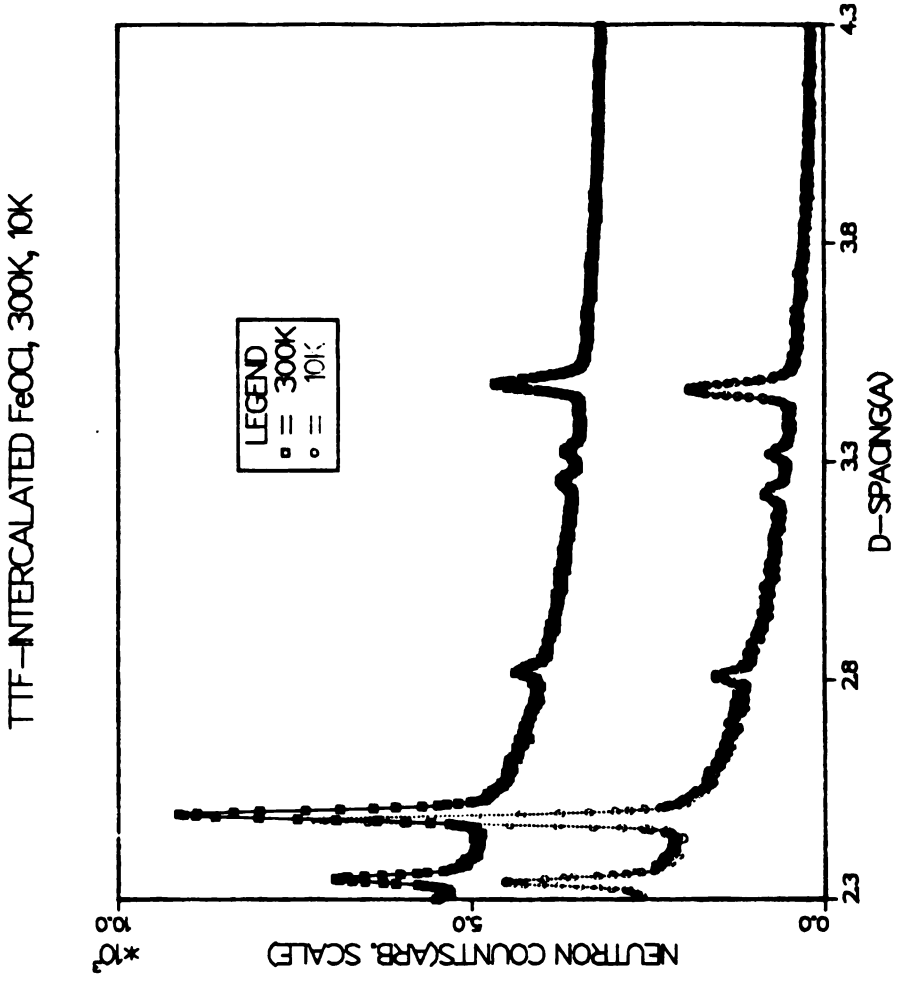

Figure 64. Neutron powder diffraction for $FeOCl(TTF)_{1/8.5}$, 300 K (top) and 10 K (bottom) data

SUMMARY

A series of intercalation compounds containing TTF and related tetrathiolene molecules with FeOCl as the host has been prepared and characterized. Solvent, impurities and host decomposition have major effects upon the rate of intercalation. It appears that polar organic solvents with electron donating ability stabilize the radical cation, thus facilitating charge transfer between the FeOCl and the guest species. Slightly different stoichiometries of the intercalates can be obtained by varying reaction times and temperatures. At temperatures greater than 70°C, however, noticeable decomposition of FeOCl occurs. The studies of the preparation of $FeOCl(TTF)_{1/9}$ and $FeOCl(TMTTF)_{1/13}$, although preliminary, provide strong evidence that the rate of intercalation is increased by the presence of impurities and host decomposition. Differences in stoichiometries obtained for distinct preparations are meaningful, but do not appear to significantly affect the physical properties measured to date.

X-ray powder diffraction data for all the intercalants can be adequately described by an orthorhombic cell with *a* unchanged, *c* increased by about 1% and *b* (the interlayer axis) expanded and doubled compared to pristine FeOCl. Analysis of the line shapes obtained from neutron powder diffraction is consistent with $FeOCl(TTF)_{1/8.5}$ being a well-ordered crystalline material. Comparison of the full widths at

half maximum of the X-ray powder diffraction data for the intercalates vs FeOCl indicates that $FeOCl(TTF)_{1/9}(tol)_{1/23}$ is the least crystalline.

Two models have been proposed based on X-ray powder diffraction and EXAFS data and on the combination of these techniques with neutron powder diffraction studies. In the first, referred to as the hard sphere model, the sulfur on the tetrathiolene and the chloride ion of the FeOCl layer are considered to be hard spheres. The sulfur-chloride distance is determined from the sum of their van der Waals radii. The model predicts that TTF must be aligned along the c axis of FeOCl and tilted at an angle $\Theta = 25°$ (where Θ is the angle with respect to perpendicular to the FeOCl layers) and requires that the FeOCl lattice be monoclinic. Thus, the TTF molecules must be almost close packed within the layers. TTN and TTT are also predicted to be aligned along the c axis of FeOCl, but two angles are necessary in order to accommodate the short S-S bond. The molecules are tilted at an angle $\Theta = 42°$ and at an angle $\phi = 14°$ (where ϕ is defined as the angle between the S-S bond and the ac plane). The only possible orientation of TMTTF is parallel to the FeOCl layers. The second model, the soft sphere model, initially was considered in order to explain the neutron powder diffraction data for $FeOCl(TTF)_{1/8.5}$. This constitutes the first time that an approach other than a hard sphere approximation has been used to consider the orientation of an intercalate. The neutron data indicate that the presence of TTF within the layers contributes to the long range order of the solid and provide conclusive evidence for a body-centered orthorhombic cell for the

intercalates, corresponding to either I222 or Immm space group. The FeOCl lattice has expanded and doubled along the b axis, so that tilting of the TTF molecule is no longer valid. The TTF molecule is proposed to be oriented perpendicular to the layers, thus locking the layers into an eclipsed configuration. The sulfurs on the TTF are then closer to the chloride ions of FeOCl (3.15 A) than the sum of the van der Waals radii (3.6 A), implying that the sulfur atoms must be considered as something other than a hard sphere. Pseudotetrahedral (sp^3) hybridization, observed for the selenium atoms in TMTSF salts, is proposed for the electronic density on the sulfur atoms of TTF. The resulting nonspherical electronic distribution about the sulfur rationalizes the short sulfur-chloride contacts. Because of the short S-S bond of TTT and TTN, these intercalants must be tilted at an angle ϕ, as defined by the hard sphere model, with respect to the FeOCl layers. The molecules are aligned along the c axis of FeOCl with Θ = 0 (Θ defined by the hard sphere model). The soft sphere model for $FeOCl(TTF)_{1/8.5}$ also indicates that the TTF molecules are approximately close packed within the layers.

The tetrathiolenes are present in the FeOCl layers as radical cations. The optical and infrared spectra exhibit a broad background absorption between about 0.3 and 1.0 eV, typical of an electronic transition observed in conducting and semiconducting materials. An absorption band due to an intervalence charge transfer could not be identified, but may be obscured by the background absorption. $FeOCl(TTF)_{1/9}$ has an absorption band centered at about 1250 nm, which may be attributed to charge transfer within the TTF dimeric units.

XANES and preliminary Mössbauer studies indicate that about 10% of the iron in the lattice is present as Fe^{+2}. Although more studies are necessary, the presence of Fe^{+2} confirms that charge transfer between the guest and host has occurred.

The electrical conductivity increases by 10^2 to 10^5 over that of pristine FeOCl ($\sigma_{RT} \sim 10^{-7}$ $(ohms\text{-}cm)^{-1}$) upon intercalation. FeOCl and the intercalates behave as semiconductors over the temperature range investigated. The band gap of 0.6 eV was confirmed for FeOCl and band gaps of 0.3 - 0.4 eV were obtained for the intercalates based on the variable temperature conductivity measurements. The lack of metallic conductivity can be attributed to several factors, including the presence of domains within the FeOCl layers, the occurrence of complete charge transfer between the tetrathiolene and FeOCl, insufficient overlap between adjacent tetrathiolene molecules, and to impurity states within FeOCl. The observed increase in electrical conductivity is attributed to electron transport within the FeOCl layers.

Variable temperature magnetic susceptibility indicates that there is strong short-range magnetic ordering at temperatures between 90 and 300 K for FeOCl. Low temperature neutron powder diffraction data show that FeOCl orders antiferromagnetically and that the ordering is long-range. The absence of magnetic peaks in the low temperature neutron powder diffraction data for $FeOCl(TTF)_{1/8.5}$ and $FeOCl(d_4\text{-}TTF)_{1/9}$ indicates that the long-range magnetic order is abolished upon intercalation. Since the iron atoms are antiferromagnetically coupled

across the b axis (the interlayer distance), one would expect that intercalation would considerably weaken any sort of long range interactions. Due to the similarities in the susceptibility curves of the intercalates and FeOCl between 90 and 300 K, it is proposed that the short-range magnetic ordering is still in effect for the intercalates.

Taken together, the physical studies indicate that the bulk properties can be attributed to the changes in electronic, magnetic and physical structure of the FeOCl lattice resulting from intercalation. Complete charge transfer has occurred between the guest and host, resulting in conductivity due to the added electrons within the FeOCl layers. The fact that the TMTTF intercalate has the highest conductivity and the lowest intercalant stoichiometry corroborates this hypothesis.

Detailed physical studies on $FeOCl(TTF)_{1/8.5}$ are consistent with the TTF molecule oriented perpendicular to the layers and dimerized. TTF contributes to the long-range order as observed by the neutron powder diffraction data. Although the analysis of the neutron data is still at a preliminary stage, the slow oscillation of the background in the neutron powder diffraction data may be attributed to short-range order within the solid.

Solid state wideline NMR spectroscopy provides further insight into the orientation and interactions of the TTF molecule within FeOCl. The ^2H NMR data indicate that d_4-TTF motion is more constrained and/or slower in $FeOCl(d_4\text{-TTF})_{1/9}$ than in crystalline d_4-TTF; the ^1H data are consistent with this interpretation. The ^1H

lineshapes and hole burning experiments together with the observation of multiple splittings in the ^2H quadrupole-dipole NMR provide evidence for more than one type of environment of TTF molecules in $FeOCl(d_4\text{-}TTF)_{1/9}$, characterized by different average TTF orientations and/or dynamics. This can be most simply interpreted as evidence for molecular domains with different structural and/or dynamic characteristics.

It appears that the sulfur atoms on the intercalant are in close proximity to the chloride ions of the FeOCl layer. There may not be sufficient overlap between adjacent intercalant molecules to result in conductivity. The question of domains within the layers needs to be pursued further by ^2H NMR spectroscopy and neutron powder diffraction, as well as by single crystal and powder X-ray diffraction. The use of the selenium analogues, which have a larger radial distribution function, will increase the possibility of overlap for the intercalants. In addition, partial, rather than complete, electron transfer needs to be achieved, possibly by intercalation of compounds with higher oxidation potentials. The use of electrochemical synthesis has not yet been explored for these compounds and may produce higher concentrations of intercalant within the layers, resulting in better overlap between the intercalant molecule. Electrochemical intercalation of single crystals may also produce higher quality crystals for X-ray diffraction than the method currently used. Before too many general conclusions about these compounds can be made, more intercalation compounds with various electron donors such as ET and TMTSF need to be prepared.

Intercalation of organosulfur compounds such as TTF has resulted in new low-dimensional materials, but high conductivity has not yet been achieved. The results to date indicate that intercalation chemistry is a promising route to low-dimensional conductors. It provides the correct orientation for the guest molecules and results in charge transfer between the guest and host species (albeit complete, rather than partial so far). Further investigations of new intercalation compounds as well as different synthetic procedures for the compounds discussed herein will result in a more complete understanding of these systems. This will allow one to predict, at least qualitatively, the properties of these new materials and consequently to be able to tailor them to meet specific demands.

LIST OF REFERENCES

LIST OF REFERENCES

1. "Physics and Chemistry of Low-Dimensional Solids"; Alcacér, L., Ed.; D. Reidel Press: Dordrecht, Holland, 1980.

2. Miller, J. S.; Epstein, A. J. Prog. Inorg. Chem. 1976, 20, 1-151.

3. Day, P. Chem. in Britain 1983, 19, 306-310.

4. Hoffman, B. M.; Ibers, J. A. Acc. Chem. Res. 1983, 16, 15-21.

5. Greene, R. L.; Street, G. B. Science, 1984, 226, 651-656.

6. Little, W. A. Sci. Amer. 1965, 212, 21-27.

7. Little, W. A. Phys. Rev. 1964, 134A, 1416-1424.

8. Underhill, A. E.; Watkin, D. M. Chem. Soc. Rev. 1980, 9, 429-448.

9. Labes, M. M.; Love, P.; Nichols, L. F. Chem. Rev. 1979, 79, 1-15.

10. Goodings, E. P. Chem. Soc. Rev. 1976, 5, 95-123.

11. Nohr, R. S.; Kuznesof, P. M.; Wynne, K. J.; Kenney, M. E.; Siebenman, P. G. J. Am. Chem. Soc 1981, 103, 4371-4377.

12. Schoch, K. F., Jr.; Kundalkar, B. R.; Marks, T. J.; J. Am. Chem. Soc. 1979, 101, 7071-7073.

13. Metz. J.; Hanack, M. J. Am. Chem. Soc. 1983, 105, 828-830.

14. Phillips, T. E.; Hoffman, B. M. J. Am. Chem. Soc. 1977, 99, 7734-7736.

15. Bechgaard, K.; Andersen, J. R. in "Physics and Chemistry of Low- Dimensional Solids", Alcacér, L., Ed.; D. Reidel Press: Dordrecht, Holland, 1980; p. 247-263.

16. Khidekel, M. L.; Zhilyaeva, E. I. Synthetic Metals 1981, 4, 1-34.

17. Bechgaard, K; Carneiro, K.; Olsen, M; Rasmussen, F. B.; Jacobsen, C. S. Phys. Rev. Lett. 1981, 46, 852.

18. Jerome, D.; Mazaud, A.; Ribault, M.; Bechgaard, K. J. Physique Lett. 1980, 41, L95-L98.

19. Bechgaard, K.; Jacobsen, C. S.; Mortensen, K.; Pedersen, H. J.; Thorup, N. Solid State Commun. 1980, 33, 1119-1125.

20. Williams, J. M.; Emge, T. J.; Wang, H. H.; Carlson, K. D.; Crabtree, G. W. Inorg. Chem. 1984, 23, 2558-2560.

21. Kobayashi, H.; Kobayashi, A.; Sasaki, Y.; Saito, G.; Enoki, T.; Inokuchi, H. J. Am. Chem. Soc. 1983, 105, 297-298.

22. Saito, G.; Enoki, T.; Toriumi, K.; Inokuchi, H. Solid State Commun. 1982, 42, 557-560.

23. Torrance, J. B. Acc. Chem. Res. 1979, 12, 79-86.

24. Ibers, J. A.; Pace, L. J.; Martinsen, J.; Hoffman, B. M. Struct. Bonding (Berlin) 1982, 50, 1-55.

25. Perlstein, J. H. Angew. Chem. Intl. Ed. Engl. 1975, 16, 519-534.

26. Lyuovskaya, R. N. Russ. Chem. Rev. 1983, 52, 736-750.

27. Gamble, F. R.; Geballe, T. H. "Treatise on Solid State Chem"; Vol. III; Hannay, N. B., Ed.; Plenum Press: New York, 1976; pp. 89-166.

28. Hullinger, F. in "Structural Chemistry of Layer-Type Phases"; Levy, F., Ed.; D. Reidel: Dordrecht, Holland; 1976.

29. "Intercalated Layered Materials"; Levy, F., Ed.; D. Reidel Press: Dordrecht, Holland; 1979.

30. "Intercalation Chemistry:; Whittingham, M. S.; Jacobson, A. J., Ed.; Academic Press: New York, 1982.

31. Schöllhorn, R. in "Inclusion Compounds"; Atwood, J. L.; Davies, J. E. D.; MacNicol, D. D., Eds.; Academic Press: New York, 1984; pp. 249-349.

32. Schöllhorn, R. Angew. Chem. Int. Ed. Engl. 1980, 19, 983-1003.

33. Gamble, F. R.; Osiecki, J. H.; Cais, M.; Pisharody, R.; DiSalvo, F. J.; Geballe, T. H. Science 1971, 174, 493-500.

34. Riekel, C.; Hohlwein, D.; Schöllhorn, R. J. C. S. Chem. Comm. 1976, 863-864.

35. Riekel, C.; Fisher, C. O. J. Solid State Chem. 1979, 29, 181-190.

36. Eckert, H.; Herber, R. H. J. Chem. Phys. 1984, 80, 4526-4540.

37. Silbernagel, B. G. Chem. Phys. Lett. 1979, 34, 298-301.

38. Dines, M. B. Science 1975, 188, 1210-1211.

39. Halbert, T. R.; Scanlon, J. C. Mater. Res. Bull. 1979, 14, 415-421.

40. Herber, R. H. Acc. Chem. Res. 1982, 15, 216-224.

41. Halbert, T. R.; Johnston, D. C.; McCandlish, L. E.; Thompson, A. H.; Scanlon, J. C.; Dumesic, J. A. Physica 1980, 99B, 128-132.

42. Schafer-Stahl, H.; Abele, R. Mat. Res. Bull. 1980, 15, 1157-1165.

43. Schafer-Stahl, H.; Abele, R. Angew. Chem. Int. Ed. Engl. 1980, 19, 477-478.

44. "Inorganic Synthesis"; Vol. 19, Shriver, D. F., Ed.; John Wiley & Sons, Inc.: New York, 1979.

45. Ferrais, J. P.; Poehler, T. O.; Bloch, A. N.; Cowan, D. O. Tet. Lett. 1973, 27, 2553-2556.

46. Nakayama, J. Synthesis 1975, 38-39.

47. Nakayama, J. Synthesis 1975, 168-169.

48. Girlando, A.; Marzola, F.; Pecile, C.; Torrance, J. B. J. Chem. Phys. 1983, 79, 1075-1085.

49. Schäfer, H.; Wartenpfuhl, F. J. Less-Common Metals 1961, 3, 29-33.

50. Venien, J. P.; Palvadeau, P.; Schleich, D.; Rouxel, J. Mat. Res. Bull. 1979, 14, 891-897.

51. Kaplan, M. L.; Wudl, F.; Haddon, R. C.; Hauser, J. J. Chemica Scripta 1980, 15, 196-202.

52. Dolphin, D.; Pegg, W.; Wirz, P. Can. J. Chem. 1974, 52, 4078-4082.

53. Marshalk, C.; Strumm, C. Bull. Soc. Chim. Fr. 1948, 15, 418-428.

54. Goodings, E. P.; Mitchard, D. A.; Owen, G. J. C. S. Perkin 1972, 1310-1314.

55. Teo, B. K.; Snyder-Robinson, P. A. Inorg. Chem. 1979, 18, 1490-1495.

56. Teo, B. K., private communication.

57. "Organic Synthesis"; Collective Vol. 3; John Wiley & Sons, Inc.: New York, 1955, p. 809.

58. Hoult, D. I.; Richards, R. E. Proc. R. Soc. Lond. A 1975, 344, 311-340.

59. Stejskal, E. O.; Schaefer, J. J. Mag. Res. 1974, 14, 160-169.

60. Bloom, M.; Davis, J. H.; Valic, M. I. Can. J. Phys. 1980, 58, 1510-1517.

61. Griffin, R. G. Met. Enzymol 1981, 72, 108-174.

62. Tegenfeldt, J.; Haberlen, U. J. Mag. Res. 1979, 36, 453-457.

63. Yemen, M. R., Ph.D. Thesis, Michigan State University, 1983.

64. Azaroff, L. V.; Buerger, M. J. "The Powder Method in X-Ray Crystallography"; McGraw-Hill: New York, 1958; pp. 46-55.

65. Antonio, M. R., Ph. D. Thesis, Michigan State University, 1983.

66. Rietveld, H. M. J. Appl. Cryst. 1969, 2, 65-71.

67. Lind, M. D. Acta. Cryst. 1972, B26, 1058-1062.

68. Mayerle, J. J.; Torrance, J. B.; Crowley, J. I. Acta. Cryst. 1979, B35, 2988-2995.

69. Perez-Albuerne, E. A.; Johnson, H., Jr.; Trevoy, D. J. J. Chem. Phys. 1971, 55, 1547-1554.

70. Kamamaru, F.; Shimada, M.; Takano, M.; Takada, T. J. Solid State Chem. 1973, 7, 297-299.

71. Wadsley, A. D. in "Nonstoichiometric Compounds"; Manderleorn, L., Ed.; Academic Press: New York, 1964, p. 101.

72. Schäfer, H.; Wittig, F,; Jori, M. Anorg. Allg. Chem. 1956, 287, 61.

73. Goldstaub, M. S. Acad. Sci.-Comptes Rendus, Paris 1934, 198, 667-669.

74. Kostimer, E.; Steger, J. J. Solid State Chem. 1971, 3, 273-275.

75. Kikkawa, S.; Kanamaru, F.; Koizumi, M. Bull. Chem. Soc. Jpn. 1979, 52, 963-966.

76. Grant, R. W.; Wiedersich, H.; Housley, R. M.; Espinosa, G. P.; Artman, J. O. Phys. Rev. B 1971, 3, 678-684.

77. Hagenmueller, P.; Rouxel, J.; Portier, J. C. R. Hebd. Seances Acad. Sci. Ser B 1972, 275, 911-913.

78. Halbert, T. R., in "Intercalation Chemistry", Whittingham, M. S.; Jacobson, A. J., Eds.; Academic Press: New York, 1982; pp. 375-403.

79. Levayer, C.; Rouxel, J. C. R. Acad. Sc. Paris C 1969, 268, 167-170.

80. Dunot, M.; Rouxel, J. C. R. Acad. Sc. Paris C 1966, 262, 1879-1881.

81. Kikkawa, S.; Kanamaru, F.; Koizumi, M. Inorg. Chem. 1976, 15, 2159-2197.

82. Kikkawa, S.; Kanamaru, F.; Koizumi, M.; "React. Solids", [Proc. Int. Symp], 8th Goeteborg: Sweden, 1977, pp. 725-729.

83. Hagenmueller, P.; Portier, J.; Barbe, B.; Bouclier, P. Z. Anorg. Alleg. Chem. 1967, 355, 209-218.

84. Schafer-Stahl, H. Synthetic Metals, 1981, 4, 65-69.

85. Maeda, Y.; Yamashita, M.; Ohshio, H.; Tsutsumi, N.; Takashima, Y. Bull. Chem. Soc. Jpn. 1982, 55, 3138-3143.

86. Antonio, M. R.; Averill, B. A. J. C. S. Chem. Comm. 1981, 382-383.

87. Percentages were calculated from the measured intensity of the 020 reflection of the intercalate and the 010 reflection of FeOCl.

88. Thompson, A. H. Nature 1974, 251, 492-494.

89. Kanamaru, F.; Koizumi, M. Japan J. Appl. Phys. 1974, 13, 1919-1920.

90. Schöllhorn, R.; Zagefka, H. D.; Butz, T.; Lerf, A. Mat. Res. Bull. 1979, 14, 369-376.

91. Johnson, J. W. Physica 1980, 99B, 141-144.

92. Herber, R. H.; Maeda, Y. Inorg. Chem. 1981, 20, 1409-1415.

93. Eckert, H., private communication.

94. Gamble, F. R.; Osiecki, J. H.; DiSalvo, F. J. J. Chem. Phys. 1971, 55, 3525-3530.

95. Clough, S.; Palvadeau, P.; Venien, J. P. J. Phys. C 1982, 15, 641-655.

96. Venien, J. P.; Palvadeau, P.; Schleich, D.; Rouxel, J. Mat. Res. Bull. 1979, 14, 891-897.

97. Kauzlarich, S. M.; Averill, B. A.; Teo, B. K. Mol. Cryst. Liq. Cryst. 1984, 107, 65-73.

98. Clement, R. P.; Davies, W. B.; Ford, K. A.; Green, M. L. H.; Jacobson, A. J. Inorg. Chem. 1978, 17, 2754-2758.

99. Kanamaru, F.; Shimada, M.; Koizumi, M.; Takano, M.; Takado, T. J. Solid State Chem. 1973, 7, 297-299.

100. Rouxel, J.; Palvadeau, P. Rev. Chim. Min. 1982, 19, 317-332.

101. Bouat, J.; Bonin, D.; Faccini, L.; Beguin, F. Syn. Met. 1983, 7, 233-242.

102. Bourdillon, A. J.; Pettifer, R. F.; Marseglia, E. A. J. Phys. C 1979, 12, 3889-3897.

103. Michalowicz, A.; Clement, R. Inorg. Chem. 1982, 21, 3872-3877.

104. Clement, R.; Garner, O.; Mercier, H.; Audiere, J. P.; Michalowicz, A.; Rousseau, B.; Setton, R. J. C. S. Chem. Comm. 1984, 1354-1355.

105. Miller, G. R.; Poranski, C. F., Jr.; Resing, H. A. J. Chem. Phys. 1984, 80, 1708-1709.

106. Molitor, M.; Müller-Warmuth, W.; Spiess, H. W.; Schöllhorn, R. Z. Naturforsch 1983, 38a, 237-246.

107. Lee, P. A.; Pendry, J. B. Phys. Rev. 1975, 11B, 2795-2811.

108. Lee, P. A.; Beni, G. Phys. Rev. 1977, 1513, 2862-2883.

109. Lee, P. A.; Citrin, P. H.; Eisenberger, P.; Kincaid, B. M. Rev. Mod. Phys. 1981, 53, 769-806.

110. Gurman, S. J. J. Mat. Sci. 1982, 17, 1541-1570.

111. Hayes, T. M.; Boyce, J. B. Sol. State Phys. 1982, 37, 173-351.

112. Teo, B. K.; Antonio, M. R.; Averill, B. A. J. Am. Chem. Soc. 1983, 105, 3751-3762.

113. Antonio, M. R.; Teo, B. K.; Orme-Johnson, W. H.; Nelson, M. J.; Groh, S. E.; Lindahl, P. A.; Kauzlarich, S. M.; Averill, B. A. J. Am. Chem. Soc. 1983, 104, 4703-4705.

114. Teo, B. K.; Lee, P. A. J. Am. Chem. Soc. 1979, 101, 2815-2832.

115. Teo, B. K. Acc. Chem. Res. 1980, 13, 412-419.

116. Victoreen, J. A. J. Appl. Phys. 1948, 19, 855.

117. "International Tables for X-Ray Crystallography"; Vol. III; Kynoch Press: Birmingham, 1962, 161, 171-173.

118. Lengeler, B.; Eisenberger, P. Phys. Rev. B. 1980, 21, 4507-4520.

119. Stern, E. A.; Kim, K. Phys. Rev. B 1981, 23, 3781-3787.

120. Goulon, J.; Ginet-Goulon, C.; Cortes, R.; Dubois, J. M. J. Physique 1982, 43, 539-548.

121. Biebesheimer, V. A.; Marques, E. C.; Sandstrom, D. R.; Lytle, F. W.; Greegor, R. B. J. Chem. Phys. 1984, 81, 2599-2604.

122. Teo, B. K. J. Am. Chem. Soc. 1981, 103, 3990-4001.

123. Kristenmacher, T. J.; Phillips, T. E.; Cowan, D. O.; Ferraris, J. P.; Bloch, A. N.; Poehler, T. O. Acta. Cryst. 1976, B32, 539-547.

124. Dideberg, O.; Toussaint, J. Acta. Cryst. 1974, B30, 2481-2485.

125. Cooper, W. F.; Kenney, N. C.; Edmonds, J. W.; Nagel, A.; Wudl, F.; Coppens, P. J. C. S. Chem. Comm. 1971, 889-890.

126. Stahl, H. Inorg. Nucl. Chem. Letts. 1980, 16, 271-276.

127. IPNS-Progress Report; Argonne National Laboratory, Argonne, Illinois, 1981-1983; pp. 2-40.

128. Rotella, F. J. "Users Manual for Rietveld Analysis of Time-of-Flight Neutron Powder Diffraction Data at IPNS"; Argonne National Laboratory, Argonne, Illinois, 1983.

129. Von Dreele, R. B.; Jorgensen, J. D.; Windsor, C. G. J. Appl. Crystallogr. 1982, 15, 581-589.

130. Shirley, R. In "Crystallographic Computing, Proceedings of 1978 Summer School, Delft University"; University Press and Oosthoeks: The Netherlands, 1978.

131. Visser, J. M. J. Appl. Crystallogr. 1969, 2, 89.

132. Hendra, P. J.; Parks, P. J. D. J. Chem. Soc. A 1968, 908-911.

133. Beagley, B.; Eckersley, G. H.; Brown, D. P.; Tomlison, D. Trans. Faraday Soc. 1969, 65, 2300-2307.

134. Wudl, F.; Nalewajek, D.; Troup, J. M.; Extine, M. W. Science 1983, 415-417.

135. Grant, P. M. Phys. Rev. B 1976, 26, 6888-6895.

136. Roder, U.; Müller-Warmuth, W.; Schöllhorn, R. J. Chem. Phys. 1981, 75, 412-417.

137. Roder, U.; Müller-Warmuth, W.; Schöllhorn, R. J. Chem. Phys. 1982, 77, 4627-4631.

138. Fukushima, E.; Roeder, S. B. "Experimental Pulse NMR. A Nuts and Bolts Approach"; Addison-Wesley Publishing Co., Inc.: Reading, Massachusetts, 1981.

139. Pake, G. E. J. Chem. Phys. 1948, 327-336.

140. Abraham, R. J.; Loftus, P. "Proton and Carbon-13 Spectroscopy"; Heyden: London, 1978; Chapter 2.

141. Mansfield, P. Prog. NMR Spectroscopy 1971, 8, 41.

142. Boden, N.; Levine, Y. K.; Lightowlers, D.; Squires, R. T. Mol. Phys. 1975, 29, 1877-1891.

143. Van Vleck, J. H. Phys. Rev. 1948, 74, 1168.

144. Swift, T. J. In "NMR of Para-magnetic Molecules"; LaMar, G. N.; Horracks, W., Jr.; Holm, R. H., Eds.; Academic Press: New York, 1973; Chapter 2.

145. Bramwell, F. B.; Haddon, R. C.; Wudl, F.; Kaplan, M. L.; Marshall, J. H. J. Am. Chem. Soc. 1978, 100, 4612-4614.

146. Mayerle, J. J.; Torrance, J. B.; Crowley, J. I. Acta Cryst. 1979, B35, 2988-2995.

147. Averill, B. A.; Kauzlarich, S. M.; Teo, B. K.; Faber, J., Jr. J. Physique 1985, in press.

148. Fyfe, C. A. "Solid State NMR for Chemists"; C. F. C. Press: Guelph, 1983; Chapter 3.

149. Spiess, H. W.; Sillescu, H. J. Mag. Res. 1981, 42, 381-389.

150. Siminovitch, D. J.; Rance, M.; Jeffery, K. R.; Brown, M. F. J. Mag. Res. 1984, 58, 62-75.

151. Diehl, P.; Tracey, A. S. Mol. Phys. 1975, 30, 1917-1920.

152. Bozio, R.; Zano, I.; Girlando, A.; Pecile, C. J. Chem. Phys. 1979, 71, 2282-2293.

153. Meneghetti, M.; Bozio, R.; Zano, I.; Pecile, C.; Ricotta, C.; Zanetti, M. J. Chem. Phys. 1984, 80, 6210-6224.

154. Kachapina, L. M.; Kaplunov, M. G.; Yagubskii, E. B.; Borod'ko, Yu. G. Chem. Phys. Lett. 1978, 58, 394-398.

155. Riga, J.; Verbist, J. J.; Wudl, F.; Kruger, A. J. Chem. Phys. 1978, 69, 3221-3231.

156. Wudl, F.; Scafer, D. E.; Miller, B. J. Am. Chem. Soc. 1976, 98, 252-254.

157. Bozio, R.; Pecile, C. in "Physics and Chemistry of Low-Dimensional Solids"; Alcacer, L., Ed.; Reidel: Dordrecht, Holland, 1980; pp. 165-186.

158. Bozio, R.; Girlando, A.; Pecile, D. Chem. Phys. Lett. 1977, 52, 503-508.

159. Torrance, J. B. in "Chemistry and Physics of One-Dimensional Metals"; Keller, H., Ed.; Plenum Press: New York, 1977, pp. 137-166.

160. Rice, M. J. Phys. Rev. Lett. 1976, 37, 36-39.

161. Kral, K. Chem. Phys. 1977, 23, 237-242.

162. Bozio, R.; Meneghetti, M.; Pecile, C. J. Chem. Phys. 1982, 76, 5785-5795.

163. Wudl, F., private communication to Professor B. A. Averill.

164. Wheland, R. C.; Gillson, J. L. J. Am. Chem. Soc. 1976, 98, 3916-3925.

165. Brec, R.; Schleich, D.; Louisey, A.; Rouxel, J. Ann. Chim. Fr. 1978, 3, 347-352.

166. Sugano, T.; Yakushi, F.; Kuroa, H. Bull. Chem. Soc. Jpn 1978, 51, 1041-1046.

167. Hush, N. S. Prog. in Inorg. Chem. 1967, 8, 391-444.

168. Clement, R.; Garnier, O.; Mathey, Y. Nov. J. Chim. 1982, 6, 13-17.

169. Averill, B. A.; Kauzlarich, S. M.; Antonio, M. R. J. Physique 1983, C44, 1373-1376.

170. Dye, J. L. Prog. Inorg. Chem. 1984, 32, 329-441.

171. Ashcroft, N. W.; Mermin, N. D. "Solid State Physics"; Holt, Rinehart and Winston: Philadelphia, 1976, pp. 562-570.

172. Averill B. A.; Kauzlarich, S. M. Mol. Cryst. Liq. Cryst. 1984, 107, 55-64.

173. Fatseas, G. A.; Palvadeau, P.; Venien, J. P. J. Solid State Chem. 1984, 51, 17-37.

174. Meyer, H.; Weiss, A. Mat. Res. Bull. 1978, 13, 913-922.

175. Schafer-Stahl, H. Mat. Res. Bull. 1982, 17, 1437-1446.

176. Herber, R. H.; Eckert, H. Phys. Rev. B 1985, 31, 34-41.

177. Ohno, Y.; Hirama, K.; Nakai, S.; Sugiura, C.; Okada, S. Syn. Metals 1983, 6, 149-155.

178. Grant, R. W. J. App. Phys. 1971, 42, 1619-1620.

179. Bizette, H.; Adam, A. C. R. Acad. Sc. Paris 1972, 275, 911-914.

180. Reiffe, W., private communication.

181. Smith, T.; Freidberg, S. A. Phys. Rev., 2nd Series 1968, 176, 660-665.

182. Wood, D. W.; Dalton, N. W. J. Phys. C 1972, 5, 1675-1686.

183. Fisher, M. E. Am. J. Phys. 1964, 32, 343-346.

184. Earnshaw, A.; Figgis, B. N.; Lewis J. J. Chem. Soc.(A) 1966, 1656-1663.

185. Adam, A.; Buisson, G. Phys. Stat. Sol (A) 1975, 30, 323-329.